

NUMERICAL COMPUTATION OF STRESS INTENSITY FACTORS FOR AIRCRAFT STRUCTURAL DETAILS BY THE FINITE ELEMENT METHOD

*AEROELASTIC AND STRUCTURES RESEARCH LABORATORY
DEPARTMENT OF AERONAUTICS AND ASTRONAUTICS
MASSACHUSETTS INSTITUTE OF TECHNOLOGY
CAMBRIDGE, MASSACHUSETTS 02139*

MAY 1976

TECHNICAL REPORT AFFDL-TR-76-12
FINAL REPORT FOR PERIOD APRIL 1974 - APRIL 1975

Approved for public release; distribution unlimited

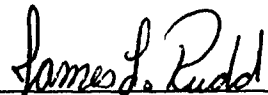
AIR FORCE FLIGHT DYNAMICS LABORATORY
AIR FORCE WRIGHT AERONAUTICAL LABORATORIES
AIR FORCE SYSTEMS COMMAND
WRIGHT-PATTERSON AIR FORCE BASE, OHIO 45433

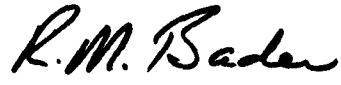
2006092/082

NOTICE

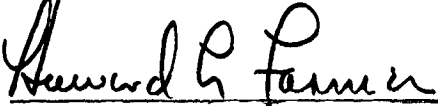
When Government drawings, specifications, or other data are used for any purpose other than in connection with a definitely related Government procurement operation, the United States Government thereby incurs no responsibility nor any obligation whatsoever; and the fact that the government may have formulated, furnished, or in any way supplied the said drawings, specifications, or other data, is not to be regarded by implication or otherwise as in any manner licensing the holder or any other person or corporation, or conveying any rights or permission to manufacture, use, or sell any patented invention that may in any way be related thereto. This report has been reviewed by the Information Office (OI) and is releasable to the National Technical Information Service (NTIS). At NTIS, it will be available to the general public, including foreign nations.

This technical report has been reviewed and is approved for publication.


JAMES L. RUDD
Project Engineer


ROBERT M. BADER, Chief
Structural Integrity Branch
Structures Division

FOR THE COMMANDER


HOWARD L. FARMER, Colonel, USAF
Chief, Structural Mechanics Division

Copies of this report should not be returned unless return is required by security considerations, contractual obligations, or notice on a specific document.

UNCLASSIFIED

SECURITY CLASSIFICATION OF THIS PAGE (When Data Entered)

REPORT DOCUMENTATION PAGE		READ INSTRUCTIONS BEFORE COMPLETING FORM
1. REPORT NUMBER AFFDL-TR-76-12	2. GOVT ACCESSION NO. NA	3. RECIPIENT'S CATALOG NUMBER NA
4. TITLE (and Subtitle) NUMERICAL COMPUTATION OF STRESS INTENSITY FACTORS FOR AIRCRAFT STRUCTURAL DETAILS BY THE FINITE ELEMENT METHOD		5. TYPE OF REPORT & PERIOD COVERED FINAL April 1974 - April 1975
		6. PERFORMING ORG. REPORT NUMBER ASRL TR 177-4
7. AUTHOR(s) Theodore H. H. Pian James W. Mar Oscar Orringer George Stalk		8. CONTRACT OR GRANT NUMBER(s) F33615-74-C-3063
9. PERFORMING ORGANIZATION NAME AND ADDRESS Aeroelastic and Structures Research Lab. Massachusetts Institute of Technology Cambridge, Massachusetts 02139		10. PROGRAM ELEMENT, PROJECT, TASK AREA & WORK UNIT NUMBERS Project 1367 Task 136703 Work Unit 13670315
11. CONTROLLING OFFICE NAME AND ADDRESS Air Force Flight Dynamics Laboratory Attn: AFFDL/FBE Wright-Patterson AFB, Ohio 45433		12. REPORT DATE May 1976
14. MONITORING AGENCY NAME & ADDRESS (if different from Controlling Office) Same		13. NUMBER OF PAGES 107
		15. SECURITY CLASS. (of this report) Unclassified
15a. DECLASSIFICATION/DOWNGRADING SCHEDULE N/A		
16. DISTRIBUTION STATEMENT (of this Report) Approved for public release; distribution unlimited.		
17. DISTRIBUTION STATEMENT (of the abstract entered in Block 20, if different from Report) Same		
18. SUPPLEMENTARY NOTES None		
19. KEY WORDS (Continue on reverse side if necessary and identify by block number) Fracture Mechanics Aircraft Structural Integrity Finite Element Analysis Hybrid Elements Stress Intensity Factor		
20. ABSTRACT (Continue on reverse side if necessary and identify by block number) The results of a program of research involving application of the hybrid finite element method to fracture mechanics analyses of several typical aircraft structural details are presented. The performance properties of the specialized finite element building blocks are reviewed. Capabilities of the computer analysis codes are discussed with regard to valid parameter ranges, core storage requirements and execution times. Numerical results obtained		

UNCLASSIFIED

SECURITY CLASSIFICATION OF THIS PAGE (When Data Entered)

UNCLASSIFIED

SECURITY CLASSIFICATION OF THIS PAGE(When Data Entered)

from extended parameter studies are presented in the form of handbook charts. Suggestions are offered for future improvements and comments are made about the limits of applicability of the data base to airframe damage tolerance analysis.

UNCLASSIFIED

SECURITY CLASSIFICATION OF THIS PAGE(When Data Entered)

FOREWORD

The developments documented in this report were carried out at the Aeroelastic and Structures Research Laboratory, Massachusetts Institute of Technology, Cambridge, Massachusetts 02139, under Contract No. F33615-74-C-3063 (Project 1367, Task 136703) from the U. S. Air Force Flight Dynamics Laboratory. Mr. James L. Rudd (AFFDL/FBE) served as technical monitor. The authors gratefully acknowledge the many contributions of Mrs. Susan E. French of the Aeroelastic and Structures Research Laboratory. This report is the fourth and last in a series covering final results from all phases of the work obtained during April 1974 - April 1975, and was submitted by the authors for technical review in November 1975. The first three reports in the series are AFFDL-TR-75-51 (Fracture Mechanics Analysis of an Attachment Lug), AFFDL-TR-75-70 (Fracture Mechanics Analysis of Centered and Offset Fastener Holes in Stiffened and Unstiffened Panels Under Uniform Tension), and AFFDL-TR-75-71 (Fracture Mechanics Analysis of Single and Double Rows of Fastener Holes Loaded in Bearing). The contractor's report number is ASRL TR 177-4.

TABLE OF CONTENTS

<u>Section</u>	<u>Page</u>
I INTRODUCTION	1
II PROGRAM OVERVIEW	4
III ATTACHMENT LUG ANALYSIS	10
IV FASTENER ROW ANALYSIS	14
V DISCUSSION AND CONCLUSIONS	22
REFERENCES	106

LIST OF ILLUSTRATIONS

<u>Figure</u>	<u>Page</u>
1 Portion of Finite Element Model Surrounding a Crack Tip	27
2 Structural Details Selected for Analysis	28
3 Error in Computed Stress Intensity Factor as a Function of Crack-Tip Position	29
4 Mesh Construction and Example Solution for Rectangular Panel	30
5 Variation of K_I Solution Accuracy with Crack Size (Hole Element Shape W/D_o Fixed)	31
6 Variation of K_I Solution Accuracy with Hole Element Shape	32
7 Attachment Lug Program Capabilities	33
8 Attachment Lug Mesh Details and Example Results	34
9 Example Results for Shear Bearing	35
10 Sensitivity of K_I to a/R_1 and R_2/R_1 for a Crack at $\theta=0^\circ$	36
11 Sensitivity of K_I to a/R_1 and R_2/R_1 for a Crack at $\theta=90^\circ$	37
12 Attachment Lug K_I Chart ($R_2/R_1=1.5$, Uniform Bearing)	38
13 Attachment Lug K_I Chart ($R_2/R_1=2$, Uniform Bearing)	39
14 Attachment Lug K_I Chart ($R_2/R_1=2.5$, Uniform Bearing)	40
15 Attachment Lug K_I Chart ($R_2/R_1=3$, Uniform Bearing)	41
16 Attachment Lug K_{II} Chart ($R_2/R_1=1.5$, Uniform Bearing)	42

LIST OF ILLUSTRATIONS (Continued)

<u>Figure</u>		<u>Page</u>
17	Attachment Lug K_{II} Chart ($R_2/R_1=2$, Uniform Bearing)	43
18	Attachment Lug K_{II} Chart ($R_2/R_1=2.5$, Uniform Bearing)	44
19	Attachment Lug K_{II} Chart ($R_2/R_1=3$, Uniform Bearing)	45
20	Attachment Lug K_I Chart ($R_2/R_1=1.5$, Cosine Bearing)	46
21	Attachment Lug K_I Chart ($R_2/R_1=2$, Cosine Bearing)	47
22	Attachment Lug K_I Chart ($R_2/R_1=2.5$, Cosine Bearing)	48
23	Attachment Lug K_I Chart ($R_2/R_1=3$, Cosine Bearing)	49
24	Attachment Lug K_{II} Chart ($R_2/R_1=1.5$, Cosine Bearing)	50
25	Attachment Lug K_{II} Chart ($R_2/R_1=2$, Cosine Bearing)	51
26	Attachment Lug K_{II} Chart ($R_2/R_1=2.5$, Cosine Bearing)	52
27	Attachment Lug K_{II} Chart ($R_2/R_1=3$, Cosine Bearing)	53
28	Single Fastener Row Program Mesh and Example Results	54
29	Comparison of a/R Sensitivity with Analytical Solutions for Similar Problems	55
30	Sensitivity of K_I to a/R and θ	56
31	Sensitivity of K_{II} to a/R and θ	57
32	Single Row K_I Chart (Center Hole Damaged, $C/D=4$)	58

LIST OF ILLUSTRATIONS (Continued)

<u>Figure</u>		<u>Page</u>
33	Single Row K_{II} Chart (Center Hole Damaged, $C/D=4$)	59
34	Sensitivity of K_I to C/D	60
35	Sensitivity of K_{II} to C/D	61
36	Comparison of K_I for Damaged Center Hole Loaded and Unloaded	62
37	Comparison of K_{II} for Damaged Center Hole Loaded and Unloaded	63
38	Single Row K_I Chart (Left Hole Damaged, $C/D=4$)	64
39	Single Row K_{II} Chart (Left Hole Damaged, $C/D=4$)	65
40	Sensitivity of K_I to C/D (Left Hole Damaged)	66
41	Double Row K_I Chart (Upper Center Hole Damaged, $C/D=4$)	67
42	Double Row K_{II} Chart (Upper Center Hole Damaged, $C/D=4$)	68
43	Double Row K_I Chart (Lower Center Hole Damaged, $C/D=4$)	69
44	Double Row K_{II} Chart (Lower Center Hole Damaged, $C/D=4$)	70
45	Double Row K_I Chart (Lower Center Hole Damaged and Unloaded, $C/D=4$)	71
46	Double Row K_{II} Chart (Lower Center Hole Damaged and Unloaded, $C/D=4$)	72
47	Double Row K_I Chart (Lower Right Hole Damaged, $C/D=4$)	73
48	Double Row K_I Chart (Lower Right Hole Damaged and Unloaded, $C/D=4$)	74

LIST OF ILLUSTRATIONS (Concluded)

<u>Figure</u>		<u>Page</u>
49	Double Row K_{II} Chart (Lower Right Hole Damaged, $C/D=4$)	75
50	Double Row K_{II} Chart (Lower Right Hole Damaged and Unloaded, $C/D=4$)	76
51	Double Row K_I Chart (Upper Left Hole Damaged, $C/D=4$)	77
52	Double Row K_I Chart (Upper Left Hole Damaged and Unloaded, $C/D=4$)	78
53	Double Row K_{II} Chart (Upper Left Hole Damaged, $C/D=4$)	79
54	Double Row K_{II} Chart (Upper Left Hole Damaged and Unloaded, $C/D=4$)	80
55	Double Row K_I Chart (Upper Right Hole Damaged, $C/D=4$)	81
56	Double Row K_I Chart (Upper Right Hole Damaged and Unloaded, $C/D=4$)	82
57	Double Row K_{II} Chart (Upper Right Hole Damaged, $C/D=4$)	83
58	Double Row K_{II} Chart (Upper Right Hole Damaged and Unloaded, $C/D=4$)	84

LIST OF TABLES

<u>Table</u>	<u>Page</u>
1 Typical Core Storage and CPU Time Requirements	85
2 Uniform Bearing ($R_2/R_1=1.5$)	86
3 Uniform Bearing ($R_2/R_1=2$)	87
4 Uniform Bearing ($R_2/R_1=2.5$)	88
5 Uniform Bearing ($R_2/R_1=3$)	89
6 Cosine Bearing ($R_2/R_1=1.5$)	90
7 Cosine Bearing ($R_2/R_1=2$)	91
8 Cosine Bearing ($R_2/R_1=2.5$)	92
9 Cosine Bearing ($R_2/R_1=3$)	93
10 Range of Parameter Study for Fastener Row Programs	94
11 Single Fastener Row (Center Hole Damaged, $C/D=4$)	95
12 Single Fastener Row (Center Hole Damaged, C/D varied)	96
13 Single Fastener Row (Center Hole Damaged and Unloaded, $C/D=4$)	97
14 Single Fastener Row (Left Hole Damaged, $C/D=4$)	98
15 Double Fastener Row (Center Hole in Upper Row Damaged, $C/D=4$)	100
16 Double Fastener Row (Center Hole in Lower Row Damaged, $C/D=4$)	102
17 Double Fastener Row (Center Hole in Lower Row Damaged and Unloaded, $C/D=4$)	104

Section I

INTRODUCTION

Air Force analysis of operational experience with aircraft fleets over the past several years has led to the establishment of damage tolerance criteria for metal airframes [1] which require the designer to verify the structural integrity of flight-safety-critical details based on fracture mechanics calculations. These calculations are distinct from and serve a different purpose than fatigue calculations based on Miner's rule or similar damage accumulation hypotheses. The damage tolerance philosophy assumes the presence of small cracks in the airframe at the time the airplane is brought into service, and seeks to protect the structure against failures which might result from the actual presence of these cracks. The methodology is based upon integration of an empirical crack growth rate relationship over the aircraft life history, as represented by loads in the vicinity of the safety-critical parts, and upon the establishment of a fracture-critical crack size for each part corresponding to a maximum expected load.

Both the crack growth calculations and the determination of fracture-critical crack sizes require the application of linear elastic fracture mechanics to compute stress intensity factors at the tip of the assumed sharp crack. Analytical solutions for stress intensity factors can be obtained for crack tips remote from other geometrical features of the structure boundary. These solutions may be extended to more complicated geometries by the techniques of conformal mapping and boundary collocation [2,3]. However, the complexities found in aircraft structural details usually involve the proximity of two different types of boundary geometry (e.g., a circular fastener hole near a linear edge) as well as load distributions which are more complicated than uniform stress, linearly varying stress, or a point load. Thus, stress intensity factor solutions by the traditional methods are often inconvenient, and may be prohibitive in some cases.

The above problems are also encountered in conventional stress analysis. The finite element methods have assumed a dominant role in conventional stress analysis over the past decade because of their inherent ability to accommodate complex boundaries and load distributions in a highly organized fashion which is also convenient for the analyst. For this same reason, the finite element methods are now beginning to be applied extensively to the field of fracture mechanics analysis. A recent paper by Pian [4] reviews several alternate approaches to finite-element fracture mechanics and compares their relative merits. The work reviewed in the present report has been based on the assumed-stress hybrid approach [5].

The key feature in applying the hybrid finite element method to fracture mechanics is the special-purpose crack-tip element shown in Fig. 1. This element possesses an assumed displacement distribution along its outer boundary which is compatible with the boundary displacement assumption for conventional quadrilateral elements. The stress assumption, which characterizes behavior within the element, includes the crack-tip singularity and several additional nonsingular terms, all of which are obtained from a complex variable elasticity solution for the material region near the crack tip [6]. In effect, what has been done is to combine the classical elasticity solution for a crack-tip stress singularity, a simple solution in the absence of neighboring boundaries and applied loads, with the flexibility of transitioning to these boundaries and loads in the piece-wise fashion permitted by the finite element methods. From a practical standpoint, the hybrid approach also proves to be convenient because it permits the creation and solution of finite element models using the well-known Matrix Displacement Method. The special crack-tip element is in this respect just another element with nodes to be coupled to the model. Its only unusual features are its shape, its possession of nine instead of four nodes, and the fact that the matrix "stress" analysis procedure one normally associates with a conventional element leads in this case to stress intensity factors instead of stresses.

Naturally, there is a price to pay for the convenience of the hybrid method. Crack tips cannot be located near other geometrical details with complete disregard for the crack-tip position relative to the boundaries of the special element. One is thus forced to accept a compromise between solution accuracy and the cost of the analysis, parameters which increase as the finite element model becomes more detailed. The present work has focussed on analysis of several typical aircraft structural details and has shown that the hybrid approach permits a reasonable compromise between cost and accuracy. Subsequent sections of this report review the scope of the program, tests for accuracy, computation cost experience, and the detailed results obtained from parametric analyses of some of the structural details.

Section II

PROGRAM OVERVIEW

The major objectives of the program were to provide numerical analysis codes to compute the mode I and mode II stress intensity factors K_I , K_{II} for four general classes of structural details: an attachment lug with a bearing hole, a rectangular stiffened or unstiffened panel with an open hole which could be centered or off-set, a single row of fastener holes near one edge of a panel, and a double staggered row of fastener holes near one edge of a panel. In all cases, cracks were to be assumed emanating radially from one of the holes: a single crack for the attachment lug and either one crack or two diametrically opposed cracks in the other configurations. The angular locations of the cracks around the hole were to be variable, and selection of the damaged hole was to be a parameter in the cases of the multi-hole details. The general configurations are illustrated schematically in Fig. 2.

The above objectives were achieved by programming individual parametric analysis codes for each configuration, using the ASRL FEABL-2 software [7] as a base. Three interim technical reports [8,9,10] discuss in detail the construction, verification and initial demonstration of each computer program. Additional information relating to accuracy analysis and the general capabilities of hybrid crack elements has also been published separately [11,12,13,14]. An additional objective to study the effect on K_I and K_{II} of an interference-fit fastener in the rectangular panel (Fig. 2B) could not be attempted within the scope of the program. The loading applied to the fastener hole row details (Fig. 2C and 2D) was changed from uniform tension on the neighboring edge to individual bearing loads on each hole during the program, when the latter situation proved to be more interesting in the light of results obtained from analyses of the rectangular panel configuration.

It should be observed that the stress intensity factors K_I , K_{II} will vary with the material Poisson ratio ν and will have

different values in plane stress and plane strain when the structure incorporates a crack tip near a constrained boundary or when it is otherwise multiply connected, as in the present cases. It has been remarked [3] that the thickness of a structure relative to its external dimensions determines whether plane stress or plane strain analysis is to be conducted, irrespective of whether plane strain conditions are achieved locally at the crack front. The plane stress state was considered to be of primary interest in the present work, and the computer codes have been programmed accordingly. In all of the analyses discussed subsequently, results were obtained based on the general properties for aluminum alloys:

$$E = 10^7 \text{ psi} \quad \nu = 0.3$$

The elastic properties E , ν are input parameters, but the sensitivity of K_I , K_{II} solutions to ν was not studied in the present program.

Where possible, the finite element solutions for stress intensity factors were compared with independently obtained analytical or boundary collocation solutions [3]. However, since independent solutions are not available for most of the configurations and crack locations considered in the present work, accuracy assessments were also made based upon the performance of individual types of finite elements under varying conditions. The isoparametric 4-node quadrilateral was used as the basic building-block in the various finite element models. Its performance has been well characterized, and it is known to give accurate displacement solutions in the presence of gradients if the element shape is kept close to a square [15]. The mesh-generation portions of the computer codes were programmed accordingly, and attention was focussed upon the behavior of the hybrid crack element (PCRK59). The element was found to have a somewhat better performance with respect to shape distortions, using accuracy of the computed K_I value as a measure. The key error parameter was found to be the position of the crack tip within the element [8,13]. The latter effect is illustrated in Fig. 3, which plots the error in computed stress intensity for the problem of a finite-width strip with symmetrical edge cracks loaded in uniform

tension. As can be seen in the figure, serious errors are introduced if the crack tip approaches the opposite edge of the PCRK59 element. This effect is attributed to the tendency of severe local gradients to "spill over" into the neighboring quadrilateral elements, which are not equipped to handle such situations. The results also seem to indicate that reasonably accurate solutions are obtained when the crack tip is near a lateral boundary of the structure (also the PCRK59 boundary), i.e., for $a/b = 0.2$ in Fig. 3. However, additional results discussed subsequently cast some doubt on this finding.

The attachment lug analysis was programmed with the quadrilateral and PCRK59 elements as the basic building blocks. However, initial attempts to design an adequate mesh for the rectangular panel led to a mesh-grading problem which was finally solved by creating another building block. As shown in Fig. 4A and 4B, the amount of refinement required near the fastener hole demands either a wasteful use of nodes and elements throughout the panel or a rapid grading to a very coarse mesh remote from the hole. While the first course of action would have resulted in a costly analysis, the second would have led to inaccuracy in the displacement solution because the mesh would have contained constant-strain triangle elements. Instead, a third alternative was chosen by using the hybrid method to create a special-purpose "hole element" which occupies the region between the square and outer circular boundaries in Fig. 4B. Since the essence of the hybrid approach to special-purpose elements is to mimic known behavior, mid-edge nodes were included on the hole element outer boundary to allow in an average sense for the type of displacement field expected in the vicinity of an open hole, and the assumed stress field was adapted from a classical elasticity solution for this type of region.

Extensive tests of the hole element with and without inner circular rings of quadrilaterals verified the element's ability to reproduce accurate stress fields for a hole unloaded, subjected to uniform pressure (interference-fit) or subjected to a bearing load;

tests with PCRK59 elements in place in the inner rings also verified the ability of the finite element model to compute stress intensity factors [9]. Figure 4C illustrates a typical solution obtained from the rectangular panel program, with the fastener hole on center and without edge stiffeners. This "butterfly" plot summarizes K_I , K_{II} as functions of the polar angle to the crack. The solution for K_I was verified for single cracks at 0° and pairs of cracks at 0° , 180° by comparison with independent solutions [3].

The results reported previously for panel program performance [9] were considered to be incomplete, partly because the independent solution which was then available did not account for finite-width effects, and partly because sensitivity to the shape of the hole element had not been thoroughly investigated. The study of both of these performance aspects has since been completed after receipt of some revisions to Ref. 3 which included finite-width solutions for cracks at 0° and 180° at a hole in a tension panel. Figure 5 illustrates the effect of the ratio of crack size to hole radius a/R on solution accuracy. The error in K_I is seen to range between -9 to +3 percent, with the best performance occurring for $0.05 \leq a/R \leq 1.2$. The upper limit is sufficient to extend the range of good solutions to regions in which the fastener hole begins to lose its influence on the crack tip. For very small crack sizes ($a = 0.005$ inch, $a/R \approx .0158$) the solution error is observed to be significantly greater than was previously estimated (Fig. 3 and discussion on pp. 5-6) for small cracks. The non-monotonic error variation shown in Fig. 5 is attributed to the manner in which the mesh generation is programmed for the interior rings of quadrilaterals (see Fig. 4B) which surround the fastener hole. The PCRK59 element is placed in the first and second, second and third, or third and fourth rings according to the crack size, so that the best chance of placing the crack tip at the element center is obtained. This leads to a non-monotonic variation of the crack-tip location in the PCRK59 element, which causes the error behavior.

The "shape" of the surrounding hole element, as expressed by the ratio of its edge dimension to its inner diameter W/D_o , is

another important performance parameter. Results obtained from earlier tests [9] indicated that reasonably accurate stresses and stress intensity factors could be obtained over the range $1.59 \leq W/D_o \leq 6.35$. It is desirable to extend this range if possible, particularly the lower limit, in order to permit the analysis of other details with closely spaced fastener holes. Since the inner-ring mesh is programmed to maintain a fixed ratio between the fastener hole diameter D and the hole element diameter D_o :

$$D_o/D = 2.52$$

the realizable center-center fastener spacing is actually given by:

$$C/D = 2.52 W/D_o$$

Therefore, some additional tests were run to determine the extent to which the shape of the hole element could be distorted. The results, illustrated in Fig. 6, show that surprisingly accurate answers are obtained over a much larger range than was previously thought possible. The worst behavior (data points at $W/D_o = 1.04, 1.1$) is seen to be about 10 percent error for K_I . Based on these results, the hole element is considered to be useful over the range:

$$1.2 \leq W/D_o \leq 10$$

The study of sensitivity to a/R (Fig. 5) was run at $W/D_o \approx 1.27$.

In the limited parameter study which was run previously to test the various panel program options [9], it was found that offsetting the hole from the panel centerline and/or placing lateral stiffeners along one or both edges had very little effect on the stress intensity factor solutions. This result should be expected for panels loaded by uniform tension, unless the crack tip is allowed to approach very closely to a free edge or a lateral stiffener. In fact, the analytical solutions obtained by Isida [16] and reproduced by finite element analysis related to the present work [14] indicate that the distance between a crack (without fastener hole) in a plate and an edge stiffener must be less than 30 percent of the crack half-length to obtain more than 20 percent change in a K_I solution which ignores the presence

of the stiffener. A similarly close approach is considered to be necessary to experience the effect of an edge or stiffener on the tip of a crack emanating from a fastener hole. However, the panel program was not designed to handle these extremely close approaches. Therefore, no further parameter studies with this code were conducted.

The attachment lug and fastener row programs gave more interesting results and were consequently exercised in extended parameter studies. The results of these studies are discussed separately in Sections 3 and 4. Computing experience for all of the programs is summarized in Table 1, which compares typical total core storage requirements and CPU times for one complete set of K_I , K_{II} solutions. A "complete set" of solutions refers to 24 to 48 pairs of K_I , K_{II} values corresponding to all angular positions of the crack around a fastener or bearing hole, for one given set of dimensions (hole radius, crack size, etc.).

Section III

ATTACHMENT LUG ANALYSIS

The attachment lug program automatically generates and analyzes the structural detail shown in Fig. 7. Although the program is able to analyze a two-material lug, with ideal bonding assumed between the bushing and the remainder of the structure, this option has not been exercised. The other available options (bearing load applied in one of the four directions indicated in the figure and representation of the load as either a cosine or uniform pressure distribution) have been exercised on analyses of single-material lug details. Detailed documentation of the program and the accuracy tests associated with it appear in the first report in this series [8].

Some of the previous results are reviewed briefly here to give a general idea of the finite element model and its capabilities. Figure 8 illustrates some of the mesh details and an example solution for the case of cosine-distributed tension bearing (load position 1 in Fig. 7). The number of quadrilateral element divisions around the bearing hole is an input parameter and is usually specified as 24, 32 or 48. Maximum shape distortion of the PCRK59 element occurs when 24 divisions are used. This distortion (Fig. 8A) is well within the limits which were established for good performance of the PCRK59 element (see Section 2). The entire mesh is graded to produce quadrilaterals with shapes as close to square as possible in the bushing region (Fig. 8B) where the largest gradients in stress and displacement are expected. Since the computer code has been programmed to confine the crack to the bushing, the outer diameter of this subregion is used to control the potential extent of crack sizes in analyses of single-material lugs. The possible crack size range is given by:

$$a/R_1 \leq 0.22 \text{ for } R_2/R_1 \leq 2$$

$$a/R_1 \leq 0.45 \text{ for } 2.5 \leq R_2/R_1 \leq 3$$

where

a = Crack size

R_1 = Radius of bearing hole

R_2 = Outer radius of lug

The stress intensity factor solutions for tension bearing characteristically exhibit K_I maxima for cracks near $\pm 90^\circ$ from the lug axis. Figure 8C illustrates two sets of solutions: 24 divisions (coarse mesh) and 32 divisions (fine mesh) around the hole. The K_I data, plotted for $0^\circ \leq \theta \leq 180^\circ$, are observed to have converged with the coarse mesh. The K_{II} data, plotted for $180^\circ \leq \theta \leq 360^\circ$, are observed to be near convergence with the fine mesh. Full plots are not required, since the solutions for tension bearing are always symmetric about the lug axis. The upper part of Fig. 8C also illustrates contour plots of the stress components in an uncracked lug with the same dimensions. These stress analyses were used to demonstrate a correlation between K_I , K_{II} for small cracks and $\sigma_{\theta\theta}$, $\sigma_{r\theta}$, respectively [8], and the stress analysis option has been retained in the final program. Figure 9 illustrates the mesh details and typical solutions for positive shear bearing (load position 2 in Fig. 7) for the same lug dimensions as shown in Fig. 8B. Stress intensity factor solutions for both uniform and cosine bearing pressures are illustrated. In these cases, K_I maxima occur for cracks positioned at unexpected angles. Similar plots for several other interesting cases appear in the original report [8].

The case of tension bearing was considered to be of primary interest in the present work. Therefore, an extended parameter study was conducted for this case to evaluate the sensitivity of stress intensity factors to a/R_1 and R_2/R_1 for both uniform and cosine bearing pressure distributions. The numerical data obtained from the lug program analyses were reduced to a form convenient for design charts. Values of the sensitivity functions $F_I(a/R_1, \theta)$ and $F_{II}(a/R_1, \theta)$ are summarized in Tables 2 through 5 (uniform bearing) and 6 through 9 (cosine bearing). For specific applications, stress intensity factors may be computed as:

$$K_I = \frac{P}{\sqrt{\pi a}} F_I(a/R_1, \theta) \quad K_{II} = \frac{P}{\sqrt{\pi a}} F_{II}(a/R_1, \theta)$$

where P is the total bearing force value. These data were obtained from lug models with 32 divisions around the bearing hole, allowing the crack to be positioned at 11.25° intervals.

Figures 10 and 11 illustrate the sensitivities of K_I for cracks at 0° and 90° respectively. For cracks at 0° , a cosine pressure distribution is seen to cause stress intensities more severe than those caused by a uniform distribution. The situation is reversed for cracks at 90° , where the stress intensities are generally the most severe. In both cases, the dimensionless parameter R_2/R_1 for the lug is observed to have a significant effect. The most rapid change in stress intensities is seen to occur between $1.5 \leq R_2/R_1 \leq 2$. This rapid change is attributed to finite-width effects similar to those which have been derived analytically for cracks in finite-width plates loaded in uniform tension. The behavior of these solutions should be noted especially for $R_2/R_1 = 1.5$ and $R_2/R_1 = 2$, where anomalies occur. The data at $a/R_1 = 0.22$ are obtained from finite element models in which the crack-tip location begins to approach close to the opposite boundary of the PCRK59 element, a situation in which significant errors are to be expected (see Section 2). Therefore, the solutions for these R_2/R_1 values are considered to be valid only for $a/R_1 \leq 0.2$. A similar but much less severe effect can be observed between $0.4 \leq a/R_1 \leq 0.45$ for $R_2/R_1 = 2.5$ and $R_2/R_1 = 3$.

The sensitivity data presented in Tables 2 through 9 are also plotted in Figs. 12 through 27. It should be noted that $F_I(a/R_1, \theta)$ assumes negative values at some points. A negative value in the linear elastic solution scheme means that the two PCRK59 element nodes which lie on opposite sides of the crack surface have overlapped one another. The proper interpretation is that a crack in such a location would be closed by the applied loading; the actual negative F_I value otherwise has no specific meaning. Values for K_{II} and F_{II} may be positive or negative according to the sense of the shear stress

field in the vicinity of the crack tip. In this case, the attachment lug program routinely computes absolute values, the sign being of no significance for interaction formulas. Comparison of Figs. 12 through 15 with Figs. 20 through 23 shows that the closure effect for cracks at 0° appears only in the case of uniform bearing for $R_2/R_1 \leq 2$. Cracks at 180° are subject to closure for both uniform and cosine bearing. However, 180° cracks may be opened by reversed (compression) loading [8]. The K_I maxima are seen to occur for cracks near 90° in uniform bearing, and for cracks near 100° in cosine bearing. Comparison of K_I with K_{II} (e.g., Figs. 12 and 16) indicates that most of the crack locations result in significant combined stress intensities, while K_{II} is negligible only in very narrowly defined regions about $\theta = 0^\circ$, 90° and 180° . When considering the effects of fatigue loading, it has been shown that a crack tends to propagate along a curved path when the K_{II} value is significant, the curvature continuing until the crack is oriented perpendicular to a principal tensile stress [17]. Finally, it may be observed that the K_I charts exhibit crossovers at $\theta = 0^\circ$ and 180° when the stress intensities are small (Figs. 12, 13, 22 and 23). The K_{II} charts also exhibit crossovers in the range $0^\circ \leq \theta \leq 90^\circ$ for small stress intensities. These effects are attributed to the usual "noisiness" which is associated with low-stress regions in a finite element solution.

Section IV

FASTENER ROW ANALYSIS

The fastener row programs automatically generate and solve finite element models of the structural details shown in Fig. 2C and 2D. A typical mesh plan and example results from the single fastener row program are illustrated in Fig. 28. The mesh plans and solutions for double fastener rows are generally similar. The single and double fastener row programs make extensive use of internal automatic substructuring and rotation transformations to avoid repeated regeneration of similar elements during parametric analyses. These programs are capable of analyzing only isotropic material. The bearing loads in each fastener hole are assumed to be cosine-distributed. Values for the total bearing force applied to each hole may be chosen separately. Up to 10 fastener holes may be accommodated in the single row program, while the double row program permits up to 8 holes per row. One or two cracks may be placed at the damaged hole, which may be chosen from any of the fastener holes represented in the finite element model. The crack sizes, hole radius and centerline spacing are all input parameters. Detailed documentation of the fastener row programs and the results of some preliminary accuracy tests were reported previously [10]. The earlier demonstration runs and the new results presented in the present report have all been carried out with models containing three fastener holes per row.

The previous attempt to verify the accuracy of the fastener row programs is considered to be incomplete because of the lack of any independent analytical solution with which a direct comparison can be made. Therefore, some further indirect comparisons were conducted by studying the sensitivity of K_I to a/R for cracks perpendicular to the applied load ($\theta = 0^\circ$ according to the angular convention in these finite element models). Analytical solutions for a cracked fastener hole in an infinite medium are available in the forms [3]:

$$K_I = \sigma_\infty \sqrt{\pi a} F(s)$$

for uniform remote tension loading σ_{∞} , where $s = a/(R+a)$, and:

$$K_I = p \sqrt{\pi a} F(s)$$

for uniform pressure loading p applied to the periphery of the hole. In order to compare the finite element results with these solutions, an "equivalent pressure" corresponding to the distributed bearing load was calculated from a solution of the biharmonic equation for an uncracked structure, which gives:

$$\sigma_{\theta\theta}(r, \theta) = \frac{2P}{\pi^2 R} \left[\left(\frac{R}{r}\right)^2 + \frac{2}{3} \left(\frac{R}{r}\right)^4 \cos 2\theta + \left\{ \frac{4}{15} \left(\frac{R}{r}\right)^6 - \frac{2}{15} \left(\frac{R}{r}\right)^4 \right\} \cos 4\theta + \dots \right]$$

where R represents the fastener hole radius and $r \geq R$. The "equivalent pressure" was defined arbitrarily for a crack at $\theta = 0^\circ$ by requiring $\sigma_{\theta\theta}(r, 0)$ to be equal to the hoop stress created by a uniform internal pressure:

$$\sigma_{\theta\theta}(r, 0) = \frac{2P}{\pi^2 R} \left[1 + \frac{8}{15} + \dots \right] \approx .377 \frac{P}{R} \equiv p \text{ (equiv.)}$$

Sensitivity factors $F(s)$ for the finite element solutions were then computed from the numerical K_I values by solution of the equivalent relationship:

$$K_I \approx .377 \frac{P}{R} \sqrt{\pi a} F(s)$$

The comparison, illustrated in Fig. 29, indicates that the fastener hole loaded by a cosine pressure distribution has a behavior intermediate between the two analytical cases, but closer to the case of uniform internal pressure than to remote tension loading.

Additional indirect verification was obtained by comparing the finite element solution with the case of a crack of length of $2a$ in an infinite medium with point loads $\pm P$ applied to opposite surfaces at the center of the crack. The analytical solution for this case is given by [3]:

$$K_I = P/\sqrt{\pi a}$$

If one plots a sensitivity function $F(s)$ for the case of a crack emanating from a fastener hole in the form:

$$K_I = \frac{P}{\sqrt{\pi a}} F_I(s, \theta)$$

then as a/R becomes large, it is reasonable to look for asymptotic behavior which makes the stress intensity trend toward:

$$K_I \rightarrow \frac{P}{\sqrt{\pi(R+a)}} \quad \text{as } a/R \rightarrow \infty$$

The above trend is equivalent to:

$$F_I(s, 0) \rightarrow \sqrt{\frac{a}{R+a}} = \sqrt{s}$$

Figure 30 illustrates the comparison for sensitivity functions $F_I(s, \theta)$ computed from the K_I values obtained in a series of analyses with the single fastener row program. The curve for $\theta = 0^\circ$ is seen to exhibit the correct trend, but it lies below the curve for \sqrt{s} . The difference may be attributed to the fact that the cosine-distributed applied loading is diffuse compared to the point load considered in the analytical solution. These comparisons, taken together with the performance tests of the rectangular panel program (Section 2) are considered to be sufficient to justify confidence in the fastener row program solutions. The rectangular panel accuracy tests are applicable in the present case because the finite element models for the fastener row details are constructed from the same basic building blocks, in the same shape ranges, as the rectangular panel models.

Another important aspect of Fig. 30 is the crossover behavior which is apparent at small crack sizes ($0.0158 \leq s \leq .0875$). This type of behavior is even more apparent in the K_{II} sensitivity functions (Fig. 31), which also show anomalously high values for $F_{II}(s, \theta)$ at $s = .0158$. The crossovers in K_I cannot be considered to result only from normal solution "noise" because cracks within $\theta = \pm 30^\circ$ are involved, and these are high-stress regions. Furthermore, one should expect K_{II} (and hence F_{II}) to approach zero as the crack size approaches zero, and this expectation is followed only for $\theta = 0^\circ, -15^\circ$ in Fig. 31. Hence, the solutions at $s = .0158$ are considered to be seriously in error. The cause is attributed to the proximity of the crack-tip location to the fastener hole surface, leading to the conclusion previously mentioned (Section 2) that the crack-tip location test of an edge-cracked semi-infinite strip is an incomplete test.

Based on the above considerations, data obtained from the fastener row programs were considered to be valid in the ranges $0.05 \leq s \leq 0.528$ for K_I and $0.1 \leq s \leq 0.528$ for K_{II} , and sensitivity charts were prepared accordingly from the results of an extended parameter study. The data were taken from models with a 5/8-inch fastener hole diameter for the seven crack sizes and corresponding s-values given in Table 10. A 5/8-inch fastener diameter was selected because this size is found in many different aircraft. For this fastener size, Table 10 indicates that the invalid K-solutions ($s = 0.0158$) correspond to crack sizes considered in the durability portion of the Air Force damage tolerance criteria, while the lower limit for the valid K-solutions corresponds to crack sizes considered for structural integrity (safety-of-flight) in the criteria [1]. Also, the upper limit, which represents the capability of the finite element meshes, is seen to be sufficiently large to have some confidence that most of the crack size range over which the fastener hole has a significant influence has been covered.

Reduced data for the sensitivity functions $F_I(s, \theta)$ and $F_{II}(s, \theta)$ for several of the cases considered in the extended parameter study are given in Tables 11 through 17. In most of the cases considered, the fastener spacing was fixed at $C/D = 4$ ($C/R = 8$). However, a limited study of the sensitivity to C/D was conducted with the single fastener row program at values $C/D = 3.2, 3.6$ and 4.8 (Table 12). The applied loads were assigned equal values for all cases except those in which the effect of an unloaded damaged hole was studied. The data have been reduced in a manner such that stress intensities for specific cases can be computed from:

$$K_I = \frac{P}{\sqrt{\pi a}} F_I(s, \theta) \quad K_{II} = \frac{P}{\sqrt{\pi a}} F_{II}(s, \theta)$$

where P represents the bearing force applied to any one fastener hole in the structure, whether the damaged hole is loaded or unloaded.

Sensitivity charts have also been prepared from the cases summarized in Tables 11 through 17, as well as for several other cases of minor interest which have not been tabulated. The sensitivity charts are presented in Figs. 32 through 58. For convenience

of visual interpolation in those cases where solutions were obtained for all seven crack sizes, the tabulated data have been used to compute the data for plotting at convenient s -values (i.e., $s = 0.05$, 0.1 etc.) by linear interpolation. All of the solutions are obtained from meshes with 24 divisions around the damaged hole (crack locations at 15° intervals).

Figures 32 and 33 illustrate the sensitivity charts for a single row of fasteners with the center hole damaged. In view of the symmetry about the vertical centerline of the structure and loading, these charts cover only $-90^\circ \leq \theta \leq +90^\circ$. The K_I maxima are observed to shift from $\theta = -30^\circ$ to $\theta = -15^\circ$ as the crack size increases. As was found in the attachment lug analyses, the K_{II} values are negligible only in fairly narrow regions near $\theta = 0^\circ, \pm 90^\circ$. Figures 34 and 35 illustrate the sensitivity for three selected crack sizes as the fastener spacing C/D is varied. These charts have been prepared to be used in conjunction with Figs. 32 and 33. For example, K_I in a specific case may be computed from:

$$K_I = \frac{P}{\sqrt{\pi a}} F_I(s, \theta) G_I(C/D, s, \theta)$$

where F_I is obtained from Fig. 32 and G_I is obtained from Fig. 34. The case $C/D = 4$ is not plotted in Figs. 34 and 35, since by definition:

$$G_I(4, s, \theta) = G_{II}(4, s, \theta) = 1$$

Some of the angular variations of G_I and G_{II} can probably be attributed to solution noise. The conclusion of primary interest about sensitivity to fastener spacing concerns the behavior of K_I for cracks in the range $-30^\circ \leq \theta \leq 0^\circ$. The data in Fig. 34 are fairly consistent over this range, indicating that the K_I value (in terms of $C/D = 4$) increases by 15 to 25 percent for $C/D = 3.2$, by 7 to 10 percent for $C/D = 3.6$, and decreases by 10 to 20 percent for $C/D = 4.8$.

Although a crack at a fastener hole is viewed primarily from the standpoint of its effect in degrading structural integrity, there is a possibility that the presence of the crack may introduce enough additional local compliance in the structure to unload the

fastener. Therefore, stress intensity factor solutions for rows of fastener holes in which the damaged hole is unloaded are of some interest. Figures 36 and 37 illustrate the effect on K_I and K_{II} in a single row of three fastener holes for three selected crack sizes. The major point of interest is that the bearing loads in the adjacent holes appear to provide about 1/6 of the total stress intensity K_I in the range $-30^\circ \leq \theta \leq 0^\circ$. Thus, even a partial unloading of the fastener in the damaged hole would have a disproportionately beneficial effect. One might also conclude tentatively from these results that the contributions of K_I from more remote fastener holes tend to die out rapidly as a function of the distance between the contributor and the damaged hole. Before acceptance, this conclusion should be verified with analyses of models with five or more holes per row.

Figures 38, 39 and 40 repeat the study of basic sensitivities for the three-fastener single row with the left hole damaged. In these cases, some asymmetry appears in the solutions because of the location of the damaged hole near a free lateral edge. In particular, the K_I values (Fig. 38) for cracks directed toward the free edge (θ near 180°) are somewhat higher than the corresponding values for interior cracks (θ near 0°). A similar effect on K_{II} can be seen in Fig. 39 (compare $\theta = 30^\circ$ with 150° and $\theta = 330^\circ$ with 210°). The sensitivity of K_I to fastener spacing (Fig. 40) appears to follow the behavior exhibited in the case of the center hole damaged. (The data for the run $s = 0.138$ were inadvertently lost for $\theta > 135^\circ$.)

The remaining charts present the results of a parameter study conducted with a double row (three fasteners per row) with $C/D = 4$. Sensitivity to fastener spacing was not included in this part of the study. Figures 41 and 42 illustrate a case in which the center hole in the upper row is damaged. These solutions are similar to the corresponding case of a single row of fasteners, except that asymmetry is exhibited because of the staggered arrangement of the holes.

Figures 43 and 44 illustrate a case in which the center hole in the lower row is damaged. Comparison with the previous case shows that the stress intensity factors for this case are significantly higher. This happens because a crack in the lower row is influenced by the bearing loads in the upper row as if these loads were remote tension [10]. Also, the solution asymmetry is much less apparent in this case. Figures 45 and 46 illustrate the effect on K_I and K_{II} when the damaged hole is unloaded. Again, significant decreases in stress intensity occur, but not to the extent observed in the case of the single fastener row. Apparently, the loads in neighboring holes in the upper row can contribute to the crack-tip stress intensity much more easily than can the loads in holes which are separated laterally from the damage site.

The remaining charts illustrate results obtained with only three selected crack sizes for some minor cases of interest. The stress intensities for a damaged hole in the lower row near the right edge are somewhat lower than for damage at the center hole, and the effects of unloading are similar (Figs. 47 through 50). When the left hole in the upper row is damaged, the results are similar to the corresponding case of a single fastener row (Figs. 38, 39), but in the present case unloading of the damaged hole results in large regions of crack closure due to the compression effects of the bearing loads in the lower row (Figs. 51, 52). The behavior of K_{II} is somewhat anomalous. Unloading causes a large decrease in the stress intensities for large cracks ($s = 0.528$), but a much smaller decrease for intermediate-sized cracks ($s = 0.39$), as shown in Figs. 53 and 54. The final case, in which the right hole in the upper row is damaged (Figs. 55 through 58) is similar to the previous case if the crack angle is reflected (i.e., the roles played by $-90^\circ \leq \theta \leq +90^\circ$ and $90^\circ \leq \theta \leq 270^\circ$ are reversed).

It should be noted that all of the sensitivity charts presented in this report have been plotted by making linear connections between the computed data points, unlike the fairing which was done in the previously reported polar plots. Linear interpolation has been used purposely in the sensitivity charts to avoid applying any bias to

the intermediate angular positions for which the programs cannot compute solutions. Obviously, the true solutions should be smooth curves. In most cases, the linear interpolations are probably close enough for engineering purposes, but it is also evident that the computed solutions have missed peaks in many places. This is particularly true for the K_{II} charts.

Finally, it must be remarked that the fastener row solutions presented here probably do not correspond directly to cases of practical interest, in which the load introduction most likely will exhibit some variation with the location of individual fasteners in the panel. However, the case of equal loads was chosen for study as the best method of illustrating general behavior without unnecessarily cluttering the presentation with additional parameter variations. In any specific case, the fastener row programs can be run with individually chosen loads at each fastener location.

Section V

DISCUSSION AND CONCLUSIONS

The results of a research program involving application of the assumed-stress hybrid finite element method to the analysis of stress intensity factors in some typical aircraft structural details have been presented. The key feature of the hybrid method which has made this work possible is a special-purpose element which contains the crack tip and its stress singularity, but which may be coupled to conventional finite elements in a standard Matrix Displacement Method analysis scheme. A secondary feature, which was developed in the course of the present program, is another special-purpose hybrid element which permits the rapid grading of a mesh from a very coarse cartesian pattern to a locally fine polar pattern for surrounding fastener holes. Tailored modular computer codes were prepared with these building blocks to create automatically generated finite element models of four classes of structural details: an attachment lug loaded in bearing through its pin hole; a rectangular stiffened or unstiffened panel loaded by remote tension containing a centered or offset open fastener hole; a single row of fastener holes loaded in bearing; and a double staggered row of fastener holes loaded in bearing.

Extended parameter studies were carried out with these computer codes to assess the general behavior of the stress intensity factor solutions and their sensitivity to crack size, fastener spacing, etc. The results of the parameter studies have been presented in the form of handbook charts which can be used to compute stress intensity factors for specific cases of interest. Solution accuracy was verified, where possible, by comparison with independent analytical solutions. In those cases for which analytical solutions are not yet available, verification was accomplished by tracking the performance of individual finite elements over ranges of distortions in shape and size which covered the ranges used in the computer codes. Also, experience with the

codes during the parameter studies demonstrated that solutions could be obtained for a complete parametric variation of the angular position of a crack with moderate core storage requirements and execution times of the order of one minute. The computer codes are therefore considered to be economically practical analysis tools which give reasonable answers for engineering purposes.

Some limitations of the finite element building blocks and in the general computer codes were encountered in the course of the extended parameter studies. The hybrid crack element appears to give good solutions when the crack-tip location is restricted to a range between 25 and 75 percent of the total distance across the crack element. Other limitations, discussed in detail below, also lead to some ideas for future improvements.

The attachment lug computer code was found to provide well-converged solutions over the range of interest in the ratio of lug width to bearing hole diameter. However, the present code is restricted somewhat in the extent of crack sizes which may be analyzed. This restriction arises only from the way in which the mesh generation scheme was programmed, not from any fundamental difficulty with the analysis method. A routine reprogramming of the mesh generation scheme would permit the study of cracks which approach the outer boundary of the lug.

The solutions obtained from the rectangular panel computer code were found to be uninteresting, in that the presence of stiffeners and/or an offset of the fastener hole had very little effect on the stress intensity factors. The solutions for a centered hole in an unstiffened panel were found to be quite useful in assessing the performance of the special-purpose hybrid elements. However, it has been concluded that too much is demanded of a mesh generation scheme which attempts to model a crack at a fastener hole together with the crack tip closely approaching a stiffener or an unstiffened free edge. These latter cases appear

to be of much greater interest, and future work in this area should concentrate on a small subregion of the panel, with the crack location restricted to little or no angular variation about the perpendicular to the applied loading. Also, the use of a bi-material crack element should be considered for crack tips which lie close to stiffeners. An element of this type has already been developed in another related program of research.

The performance of the special-purpose fastener hole element was tested extensively. It was found to give accurate answers down to a lower limit of 1.27 in the ratio of its outer edge dimension to its inner diameter. With four rings of conventional quadrilaterals and the crack element placed inside to model the material immediately around the fastener hole, this results in a lower limit of 3.2 in the ratio of fastener spacing to fastener diameter. The special element performance tests also indicated that the spacing ratio could be pushed down to 3.0, probably with some loss in solution accuracy. The primary impact of these limits occurs in the fastener row computer codes, which are intended to analyze chordwise wing skin splices.

While a spacing ratio of 3.0 to 3.2 is probably adequate for many cases, very highly stressed splices such as are found in the wing roots of the Boeing 747 and Lockheed C-5A are designed with smaller spacing ratios and cannot be analyzed with the computer codes in their present forms. An improvement of the codes in this respect would appear to be desirable, since highly stressed chordwise splices are likely to continue to be of great interest in future considerations of airframe structural integrity. The most straightforward way to gain this improvement would be to reduce the number of quadrilateral rings in the interior mesh from four to two (at least two rings are required to accommodate the crack element). If the approach which was adopted for proportioning the interior mesh is not changed, the reduction from four to two rings would lead to a capability to analyze details

with fastener spacing ratios as small as 1.7 to 1.8, without requiring any modifications to the special-purpose hole element. However, a new series of verification tests using the rectangular panel program should be conducted if this approach is adopted. Also, it should be noted that a trade-off in capabilities would result. With the present four-ring interior mesh, it is possible to analyze cracks as long as the fastener hole radius; if the interior mesh were reduced to two rings, the maximum crack length would be reduced to about 30 percent of the fastener hole radius if no other modifications were made in the existing codes.

Finally, some remarks are in order regarding the uses to which the solutions presented in this report may be put. The application of fracture mechanics to airframe damage tolerance analysis follows two main avenues: the prediction of failure loads based on comparisons of stress intensity factors with material fracture toughness properties and the prediction a crack sizes as functions of time during stable crack propagation under fatigue loading. In both cases, the stress intensity factor solutions of linear elastic fracture mechanics are associated with an implicit assumption that the next increment of stable or unstable crack propagation will occur tangent to the orientation of the crack at its tip. However, crack propagation experiments have shown that fatigue cracks tend to follow curved paths in regions where they are subjected simultaneously to mode I and mode II stress intensities, the curvature continuing until the crack is advancing in a direction perpendicular to a principal tensile stress. Therefore, some caution should be exercised in applying the results presented in this report to fatigue crack growth analysis. It so happens that for most of the cases considered, the worst or nearly worst situation of mode I stress intensity coincides with negligible mode II stress intensity. Hence, cracks which are assumed to begin in these angular positions may also be safely assumed to propagate in

straight lines, and crack growth calculations can be conducted. However, it is not valid to use the stress intensity solutions by taking values for a series of cracks of increasing length and varying angular position in an attempt to trace the tip of a crack which propagates along a curved path. The restriction on use of the solutions for failure load prediction is somewhat less severe, since interaction formulas may be used for straight initial cracks which occupy angular positions such that both mode I and mode II stress intensities are present.

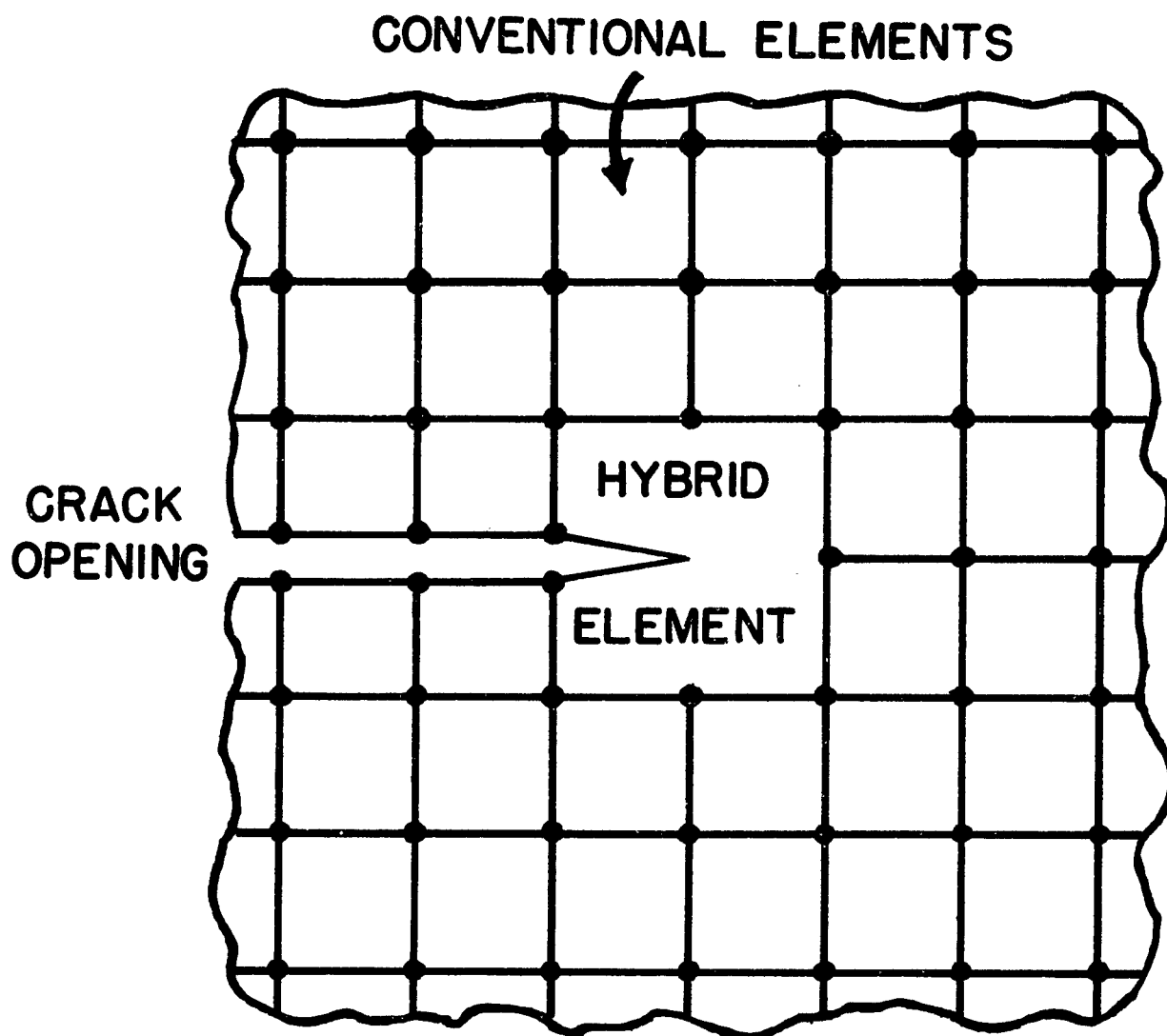
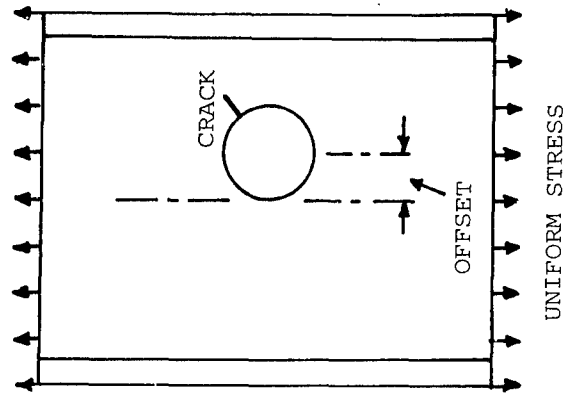
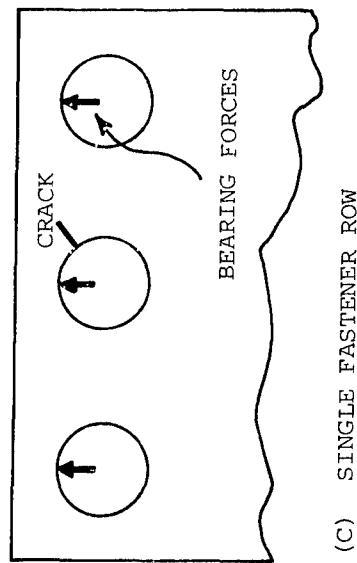


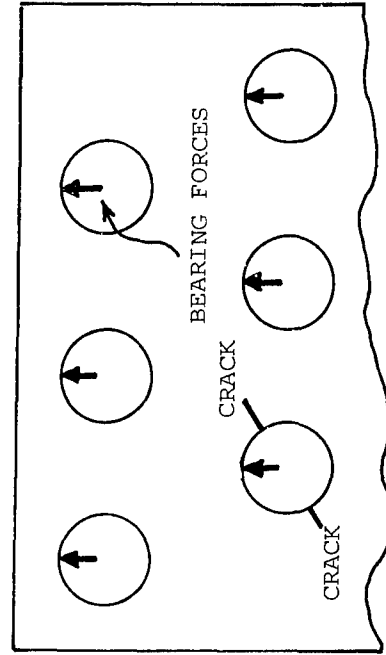
Figure 1. Portion of Finite Element Model Surrounding a Crack Tip



(B) RECTANGULAR PANEL



(C) SINGLE FASTENER ROW



(D) DOUBLE FASTENER ROW

Figure 2. Structural Details Selected for Analysis

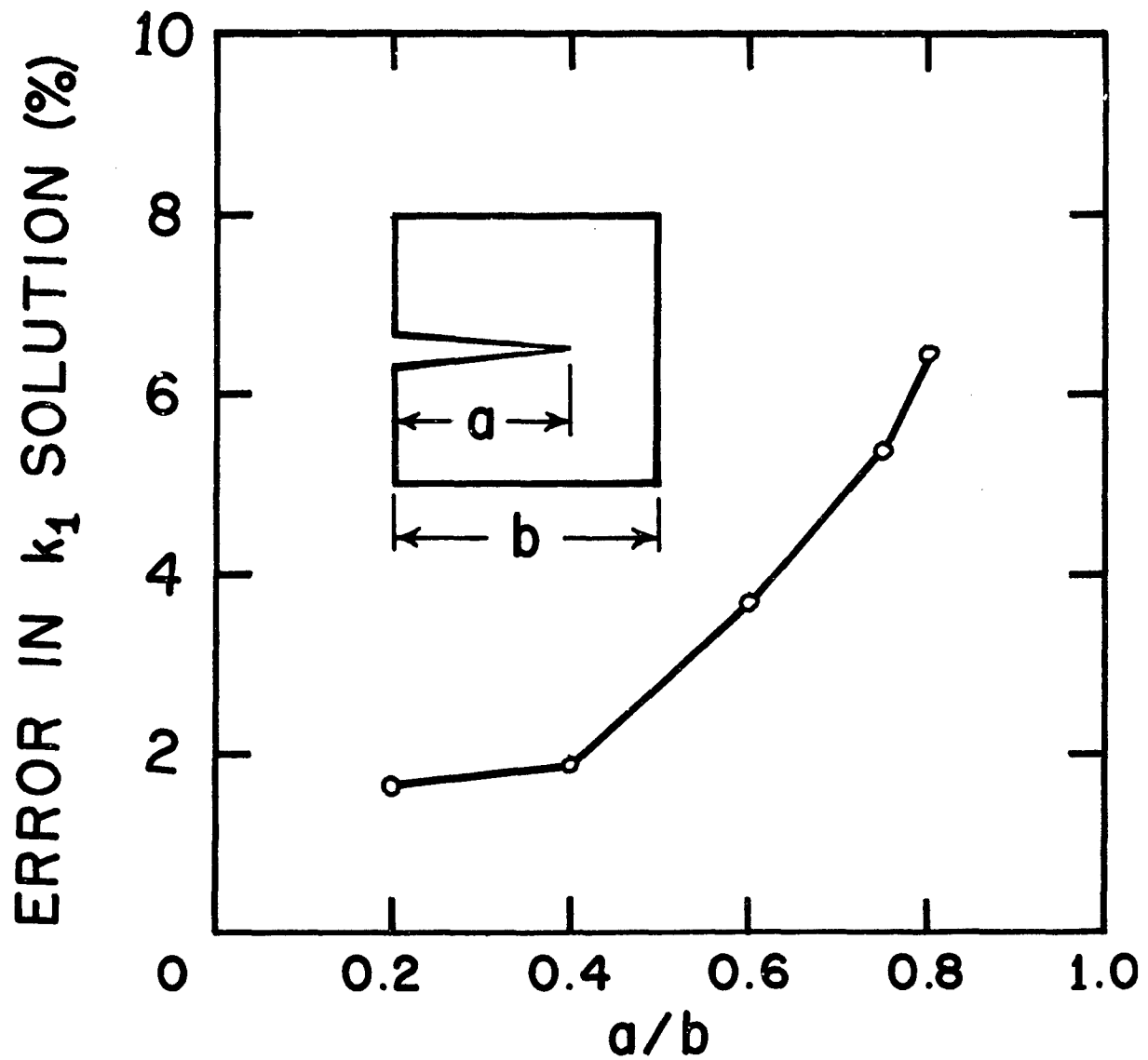


Figure 3. Error in Computed Stress Intensity Factor as a Function of Crack-Tip Position

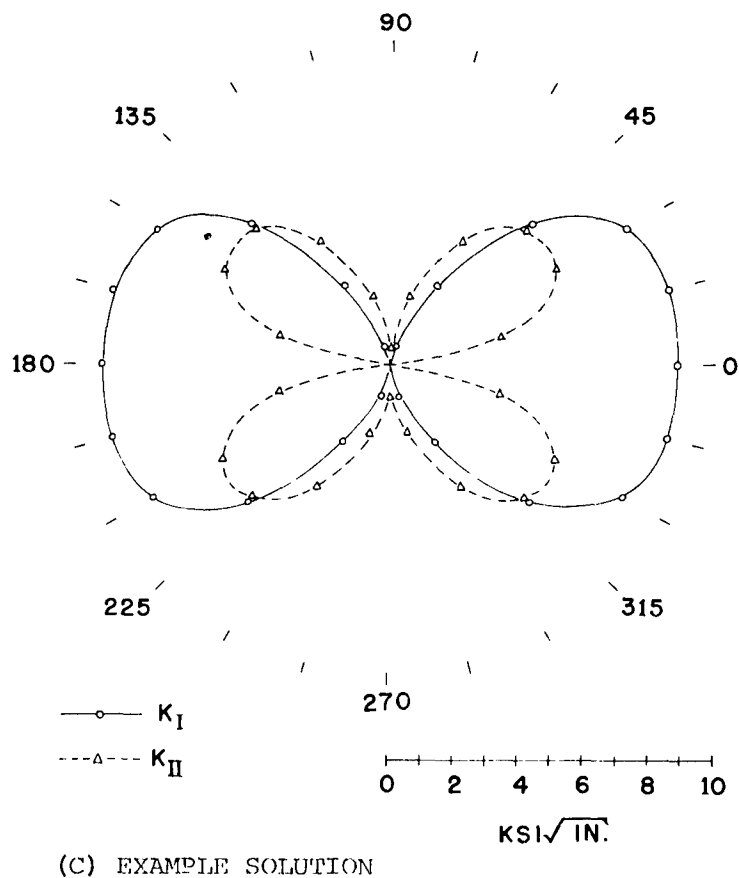
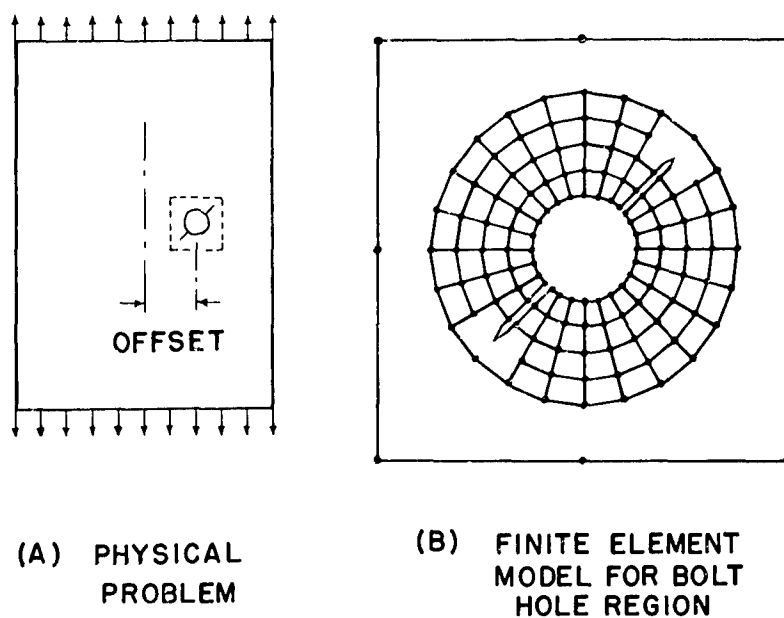


Figure 4. Mesh Construction and Example Solution for Rectangular Panel

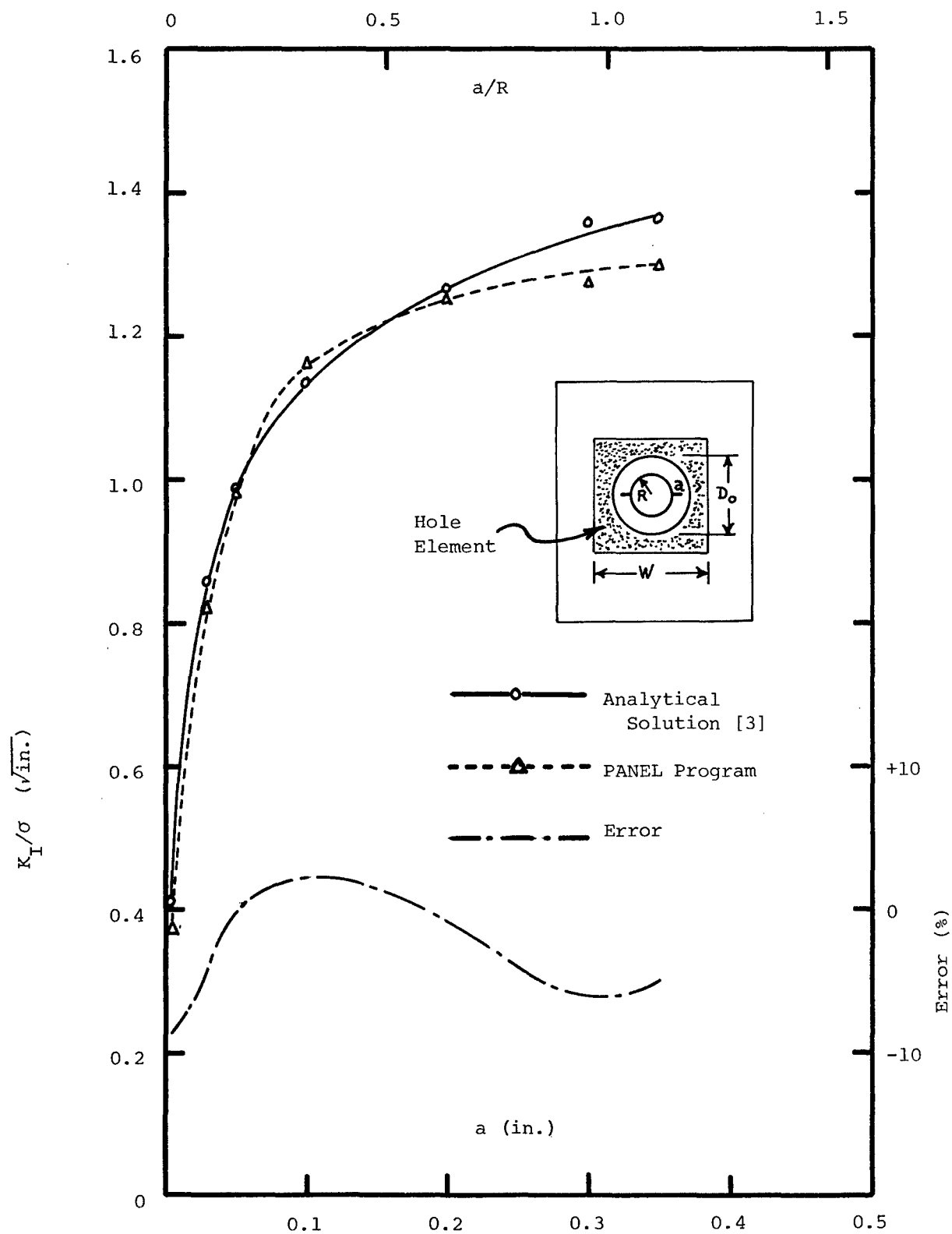


Figure 5. Variation of K_I Solution Accuracy with Crack Size (Hole Element Shape W/D_o Fixed)

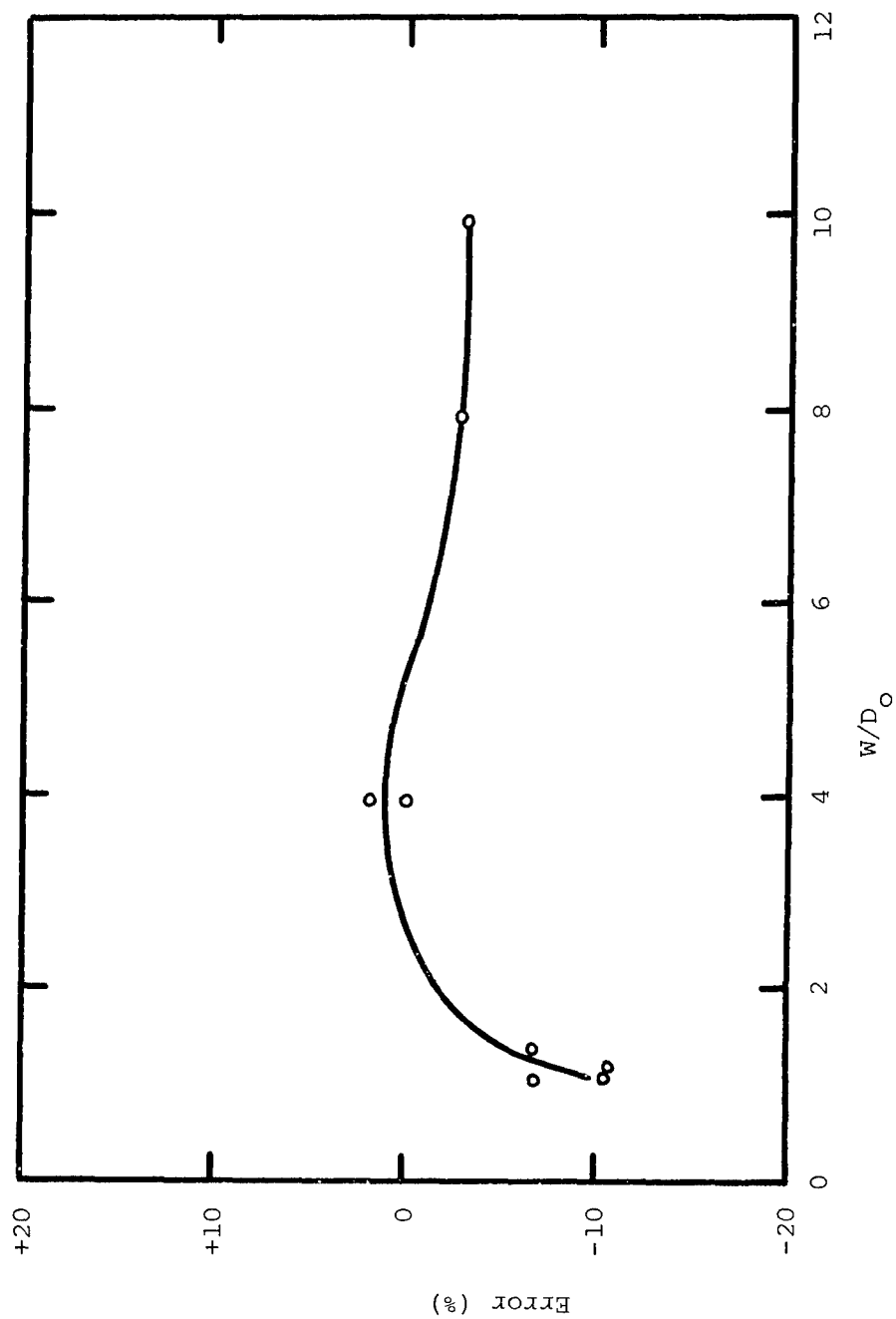


Figure 6. Variation of K_I Solution Accuracy with Hole Element Shape

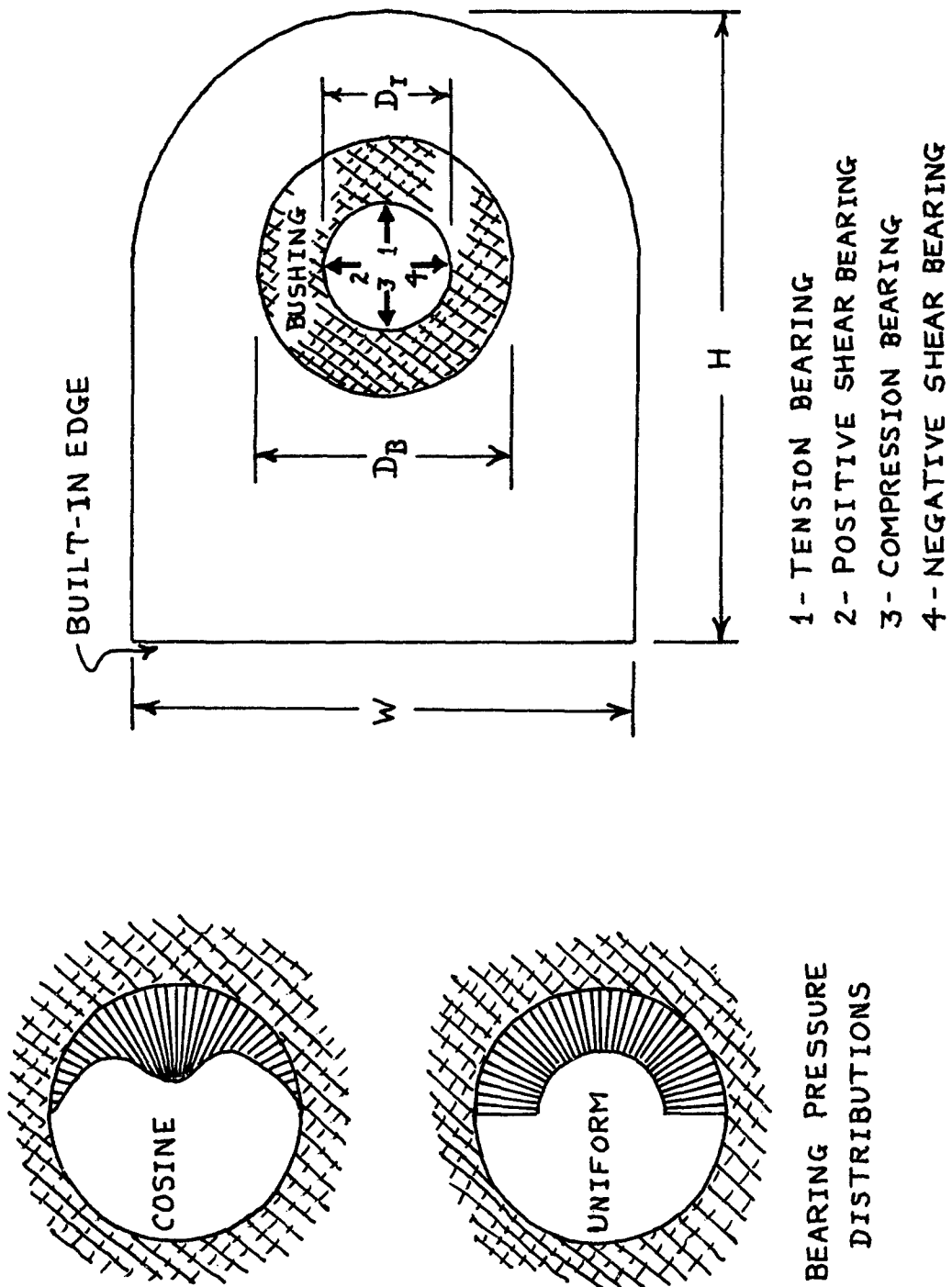
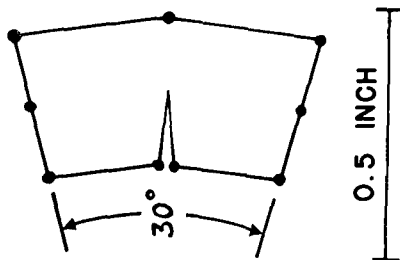
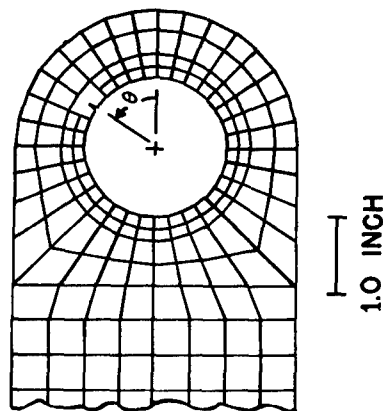


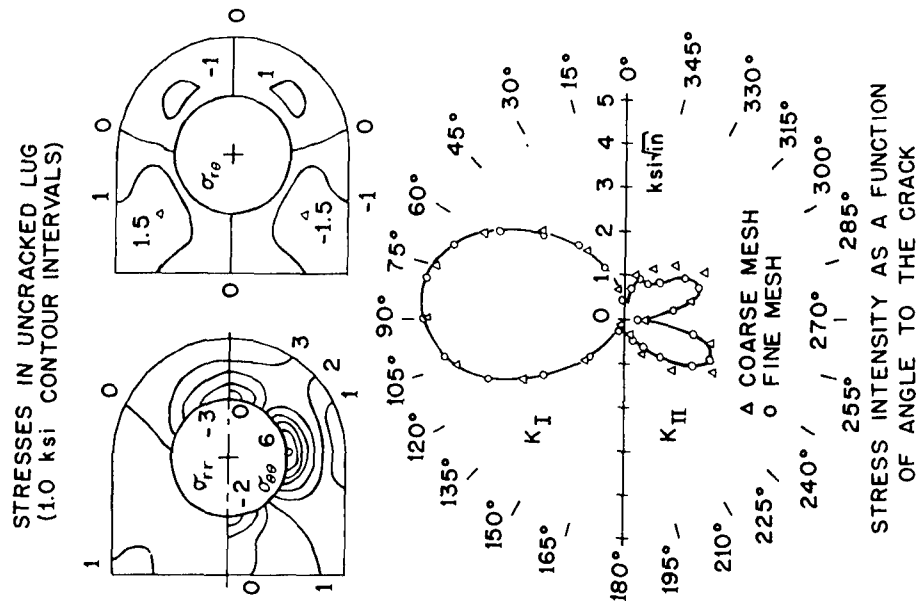
Figure 7. Attachment Lug Program Capabilities



(a) MAXIMUM ELEMENT DISTORTION
(24 DIVISIONS AROUND HOLE)



(b) LUG MODEL WITH 32 DIVISIONS
AROUND HOLE



(c) EXAMPLE RESULTS (TENSION BEARING)

Figure 8. Attachment Lug Mesh Details and Example Results

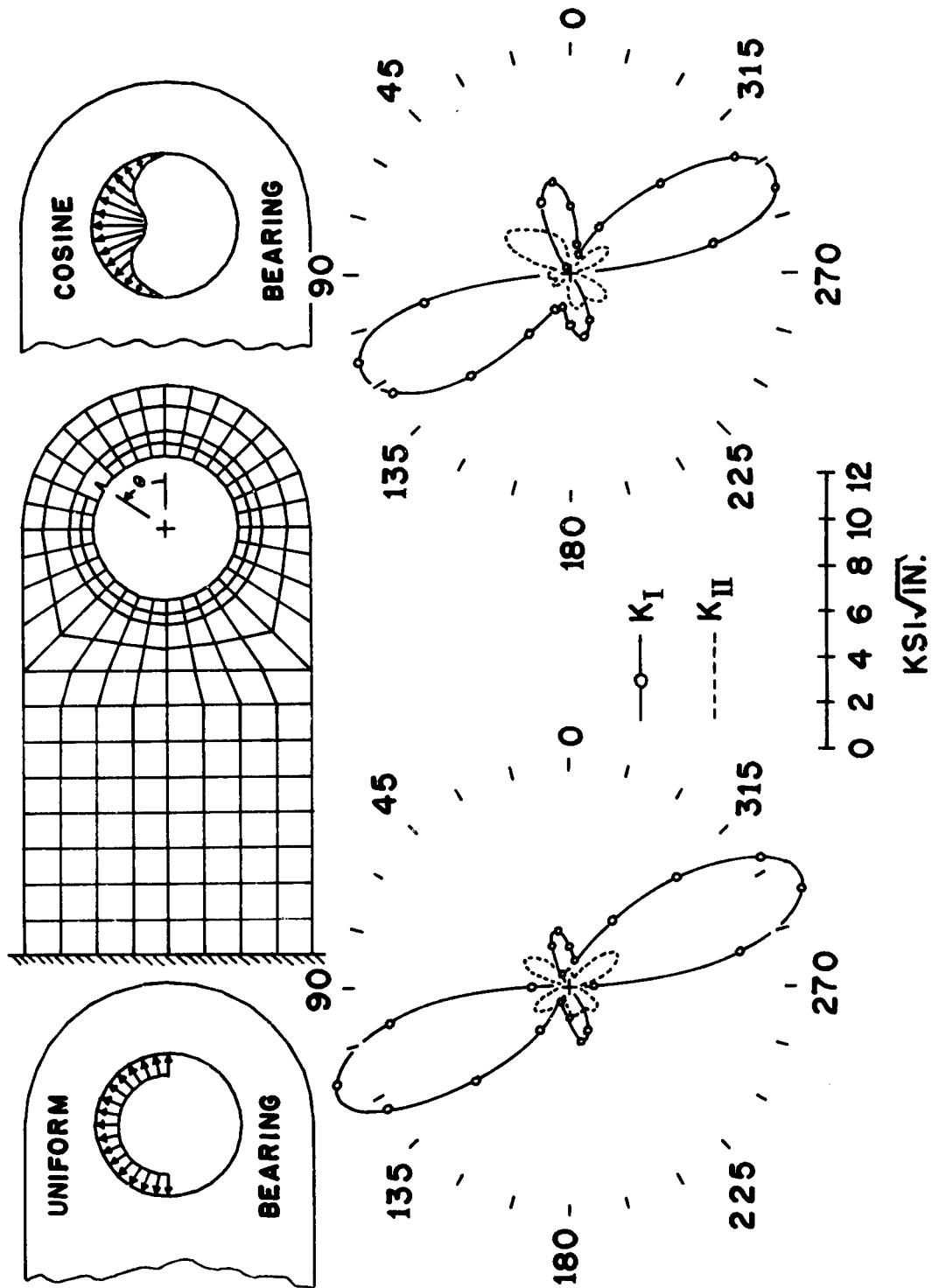


Figure 9. Example Results for Shear Bearing

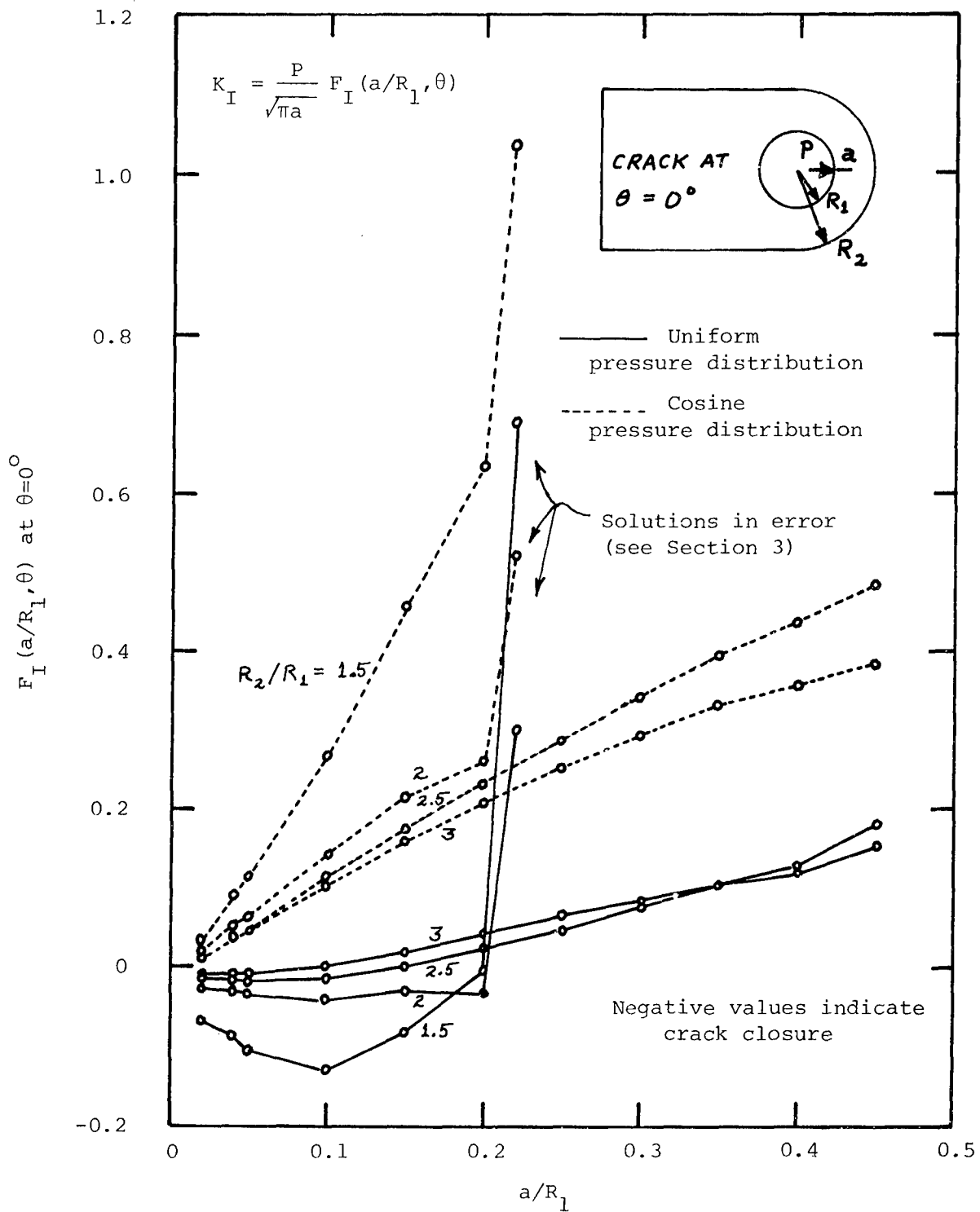


Figure 10. Sensitivity of K_I to a/R_1 and R_2/R_1 for a Crack at $\theta=0^\circ$

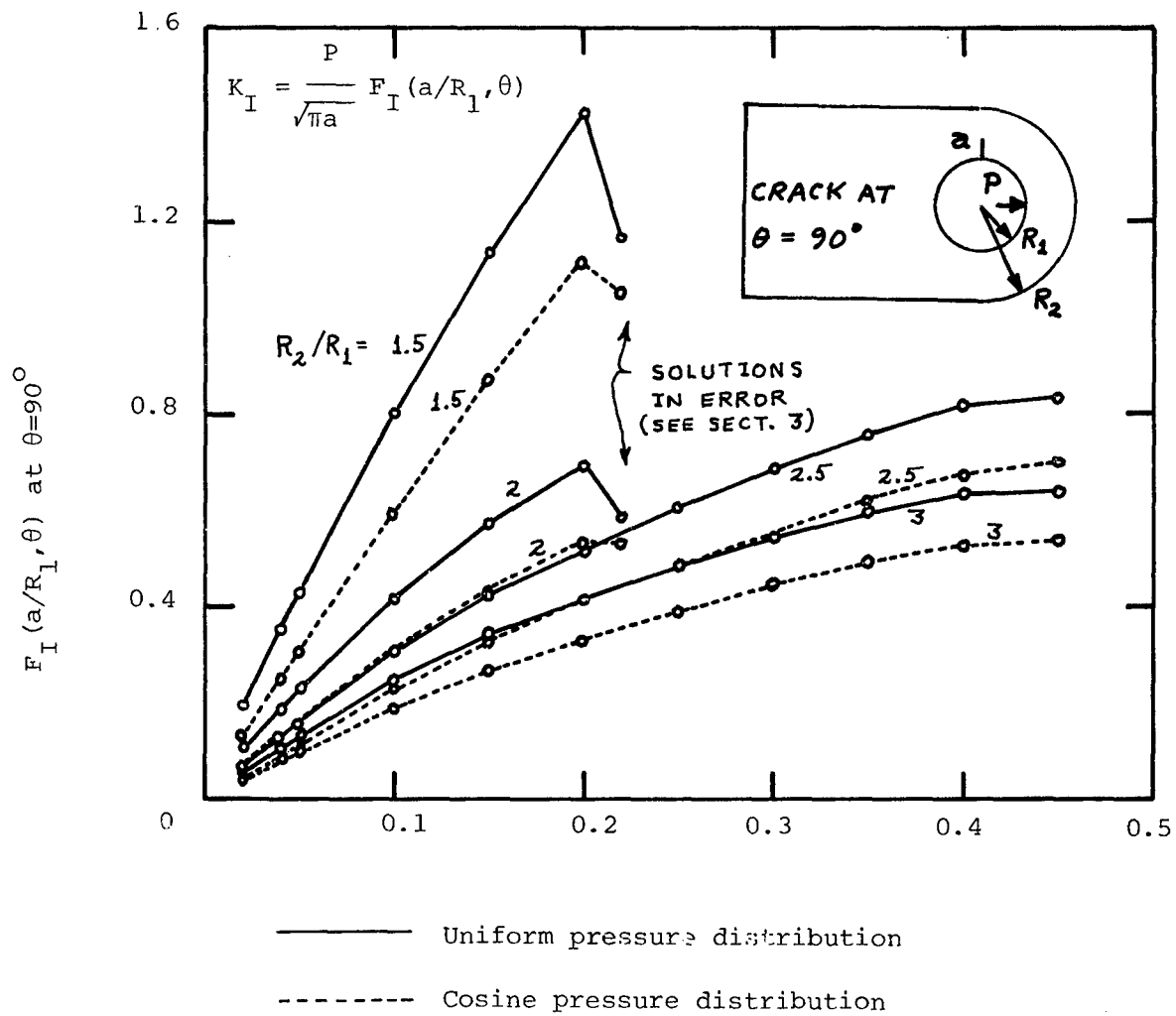


Figure 11. Sensitivity of K_I to a/R_1 and R_2/R_1 for a Crack at $\theta=90^\circ$

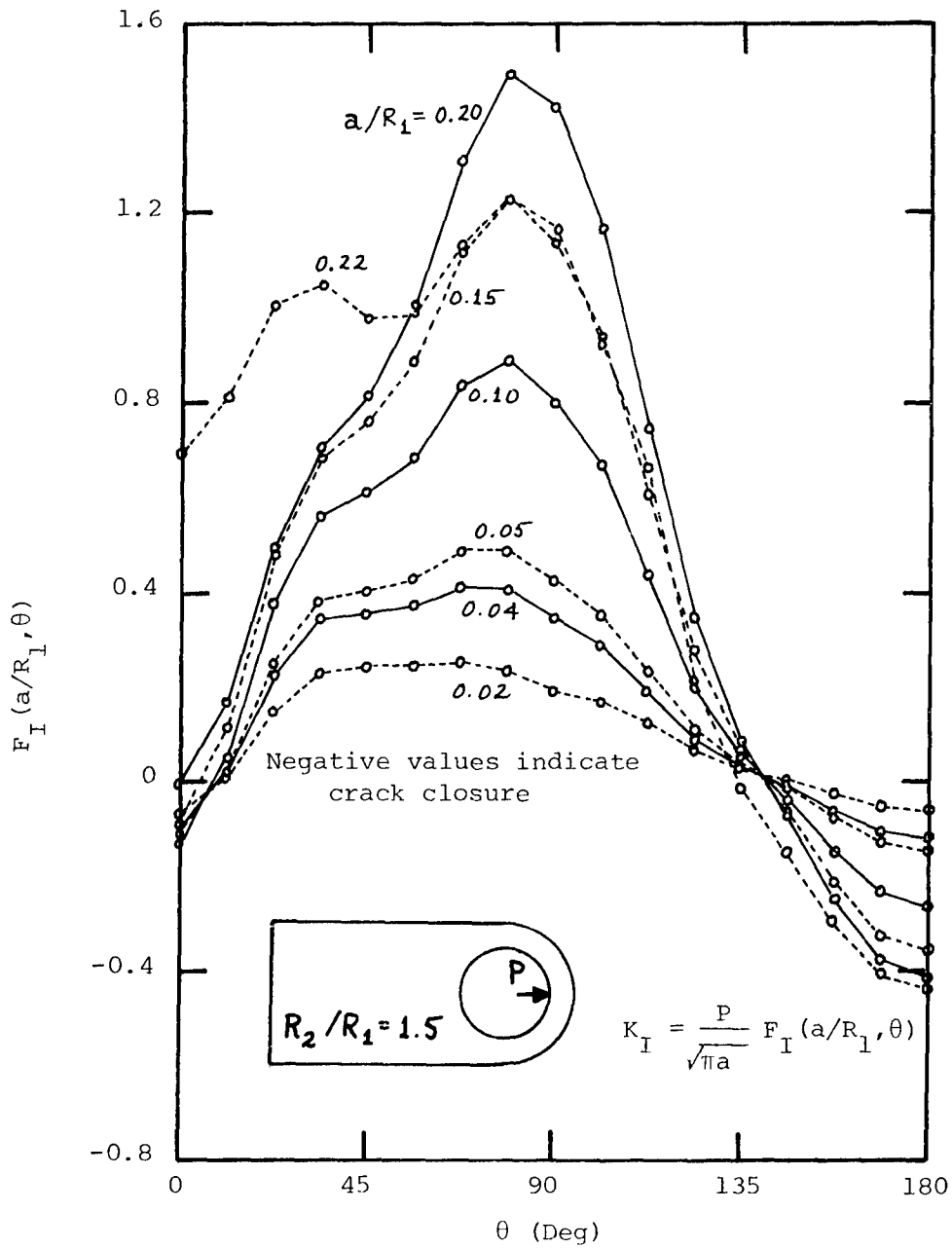


Figure 12. Attachment Lug K_I Chart ($R_2/R_1=1.5$, Uniform Bearing)

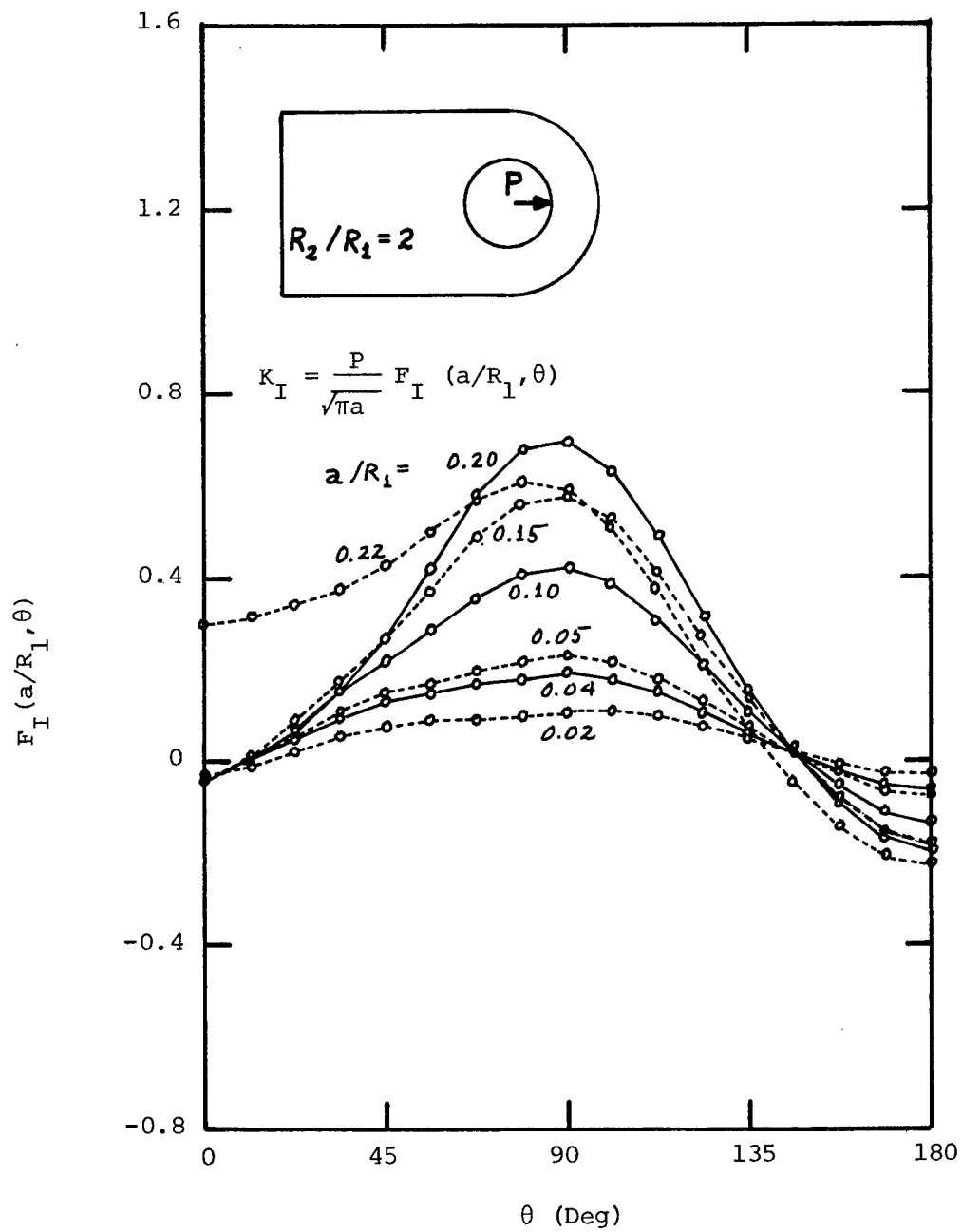


Figure 13. Attachment Lug K_I Chart ($R_2/R_1=2$, Uniform Bearing)

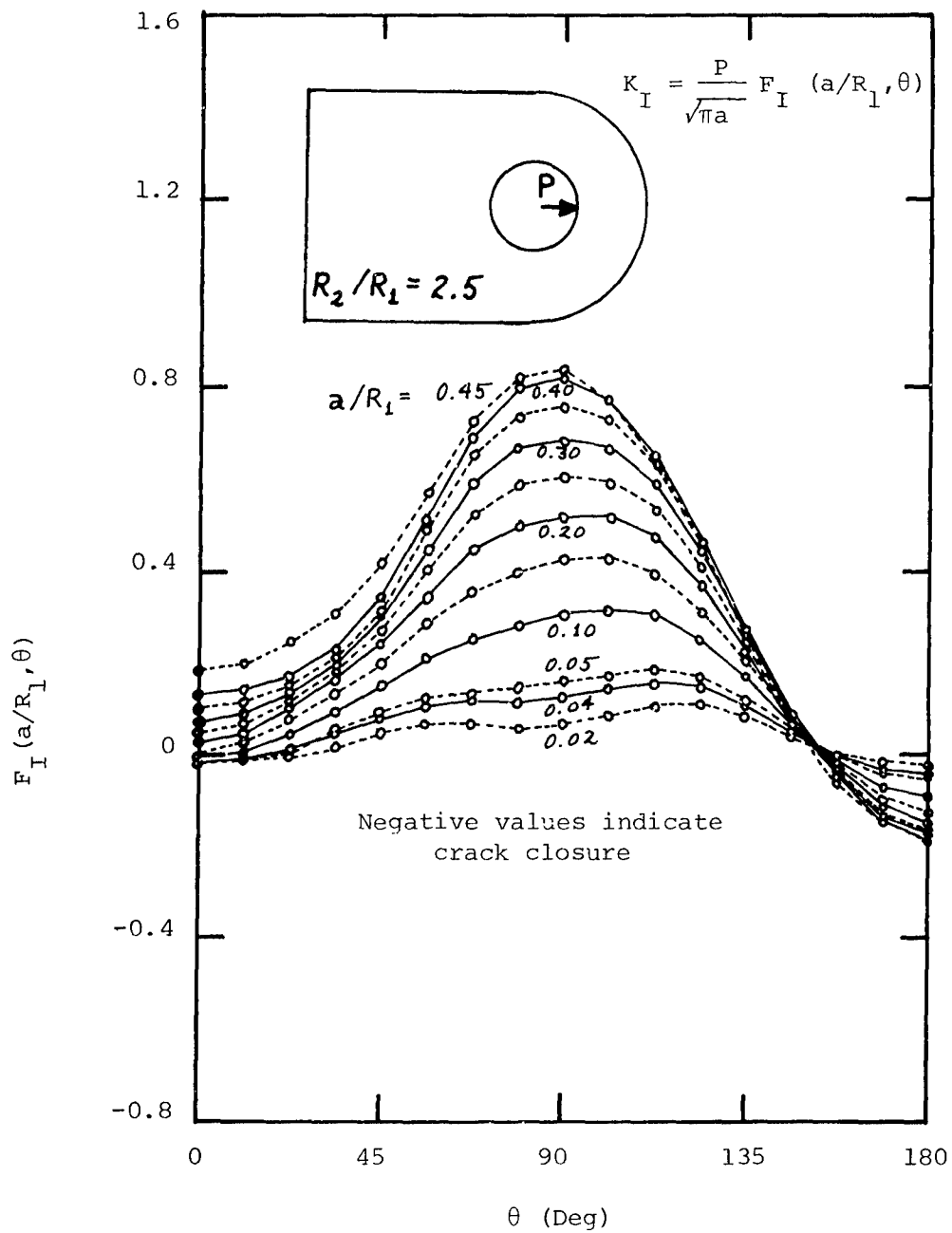


Figure 14. Attachment Lug K_I Chart ($R_2/R_1=2.5$, Uniform Bearing)

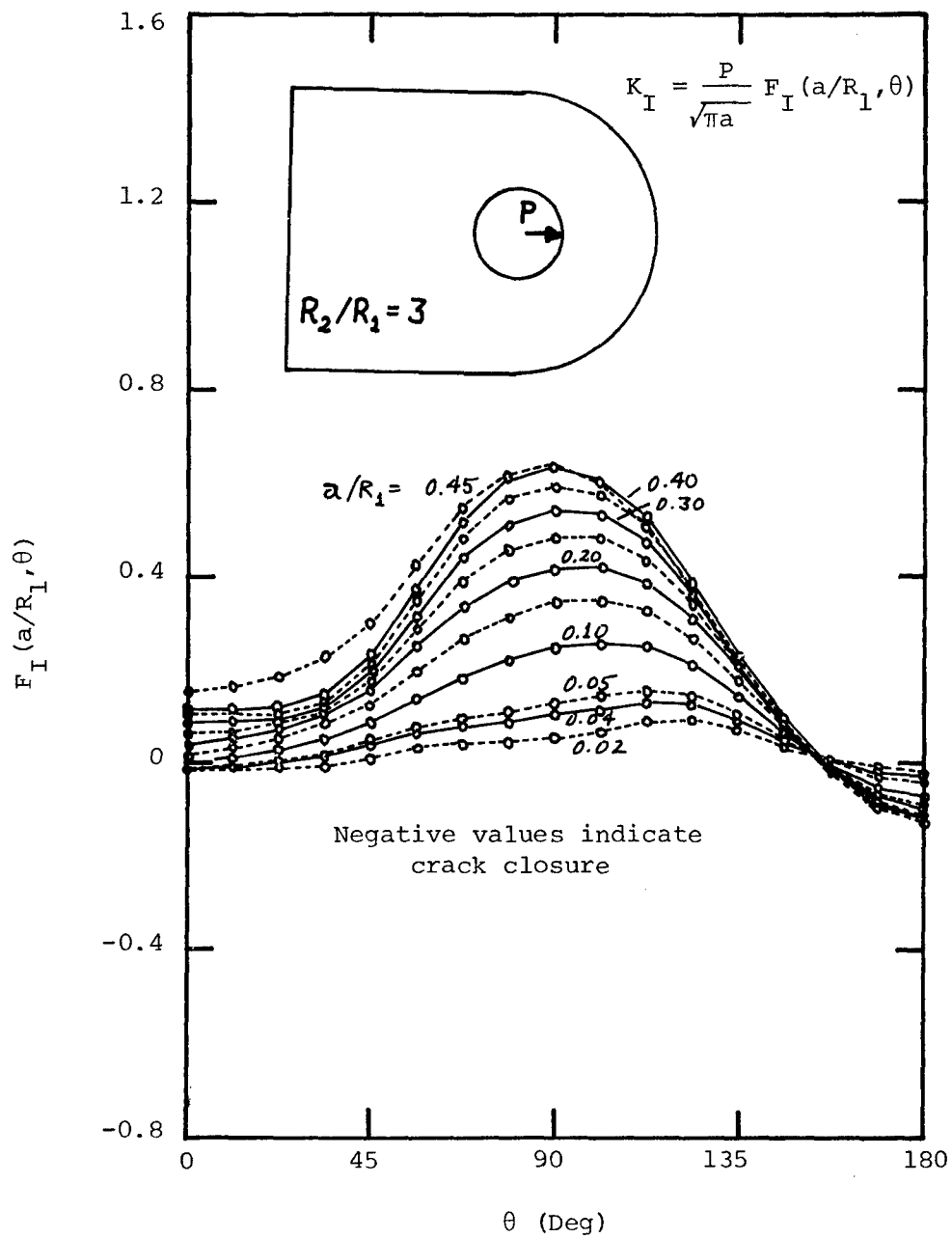


Figure 15. Attachment Lug K_I Chart ($R_2/R_1=3$, Uniform Bearing)

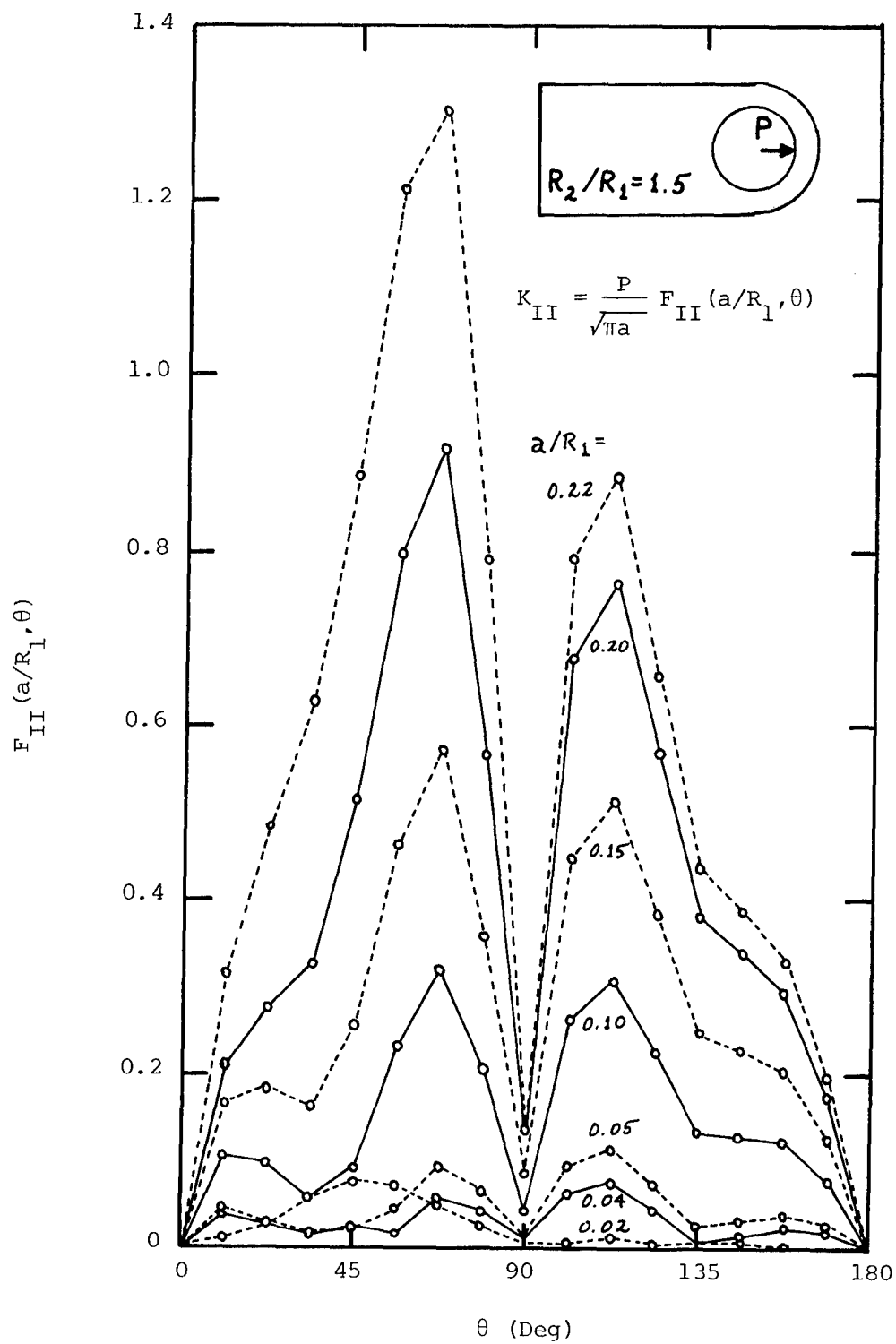


Figure 16. Attachment Lug K_{II} Chart ($R_2/R_1=1.5$, Uniform Bearing)

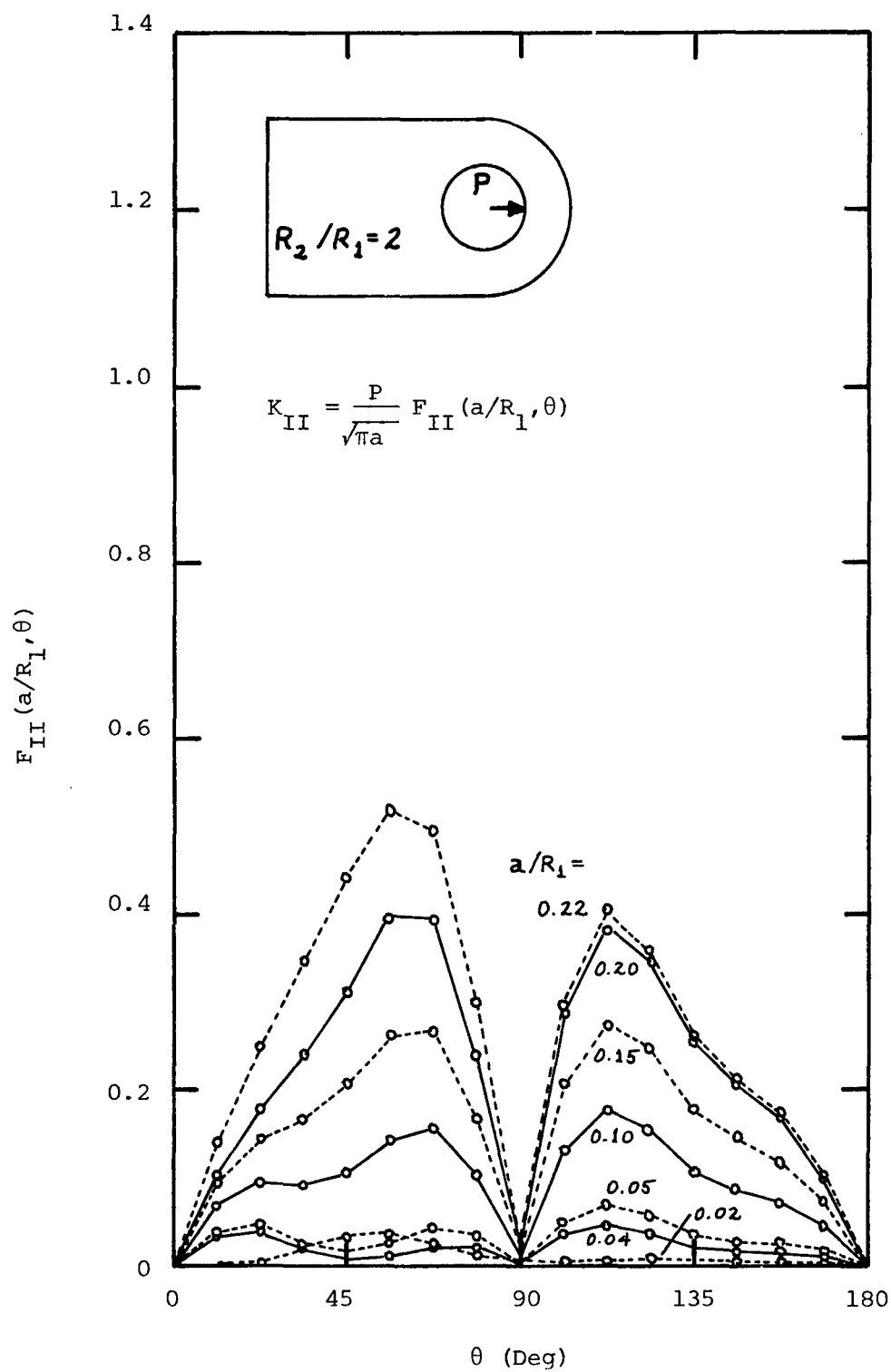


Figure 17. Attachment Lug K_{II} Chart ($R_2/R_1=2$, Uniform Bearing)

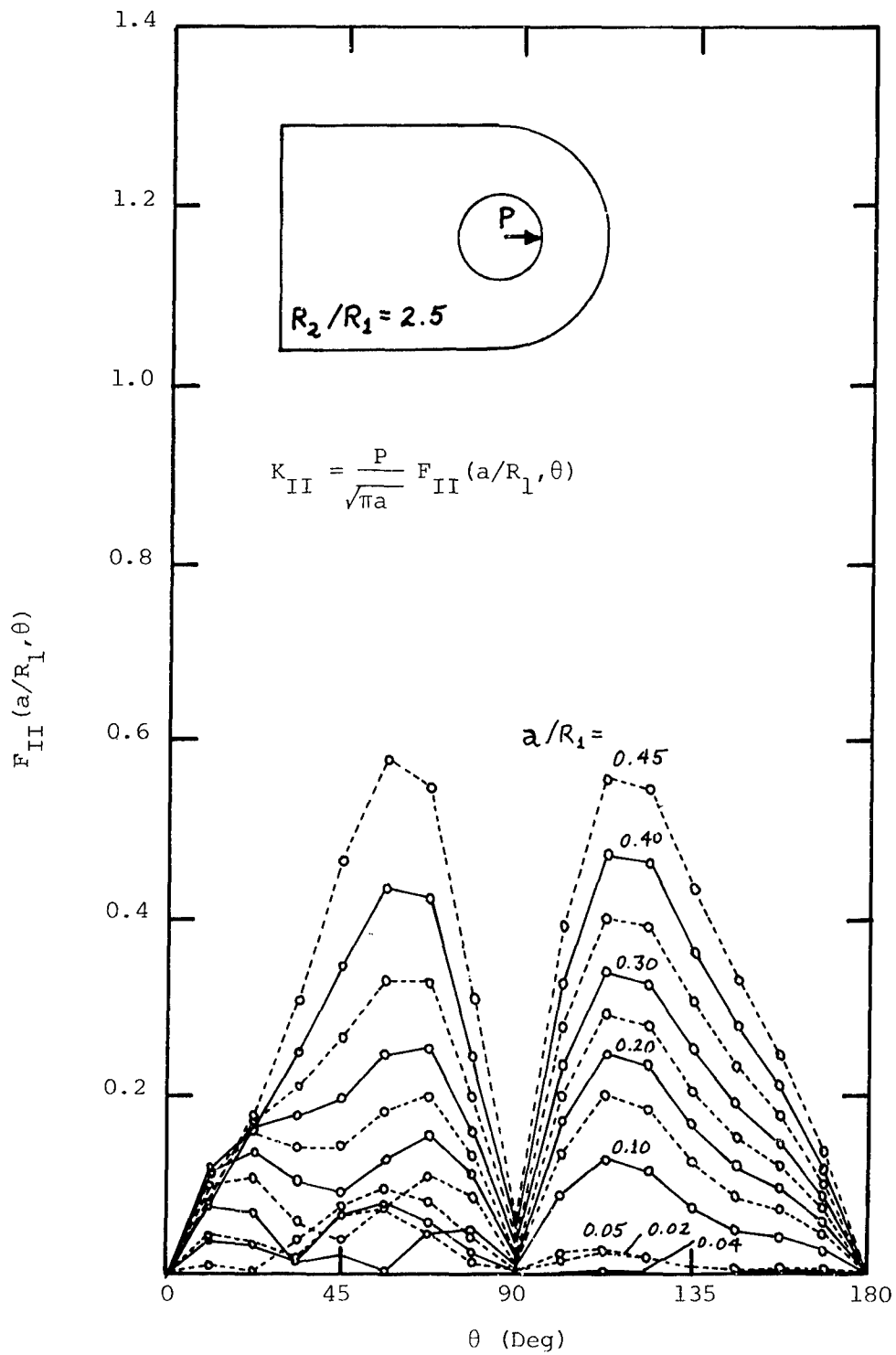


Figure 18. Attachment Lug K_{II} Chart ($R_2/R_1=2.5$, Uniform Bearing)

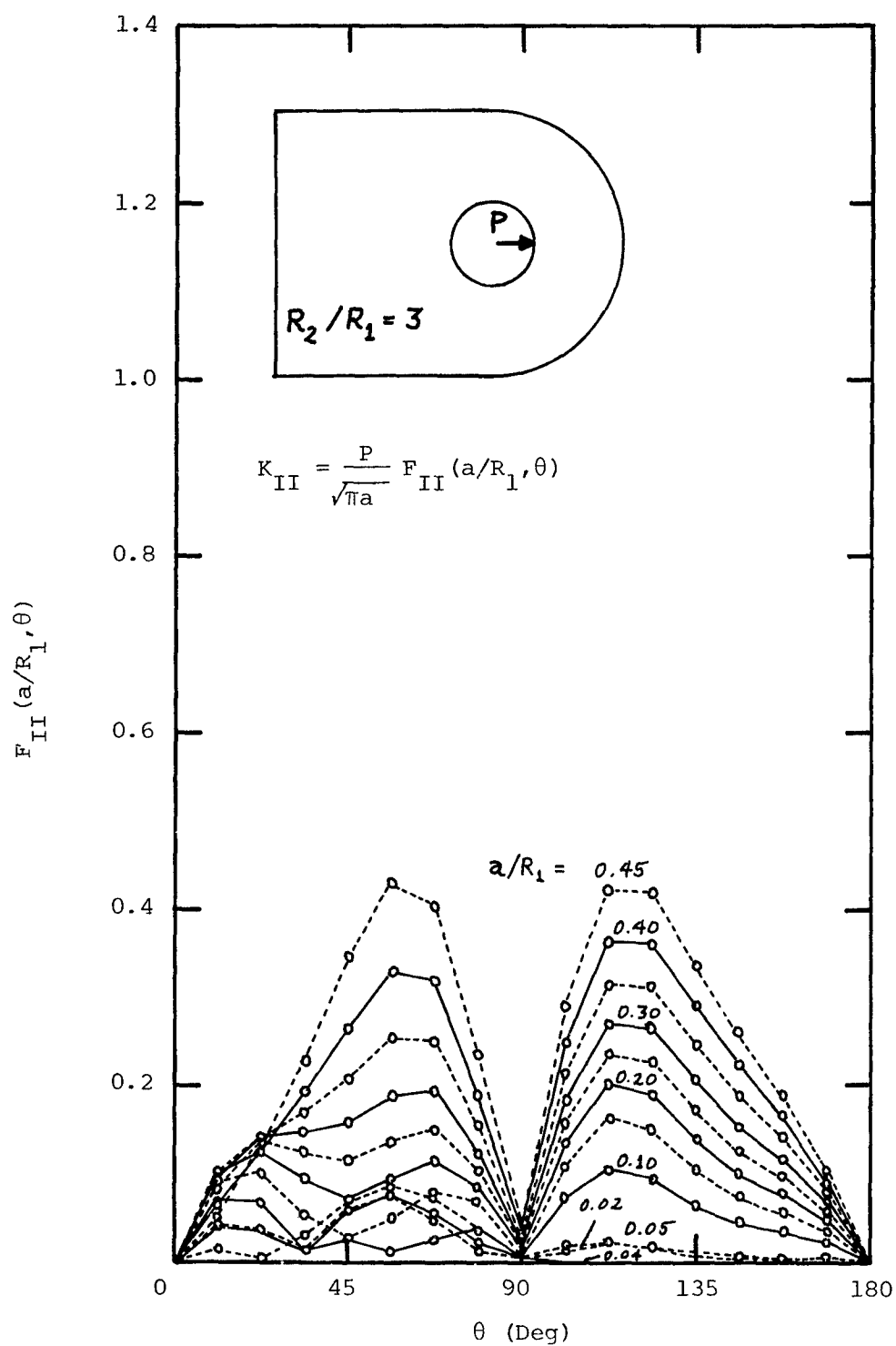


Figure 19. Attachment Lug K_{II} Chart ($R_2/R_1=3$, Uniform Bearing)

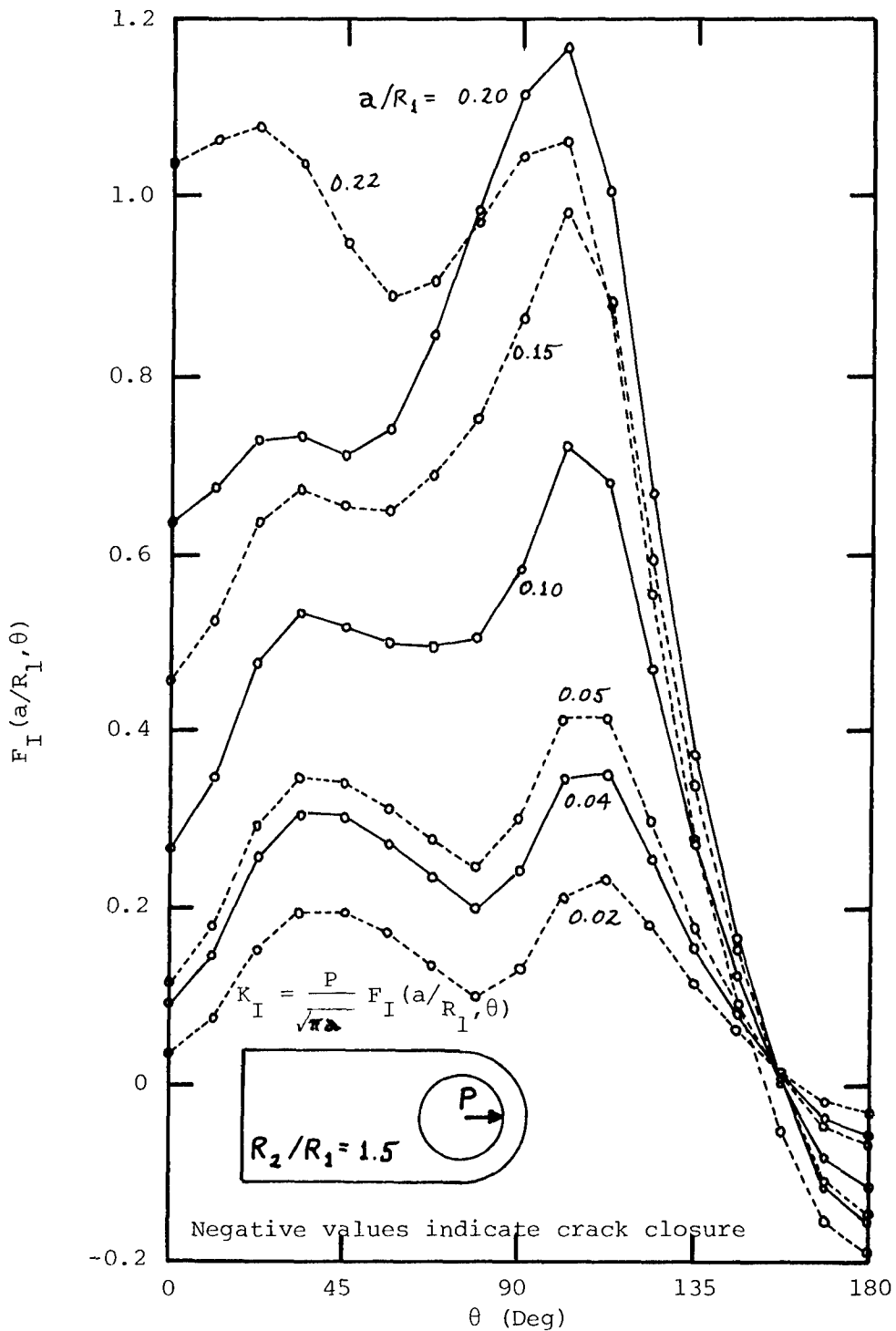


Figure 20. Attachment Lug K_I Chart ($R_2/R_1=1.5$, Cosine Bearing)

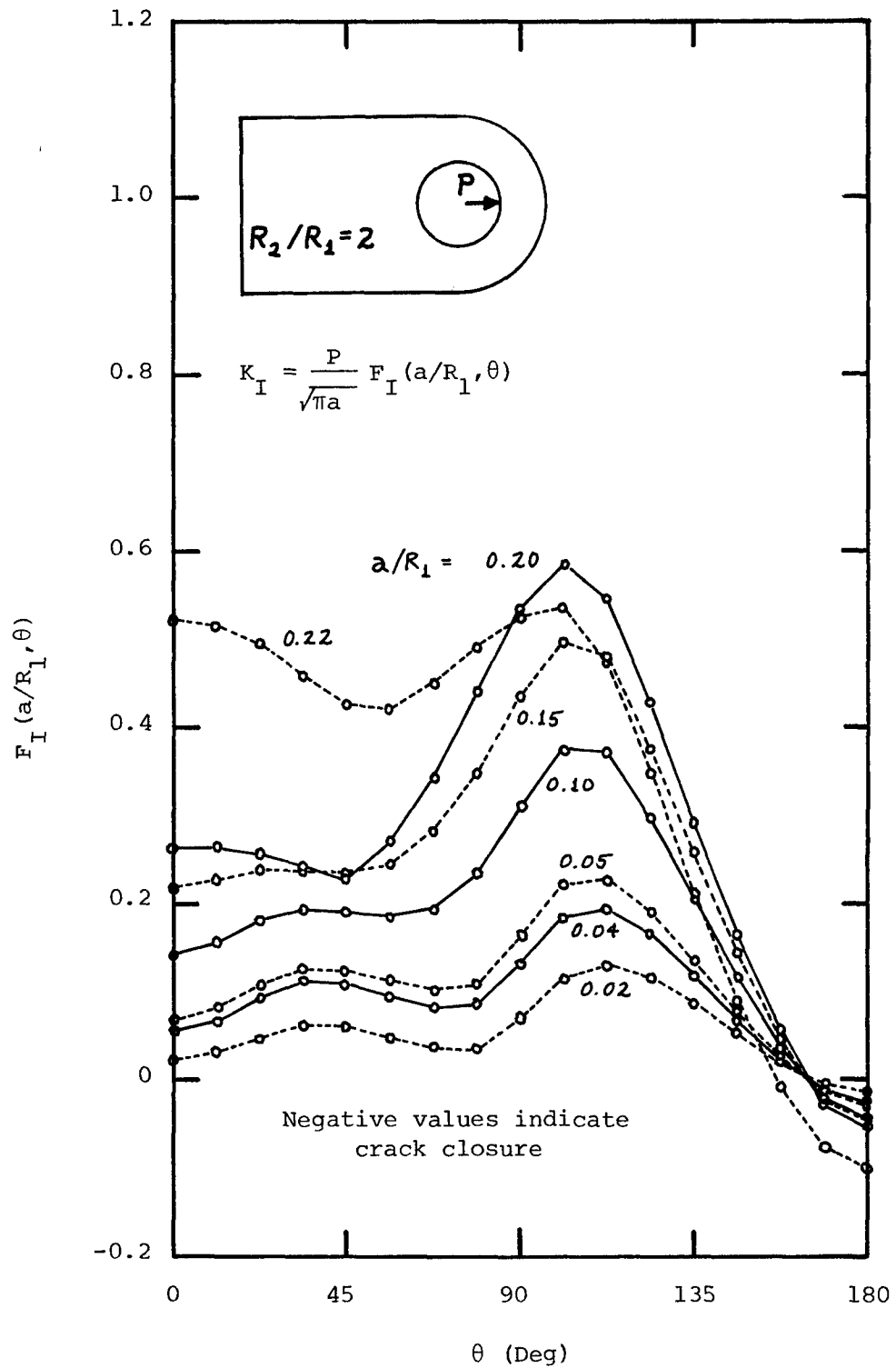


Figure 21. Attachment Lug K_I Chart ($R_2/R_1=2$, Cosine Bearing)

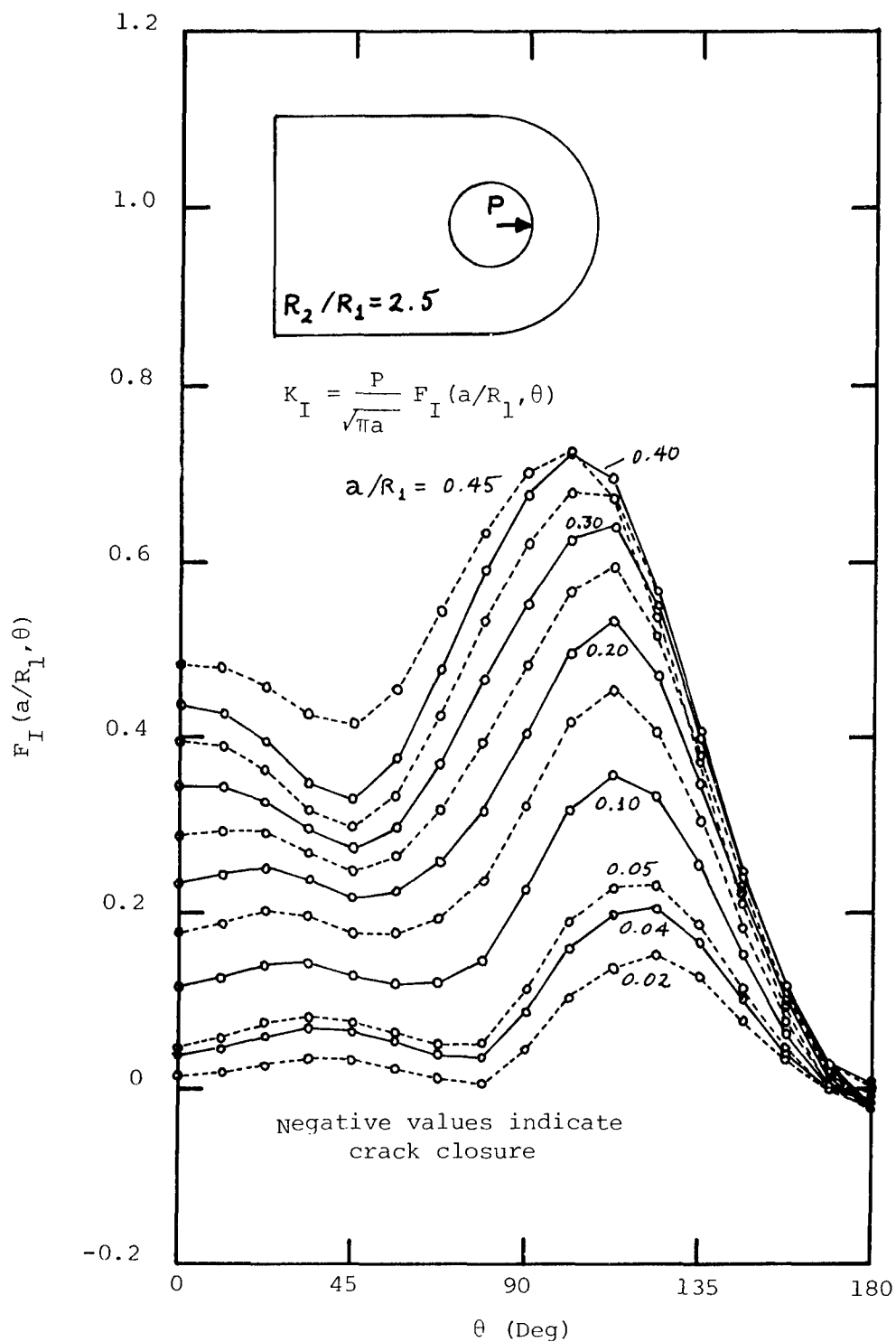


Figure 22. Attachment Lug K_I Chart ($R_2/R_1=2.5$, Cosine Bearing)

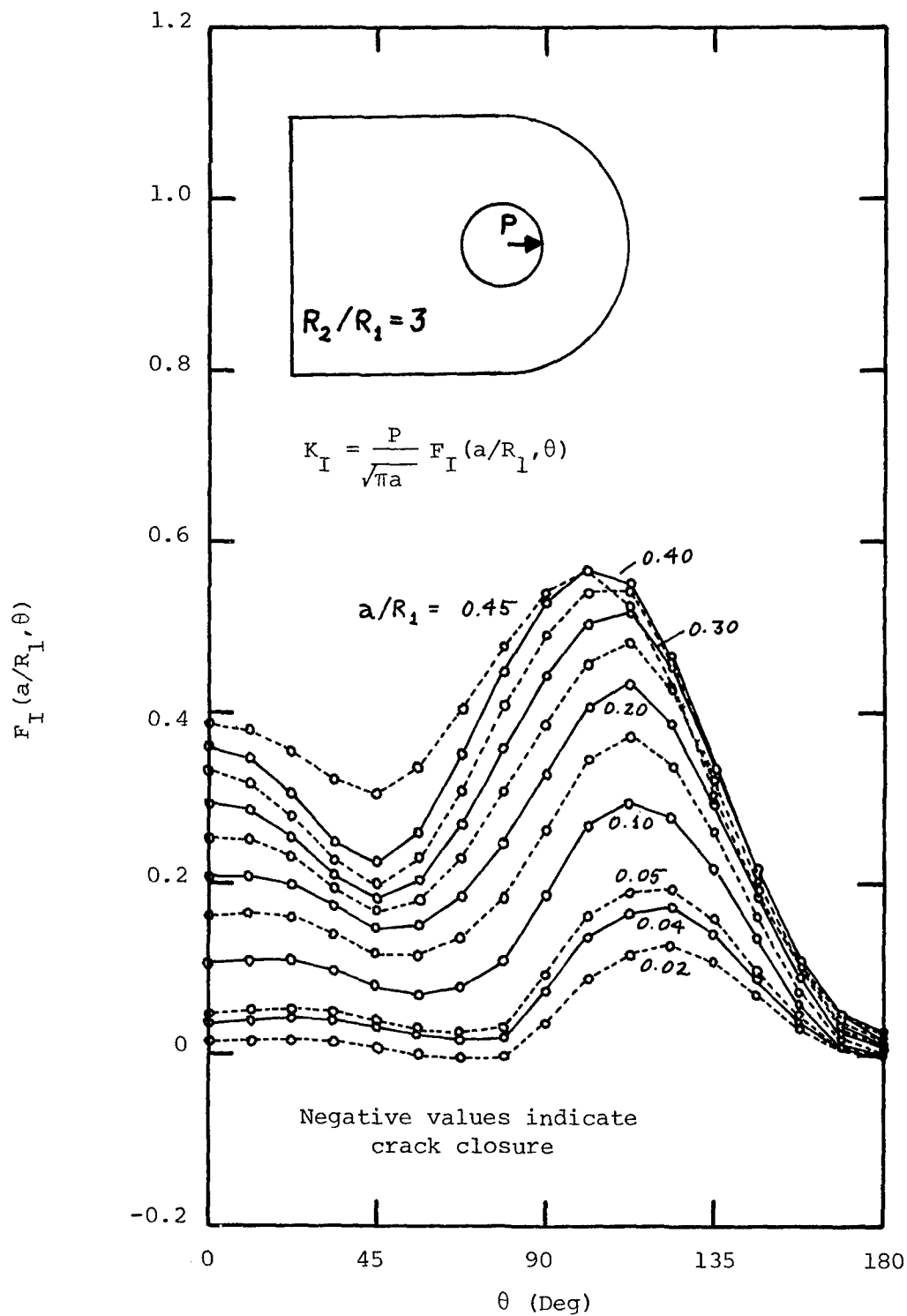


Figure 23. Attachment Lug K_I Chart ($R_2/R_1=3$, Cosine Bearing)

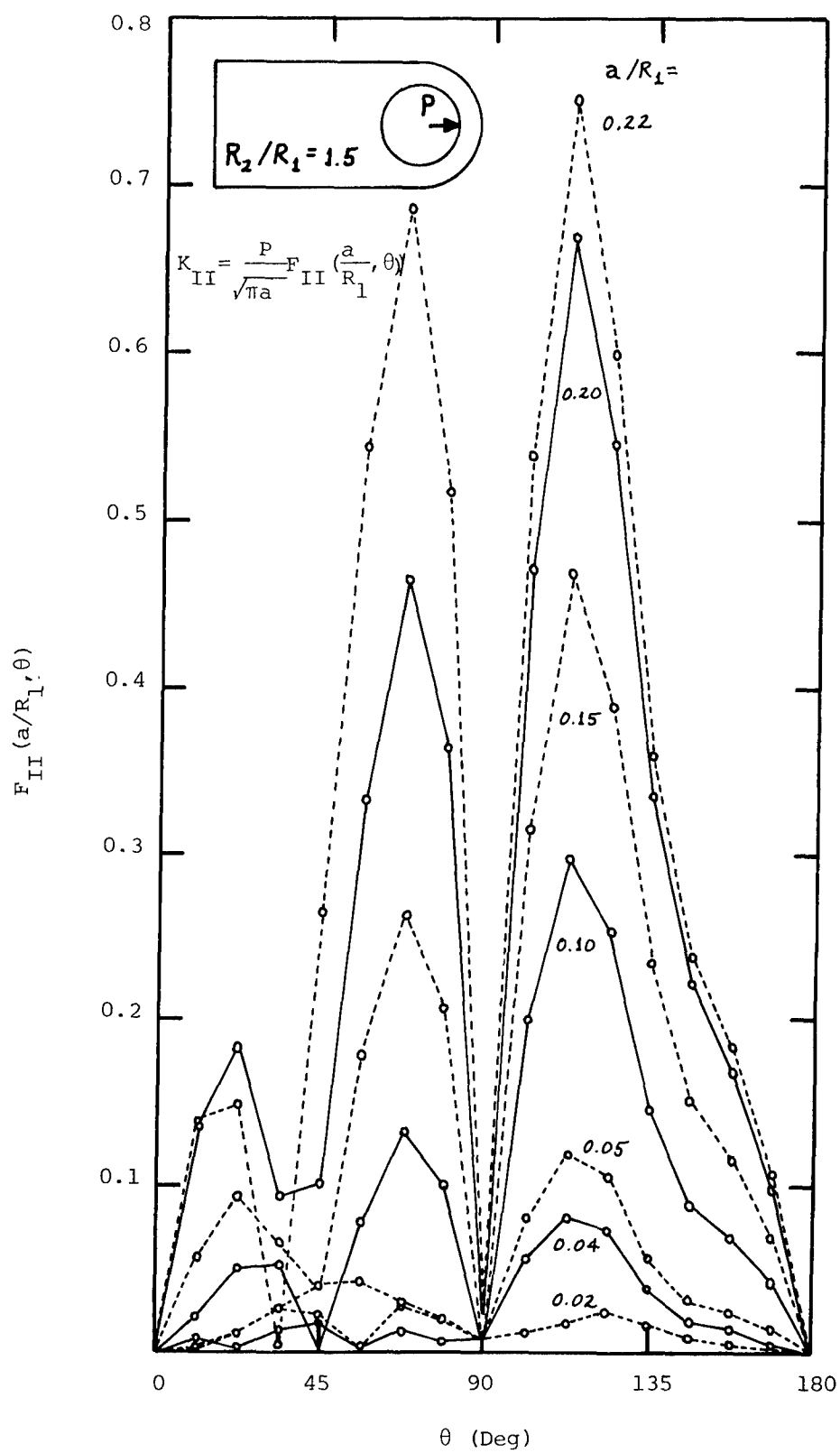


Figure 24. Attachment Lug K_{II} Chart ($R_2/R_1=1.5$, Cosine Bearing)

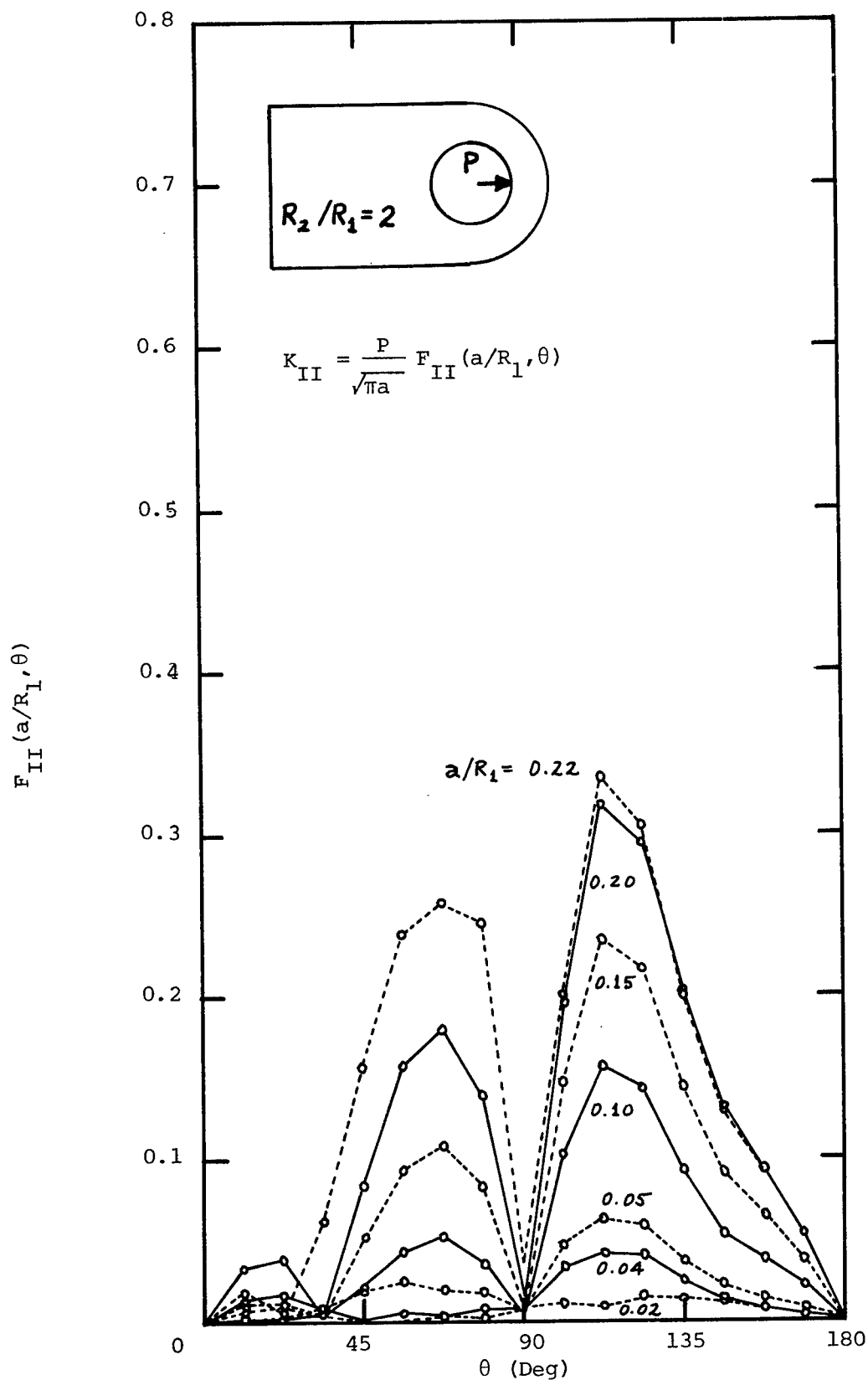


Figure 25. Attachment Lug K_{II} Chart ($R_2/R_1=2$, Cosine Bearing)

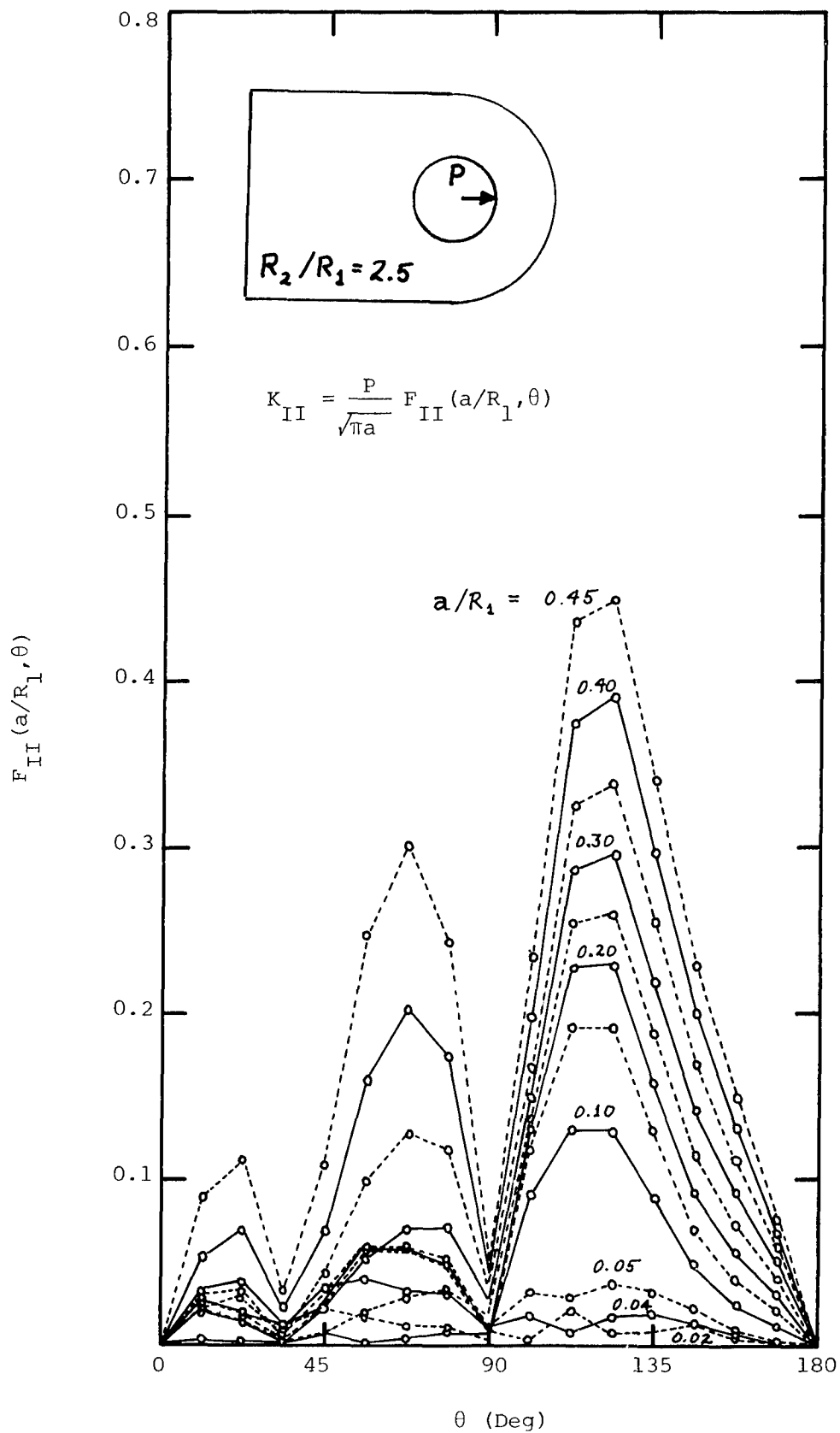


Figure 26. Attachment Lug K_{II} Chart ($R_2/R_1=2.5$, Cosine Bearing)

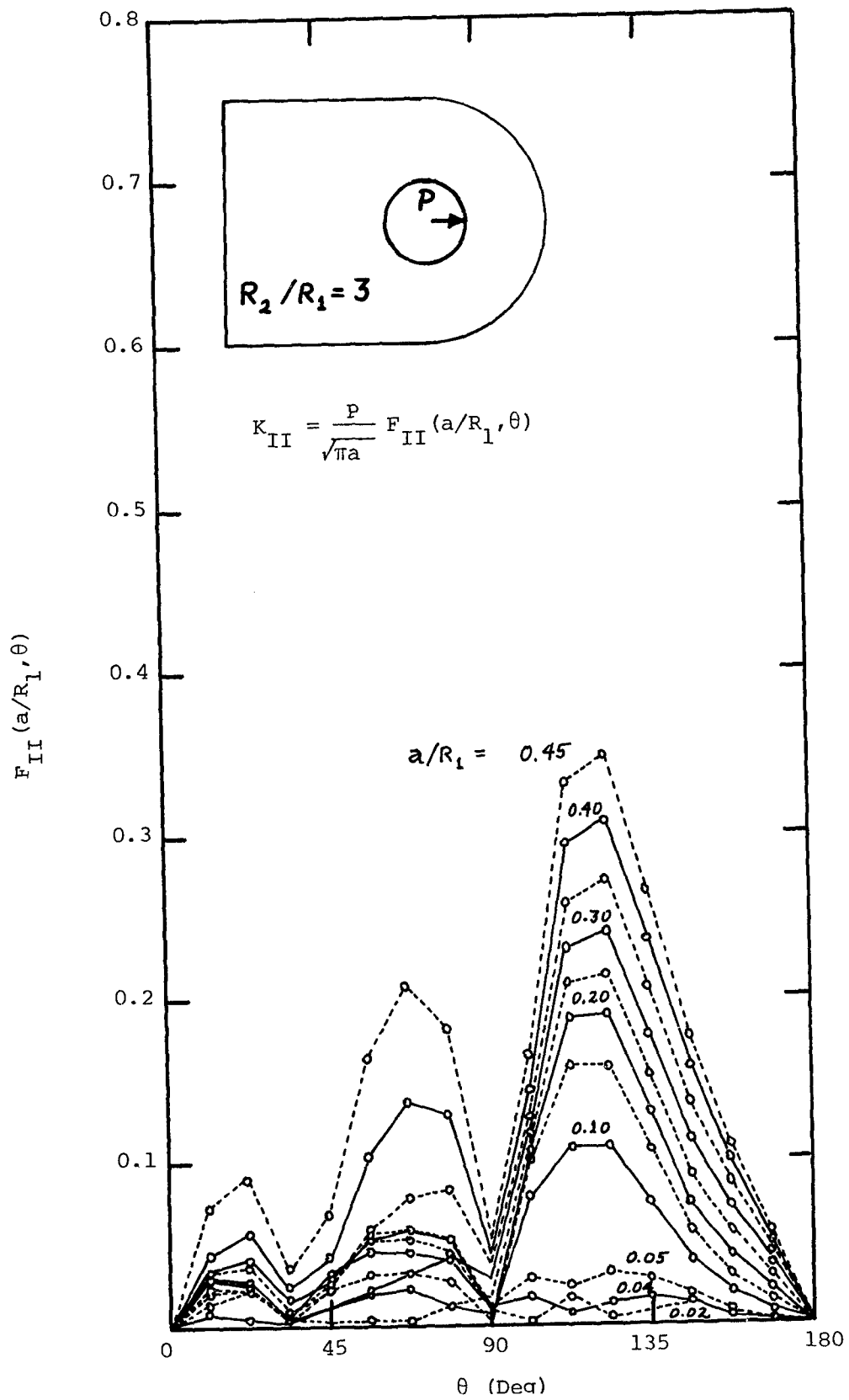
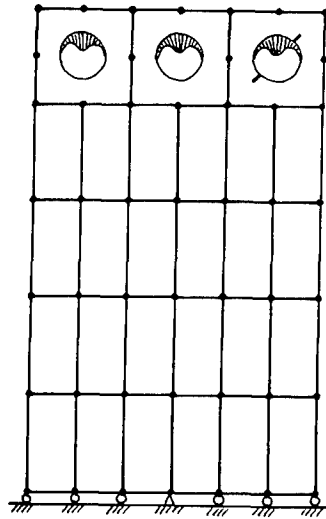
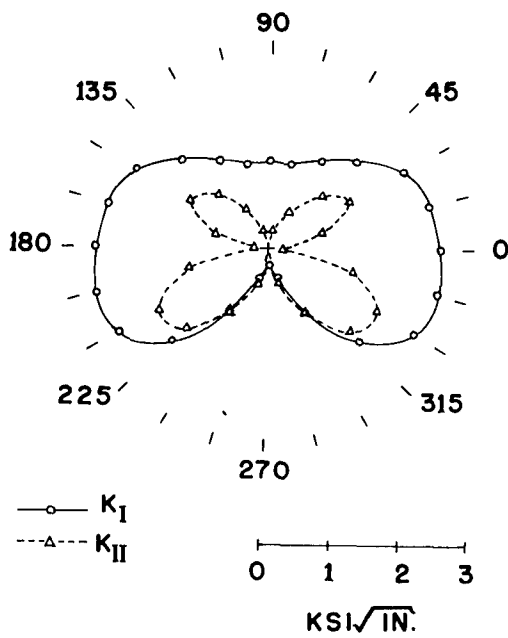


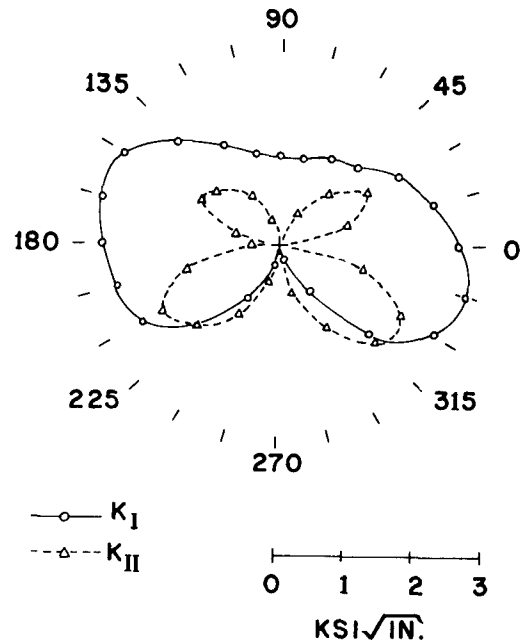
Figure 27. Attachment Lug K_{II} Chart ($R_2/R_1=3$, Cosine Bearing)



(A) TYPICAL FINITE ELEMENT MESH



(B) EXAMPLE RESULT (CENTER HOLE DAMAGED)



(C) EXAMPLE RESULT (RIGHT HOLE DAMAGED)

Figure 28. Single Fastener Row Program Mesh and Example Results

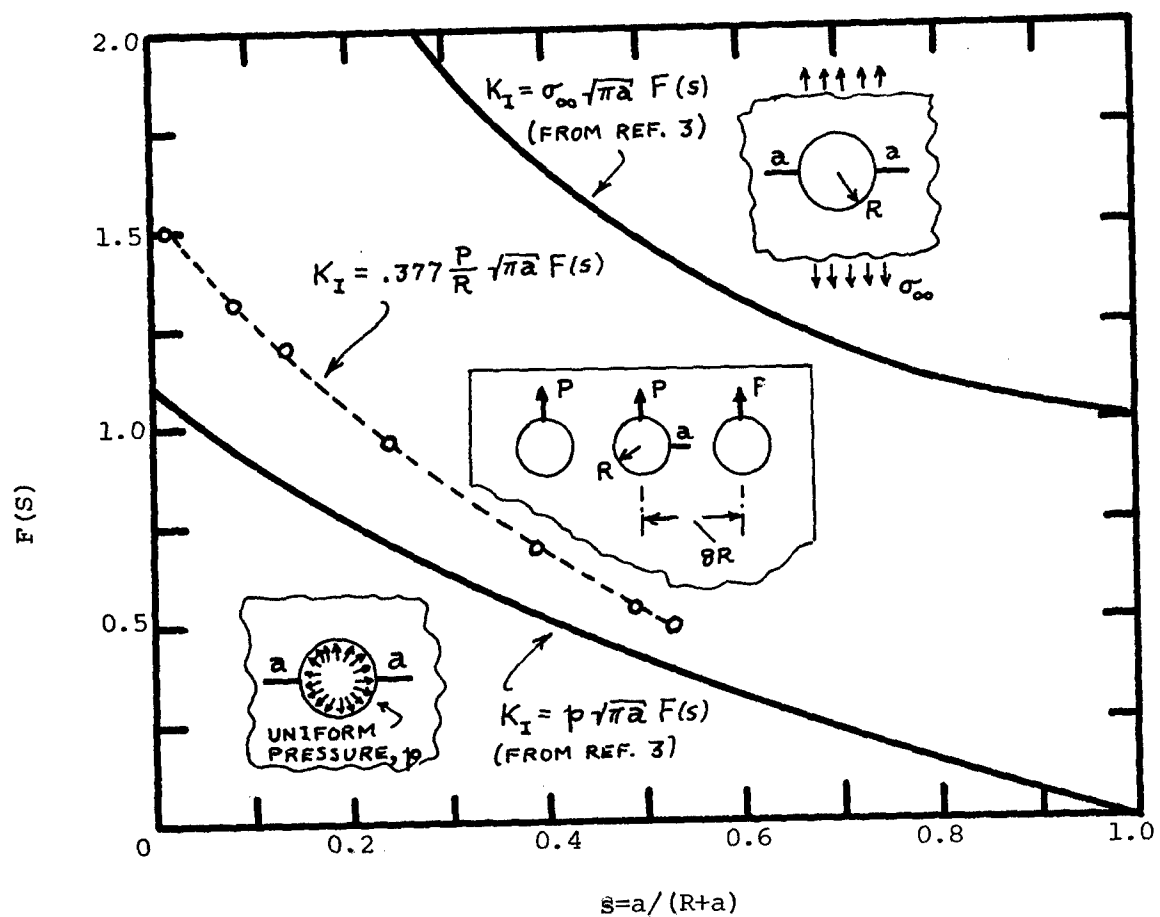


Figure 29. Comparison of a/R Sensitivity with Analytical Solutions for Similar Problems

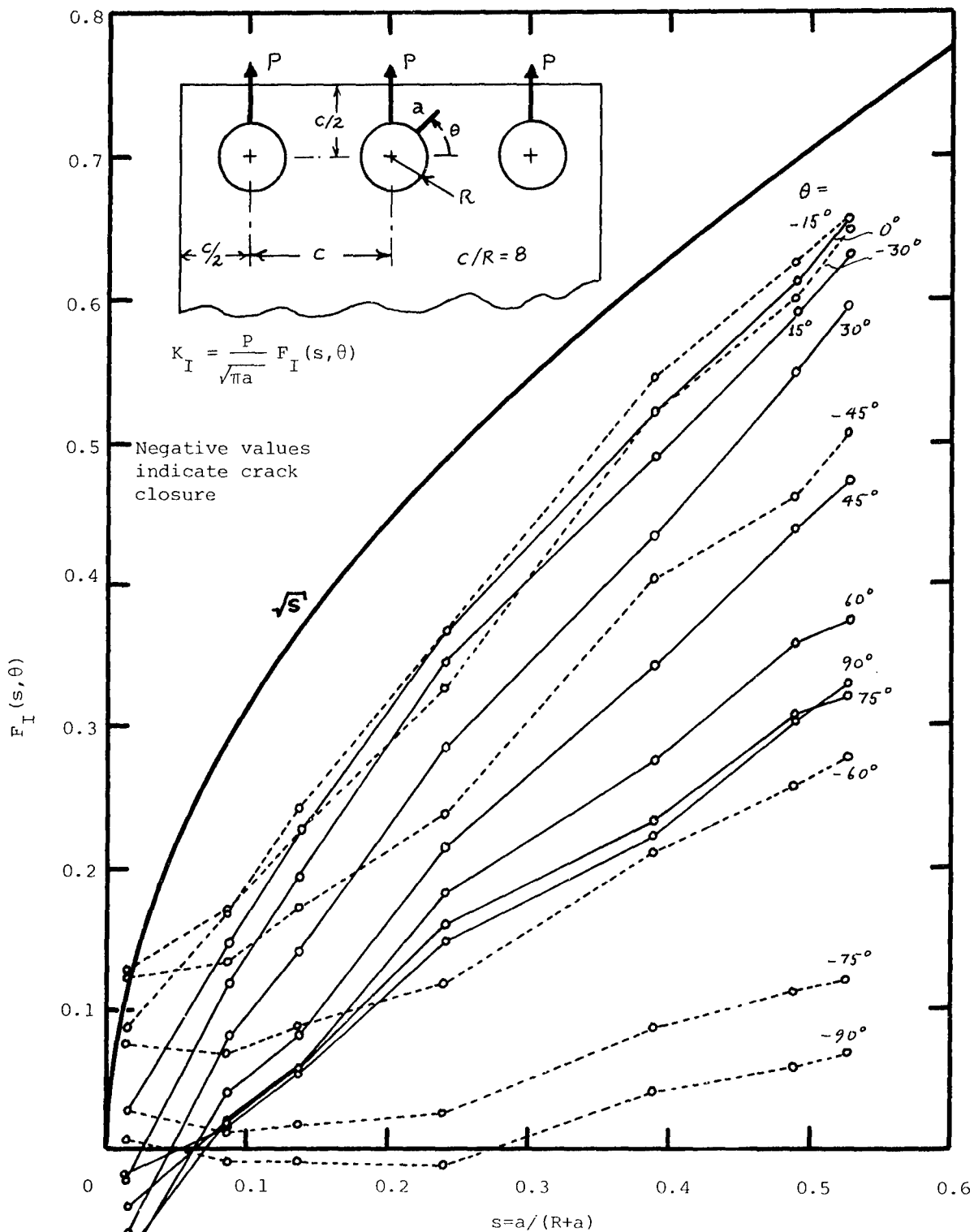


Figure 30. Sensitivity of K_I to a/R and θ

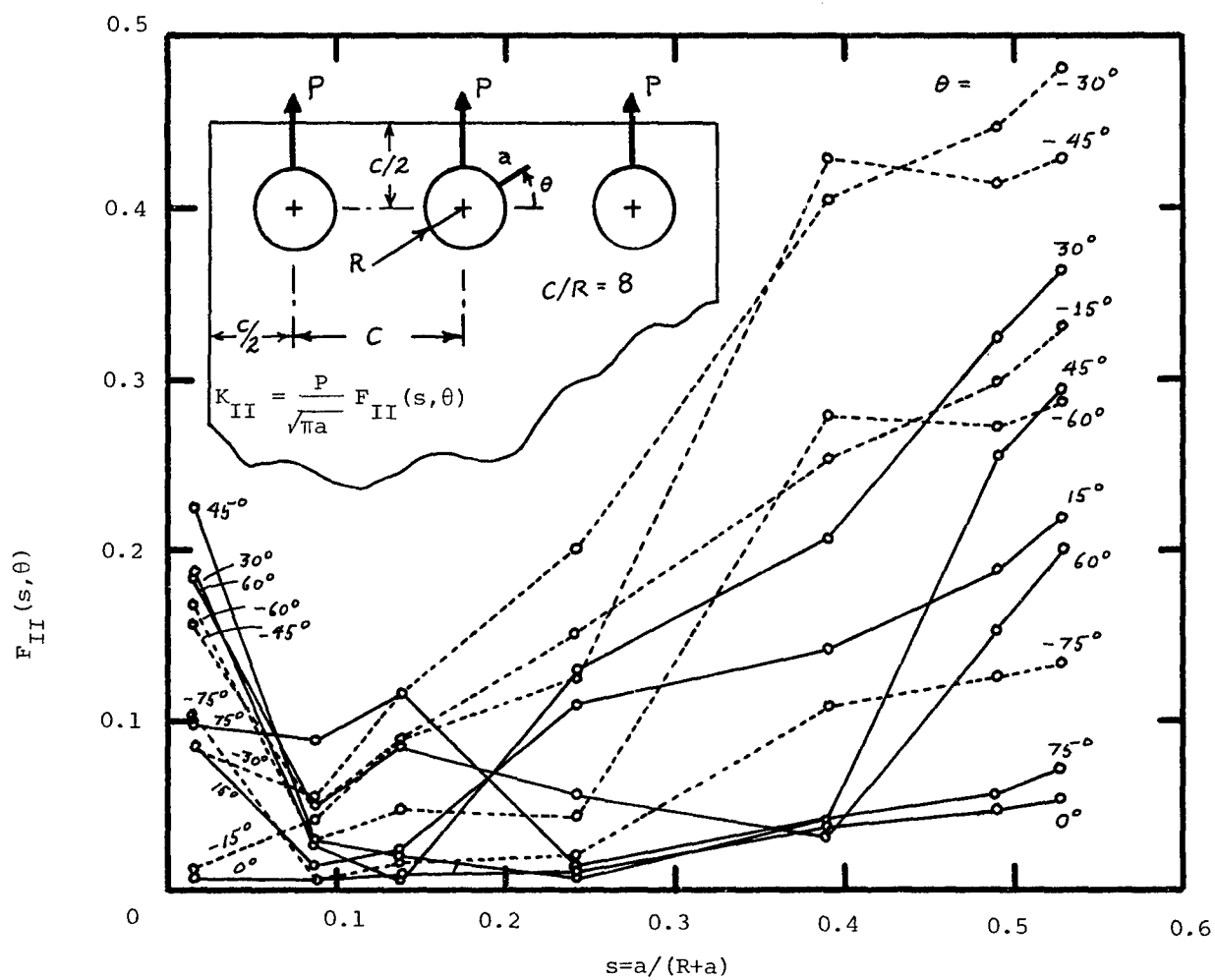


Figure 31. Sensitivity of K_{II} to a/R and θ

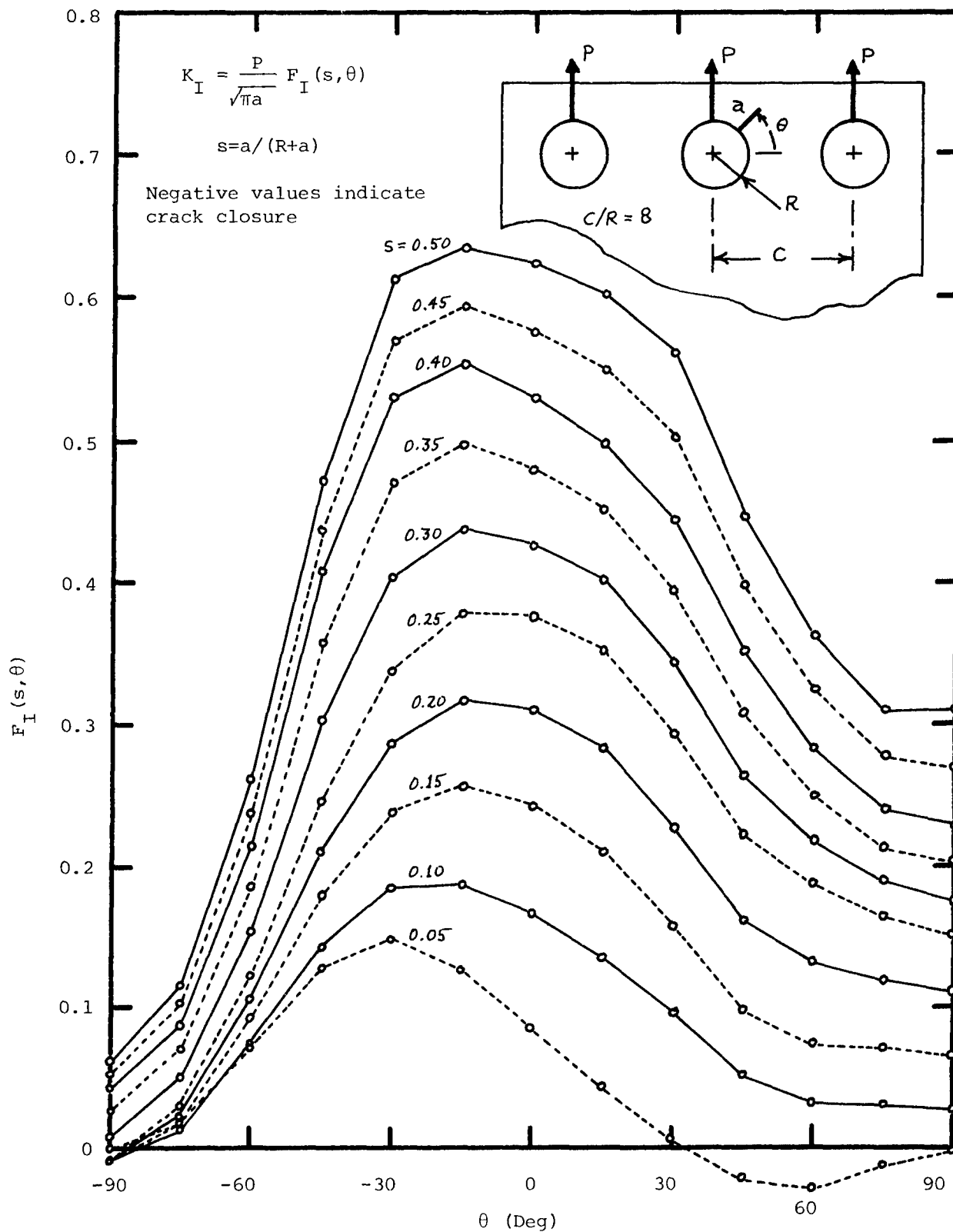


Figure 32. Single Row K_I Chart (Center Hole Damaged, $C/D=4$)

$$K_{II} = \frac{P}{\sqrt{\pi a}} F_{II}(s, \theta)$$

$$s = a / (R + a)$$

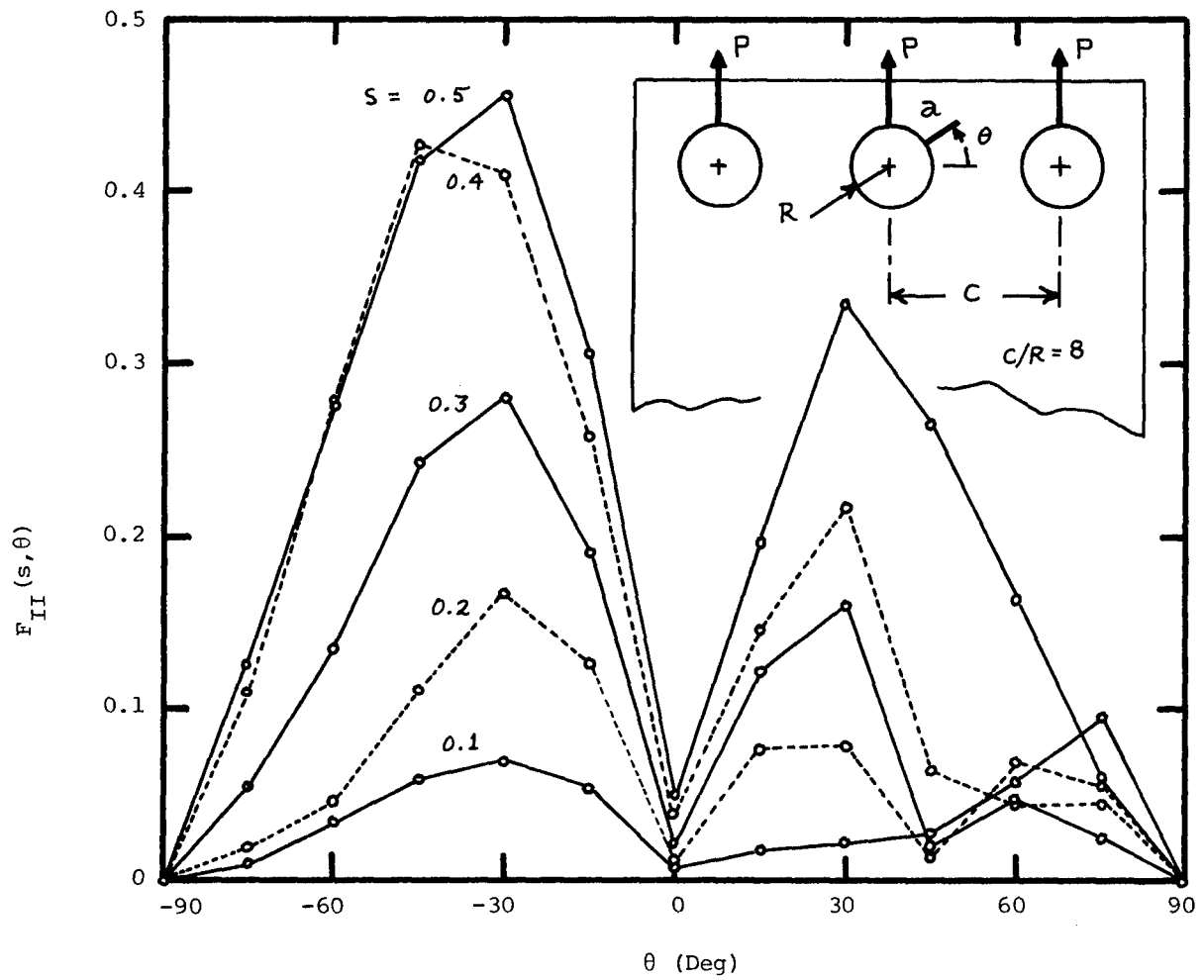


Figure 33. Single Row K_{II} Chart (Center Hole Damaged, $C/D=4$)

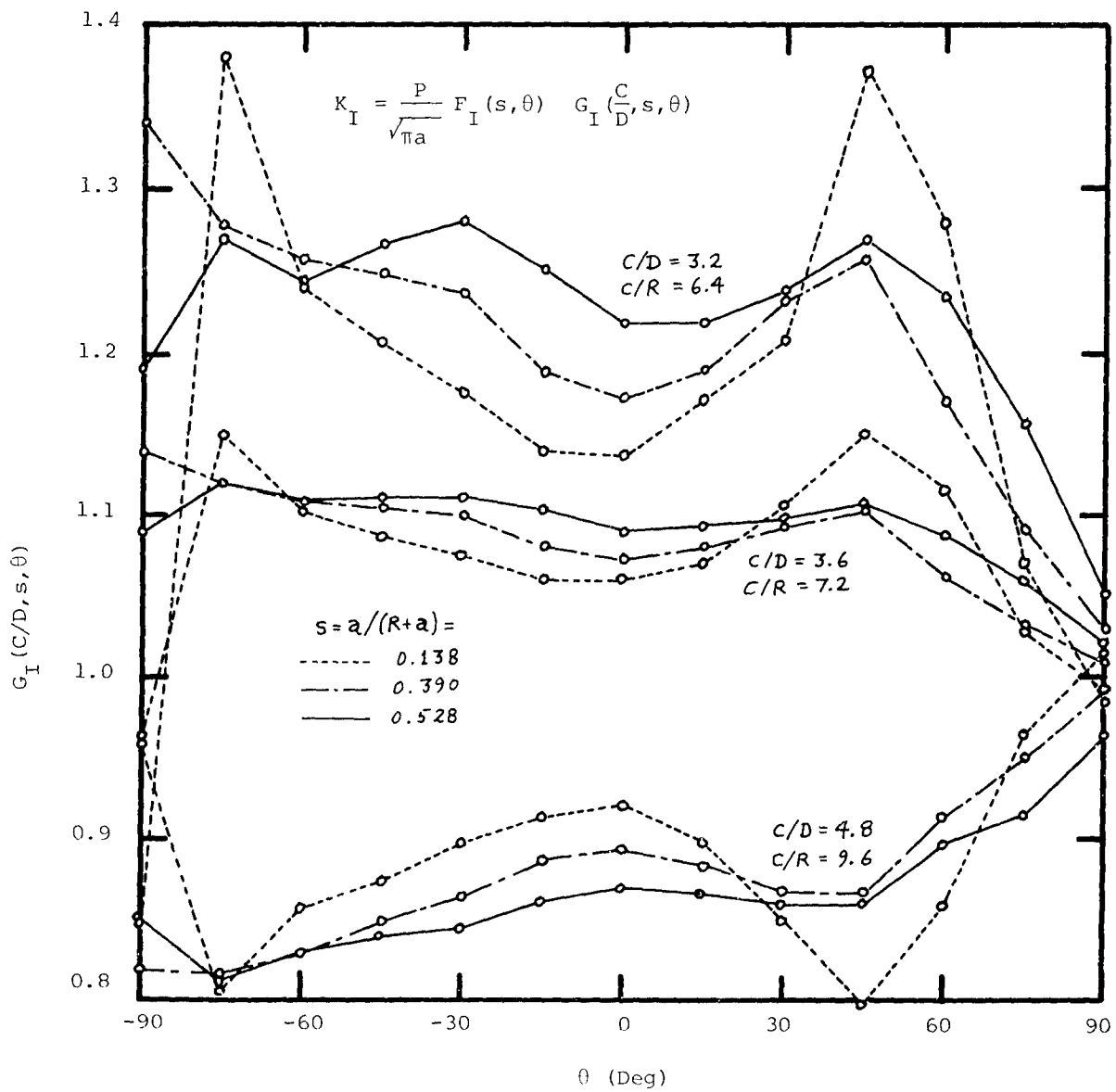


Figure 34. Sensitivity of K_I to C/D

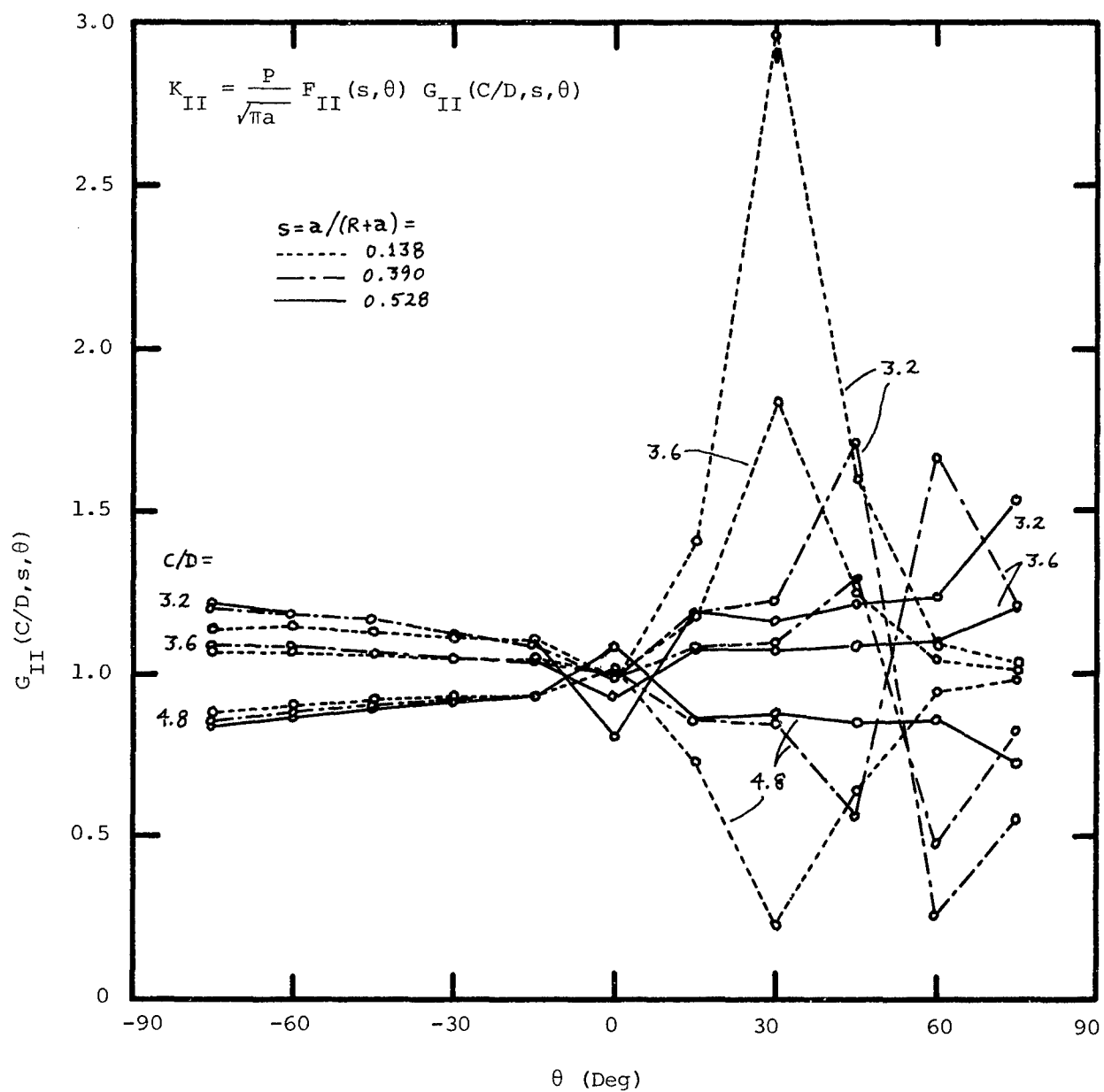


Figure 35. Sensitivity of K_{II} to C/D

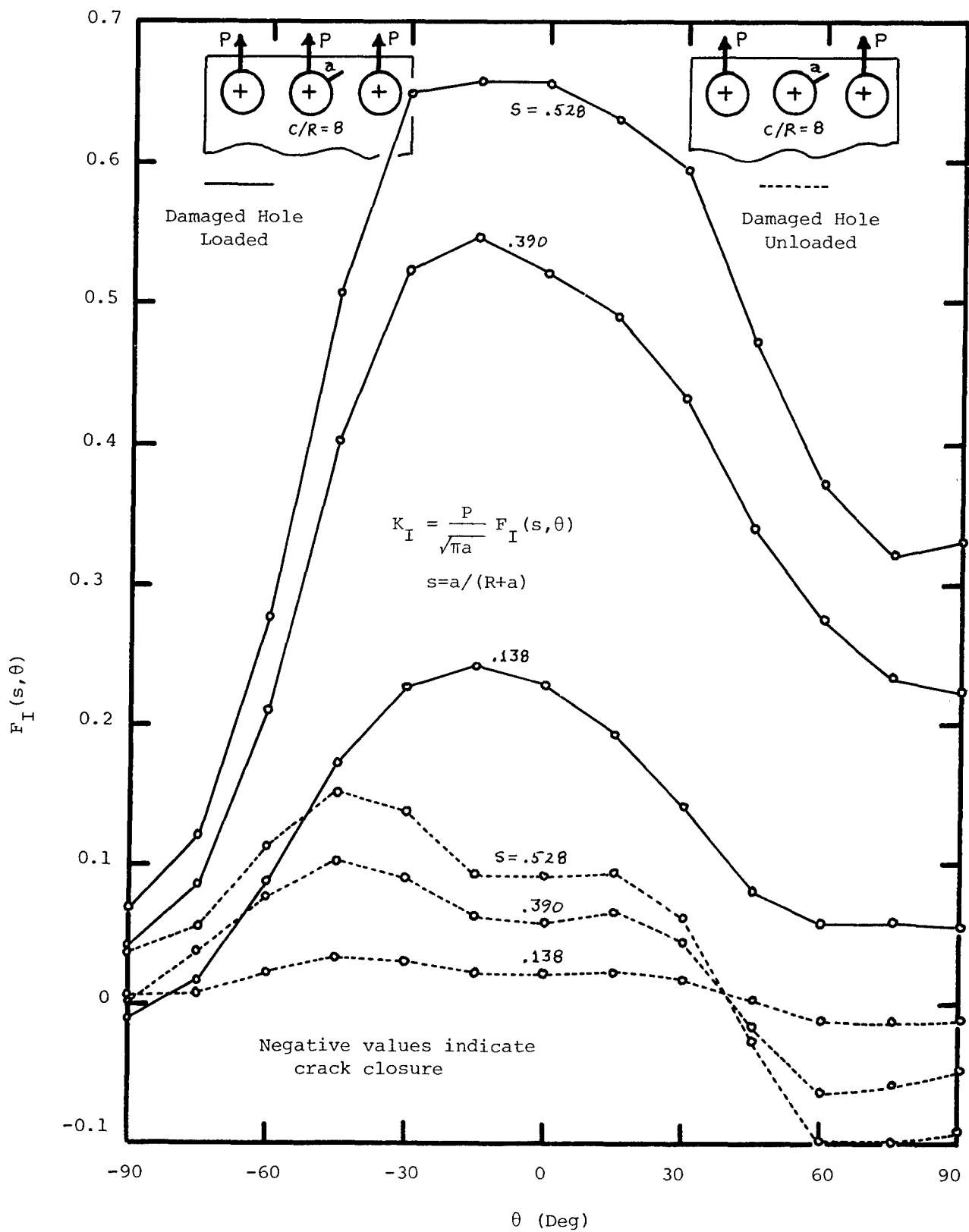


Figure 36. Comparison of K_I for Damaged Center Hole Loaded and Unloaded

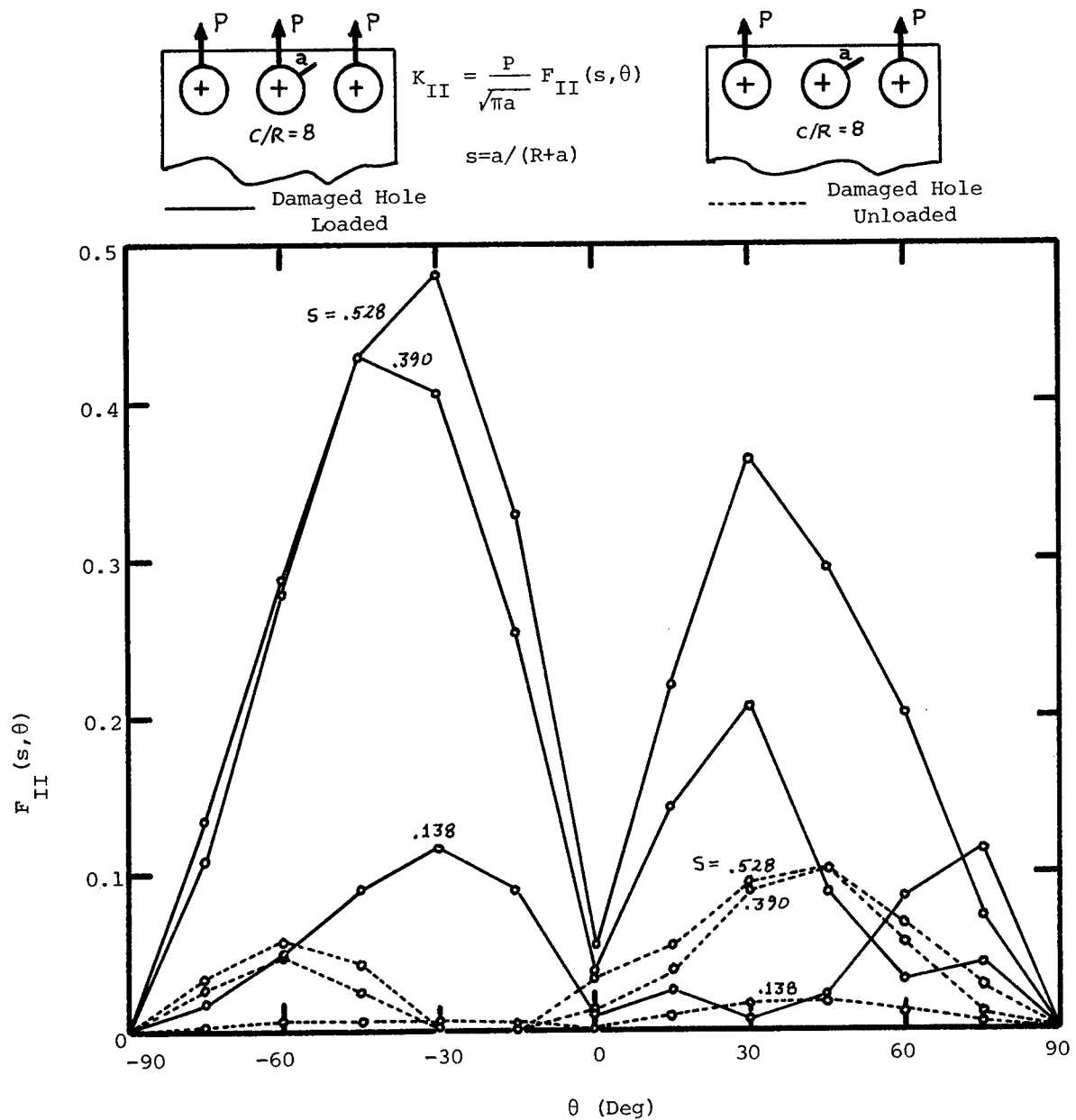


Figure 37. Comparison of K_{II} for Damaged Center Hole Loaded and Unloaded

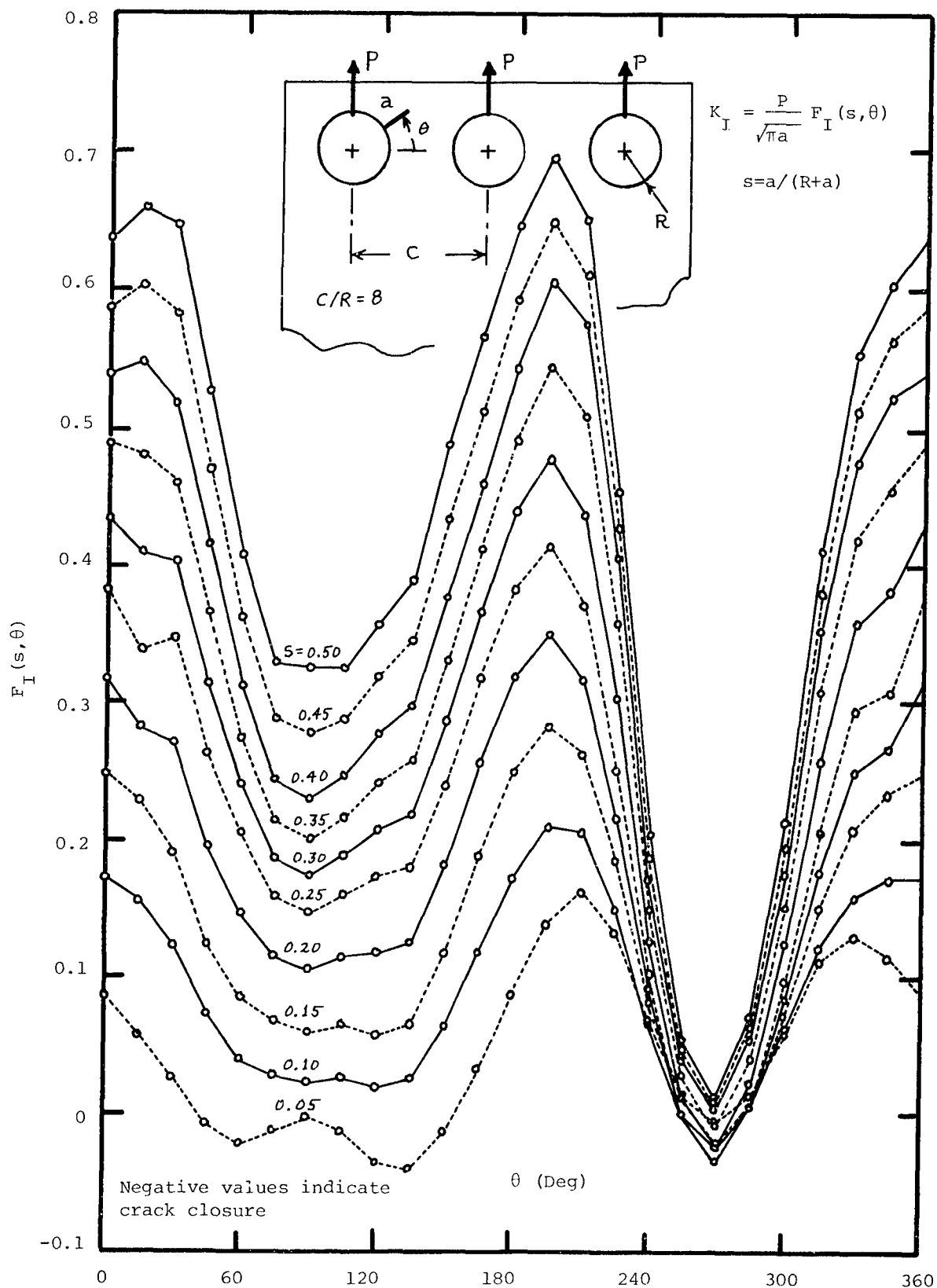


Figure 38. Single Row K_I Chart (Left Hole Damaged, $C/D=4$)

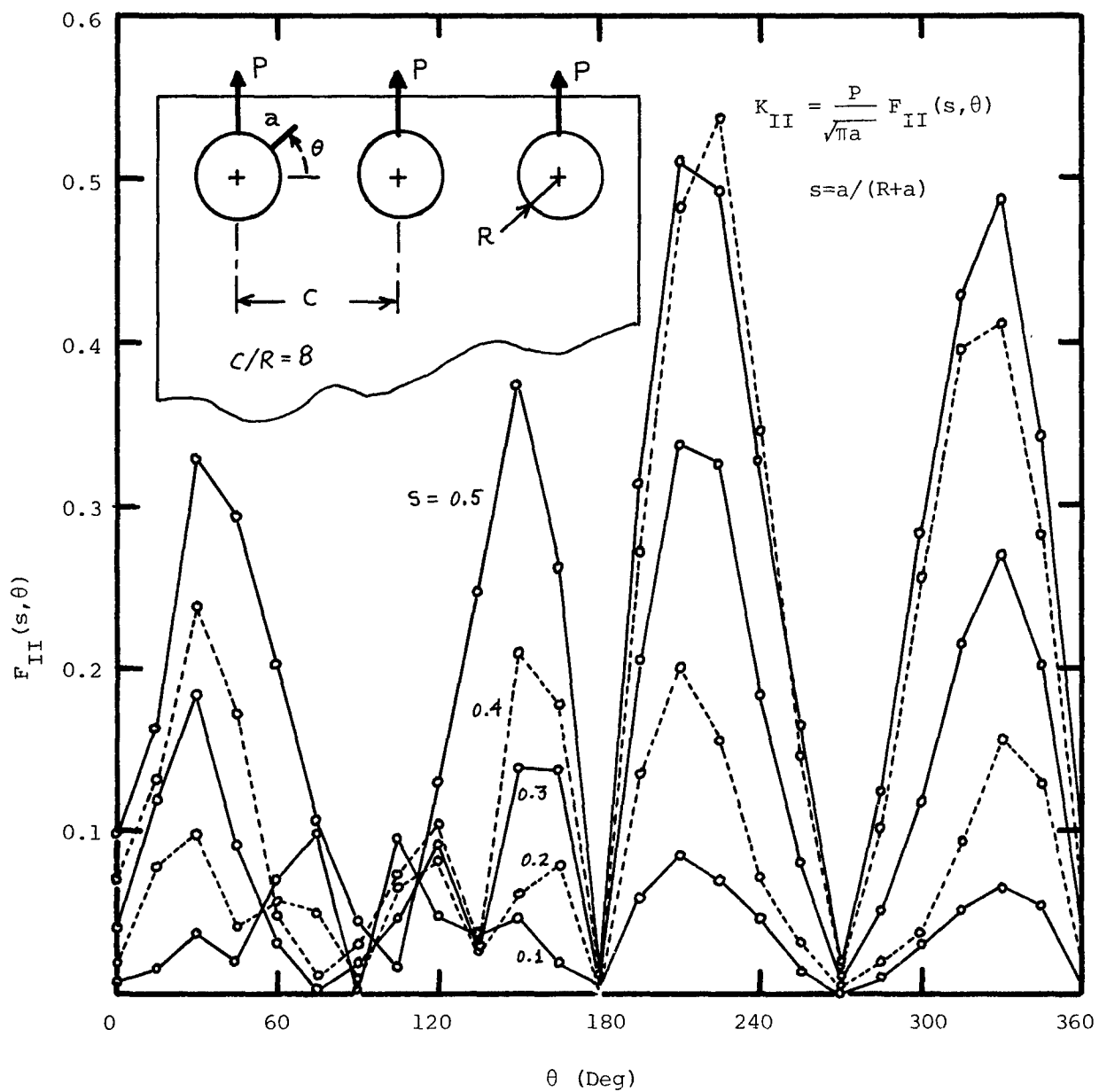


Figure 39. Single Row K_{II} Chart (Left Hole Damaged, $C/D=4$)

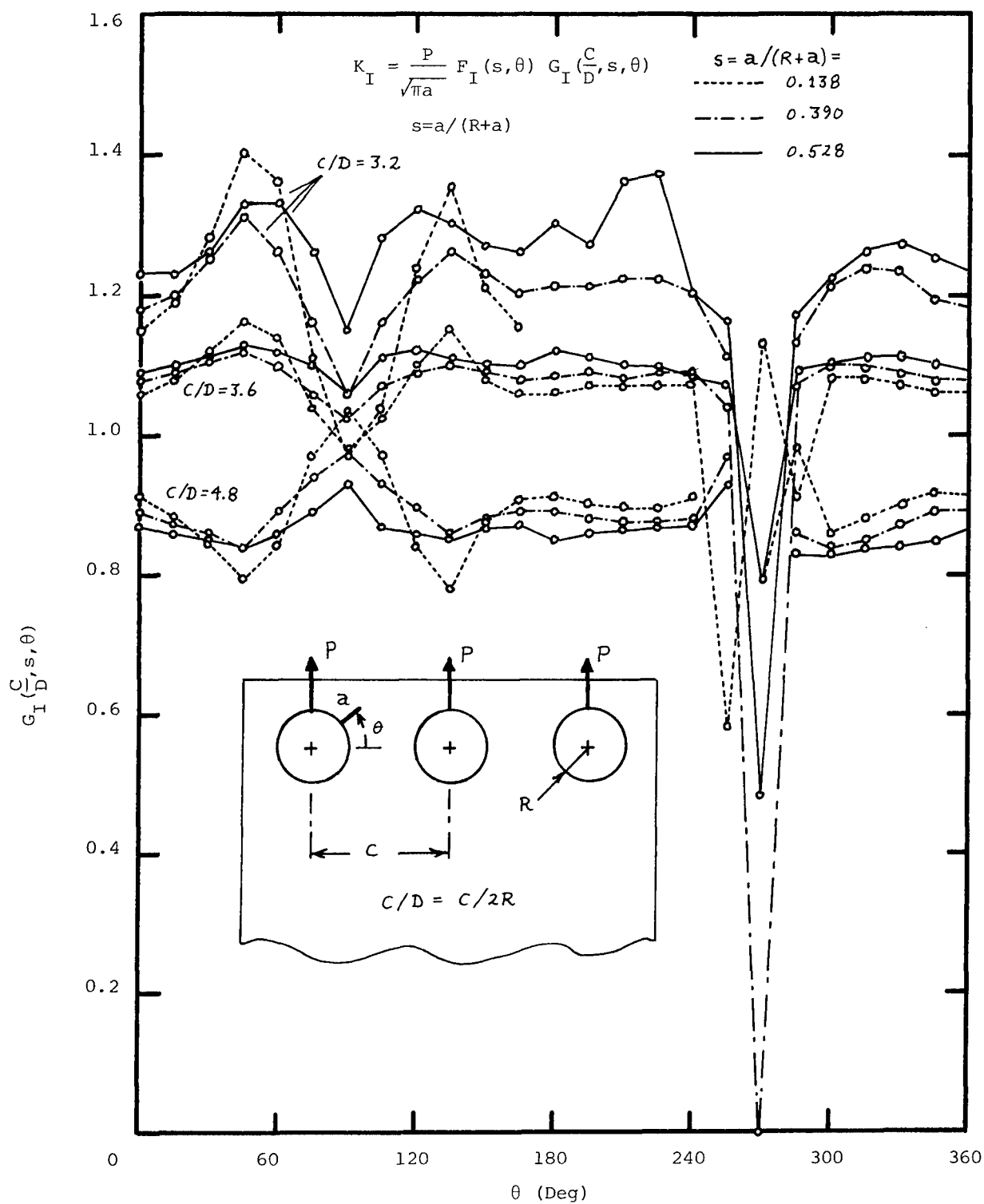


Figure 40. Sensitivity of K_I to C/D (Left Hole Damaged)

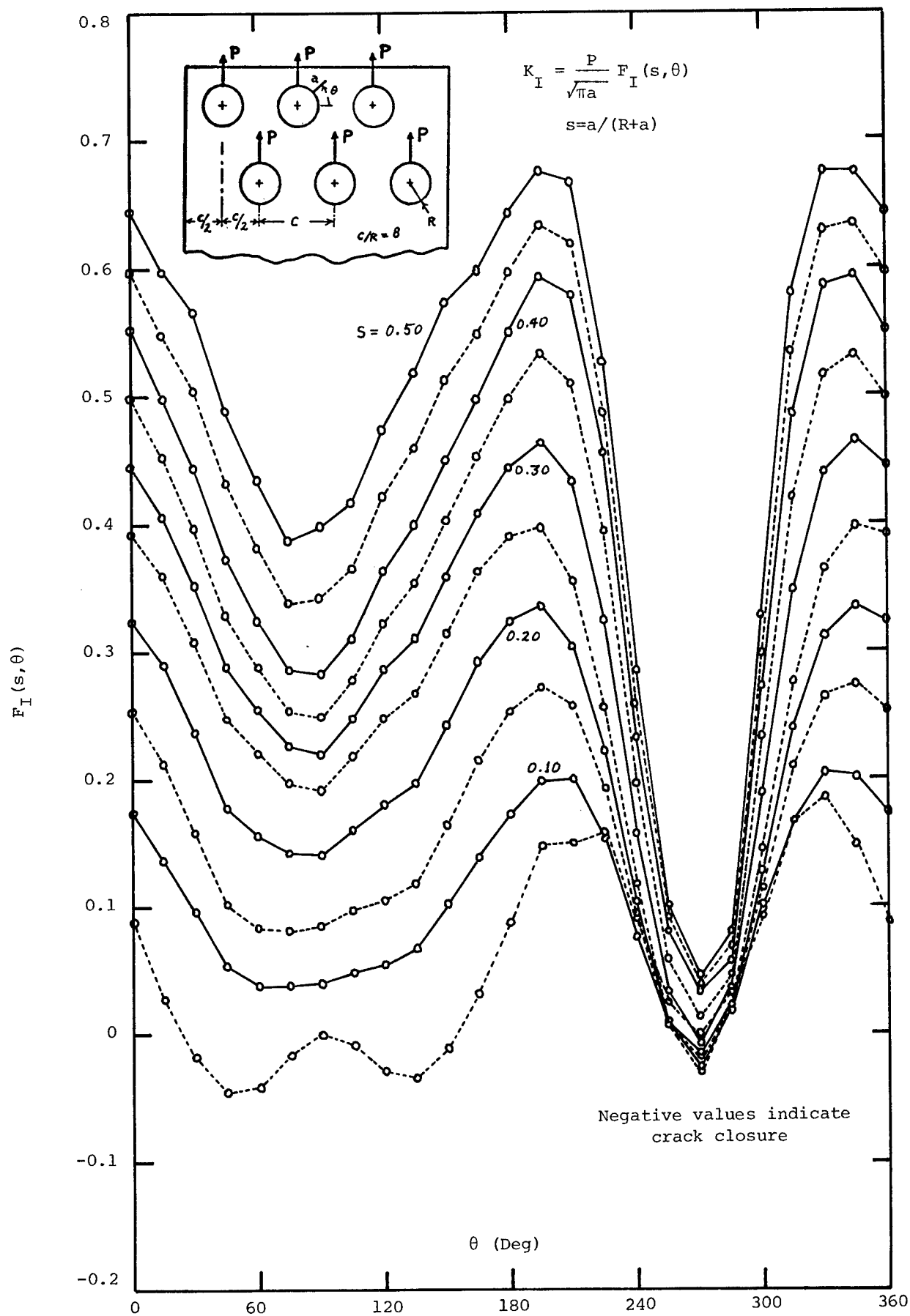


Figure 41. Double Row K_I Chart (Upper Center Hole Damaged, $C/D=4$)

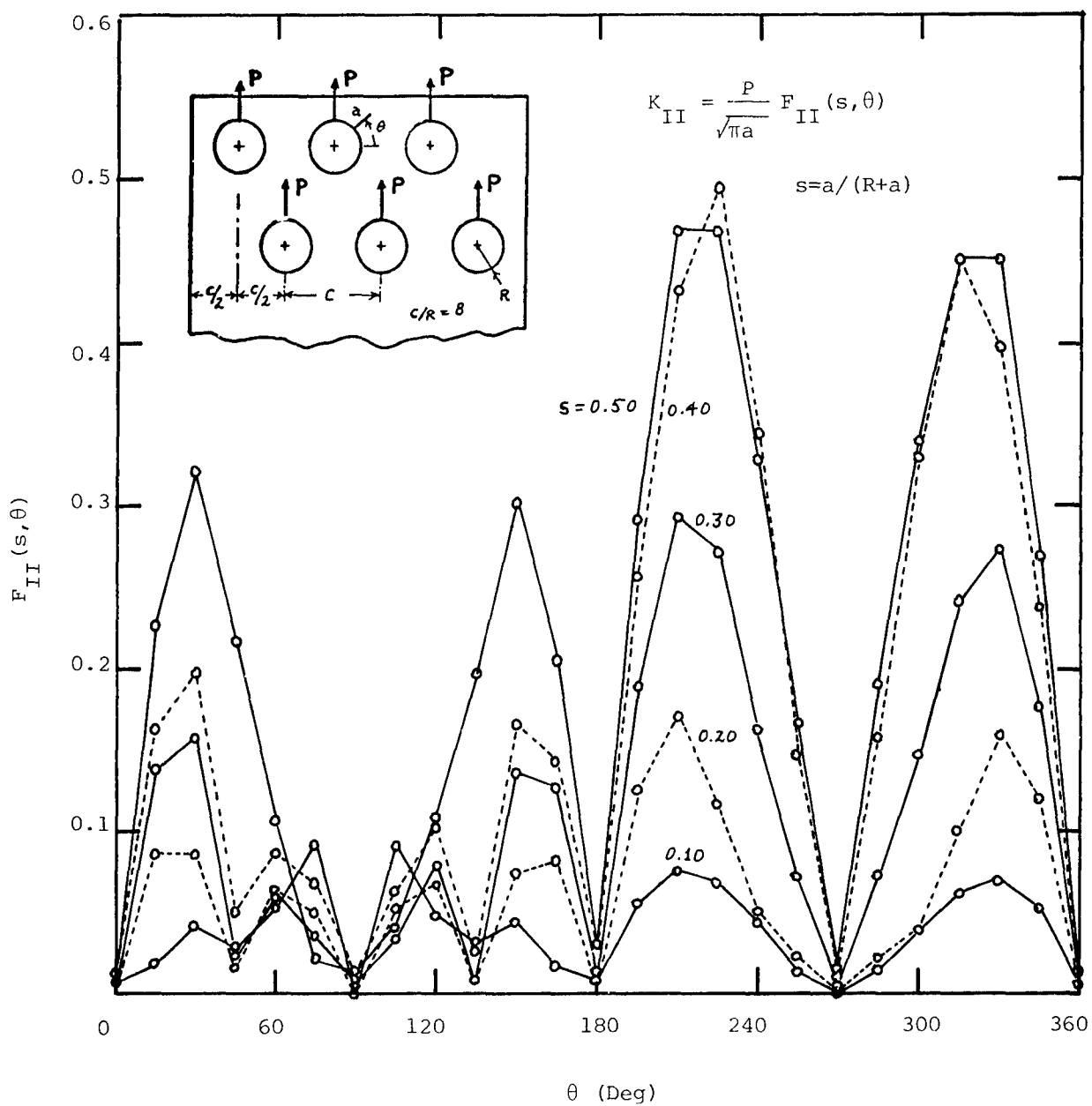


Figure 42. Double Row K_{II} Chart (Upper Center Hole Damaged, $C/D=4$)

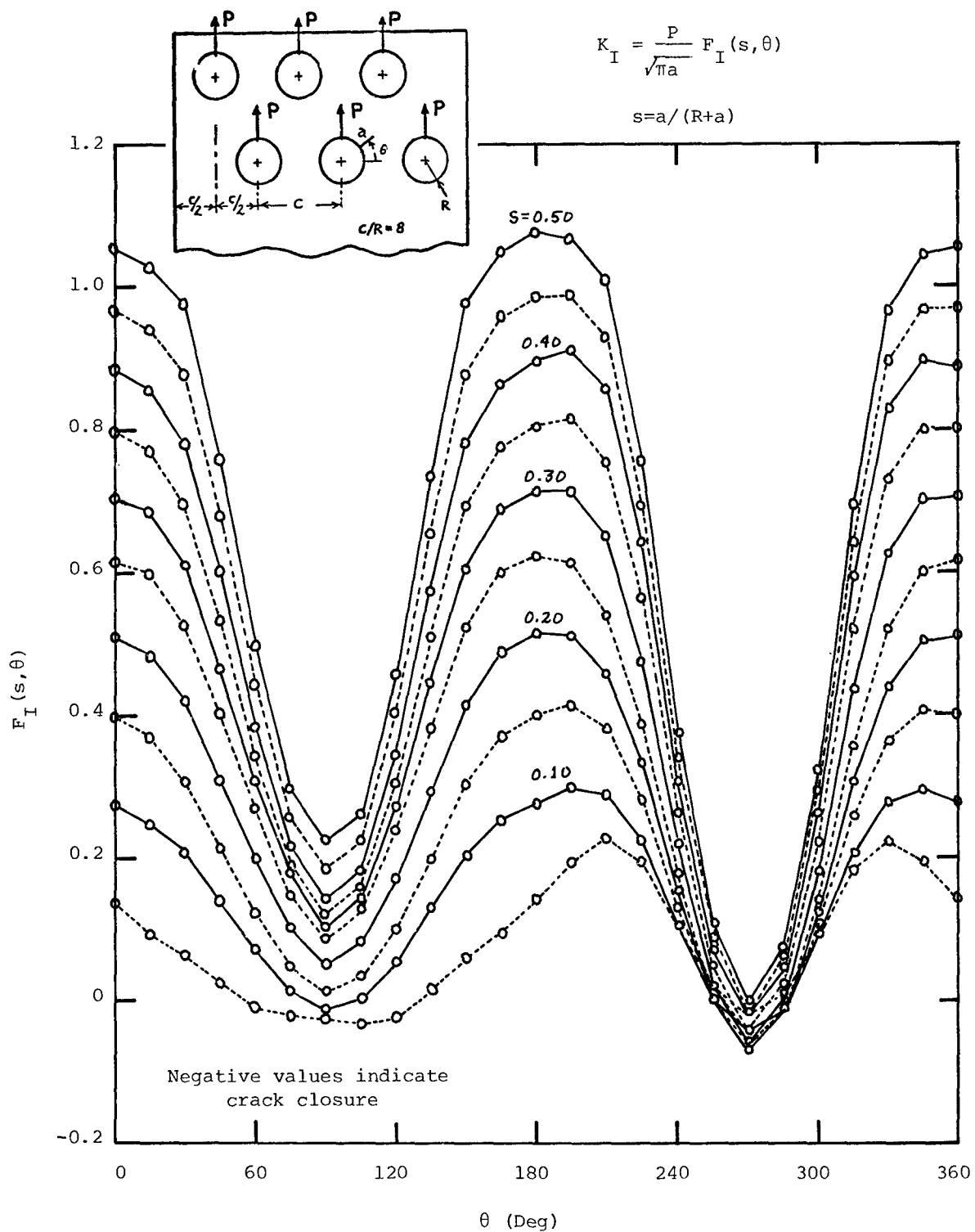


Figure 43. Double Row K_I Chart (Lower Center Hole Damaged, $C/D=4$)

$$K_{II} = \frac{P}{\sqrt{\pi a}} F_{II}(s, \theta)$$

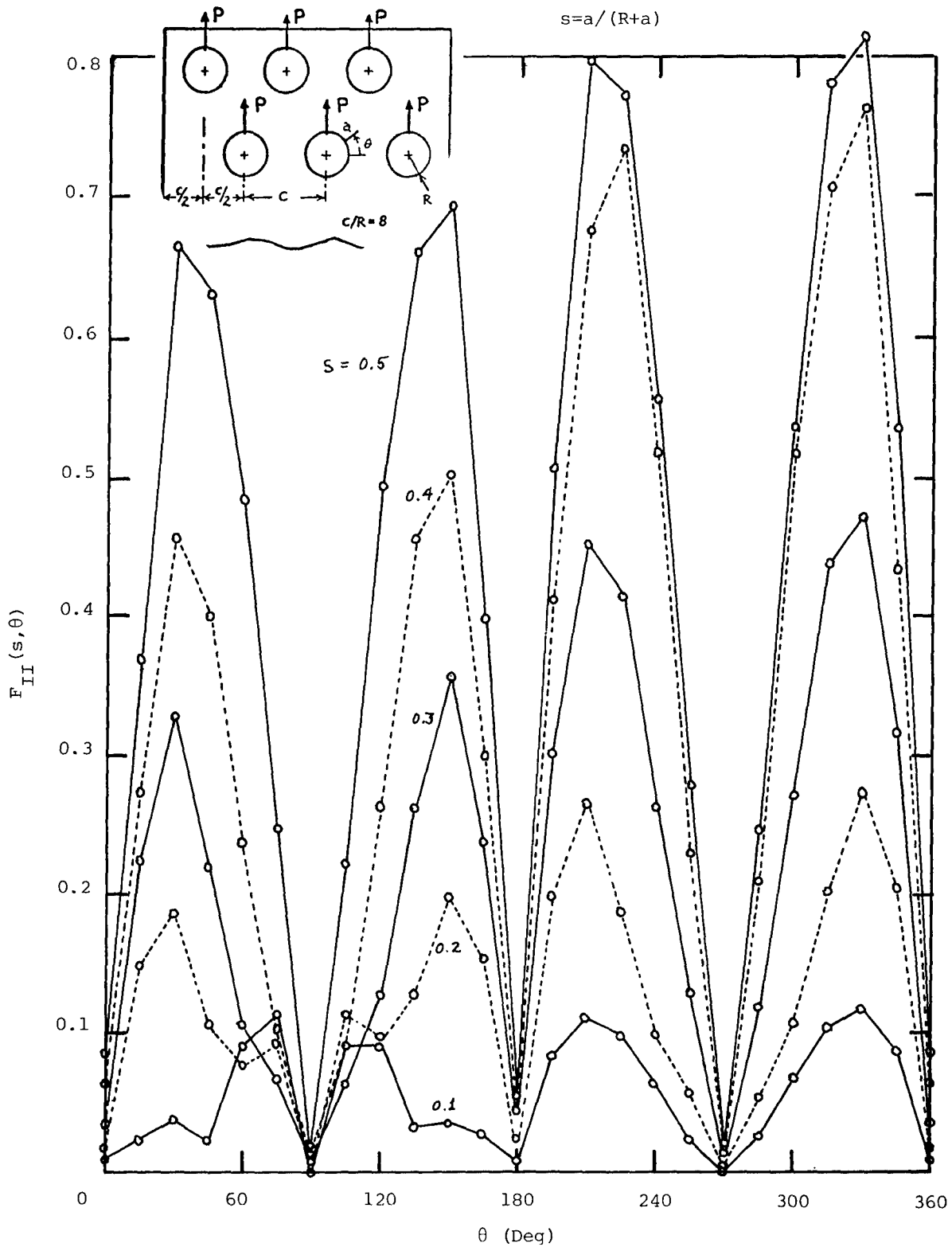


Figure 44. Double Row K_{II} Chart (Lower Center Hole Damaged, $C/D=4$)

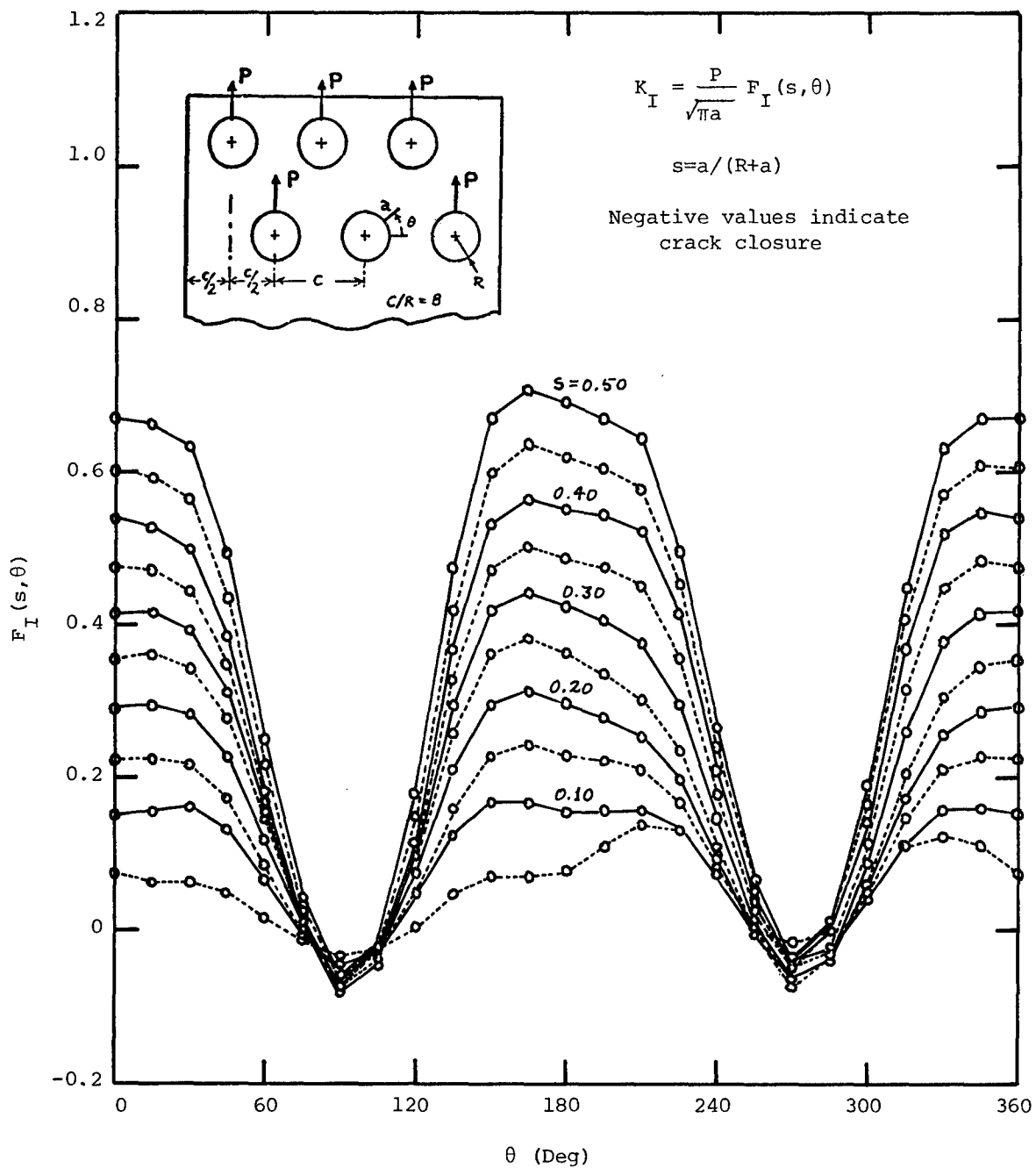


Figure 45. Double Row K_I Chart (Lower Center Hole Damaged and Unloaded, $C/D=4$)

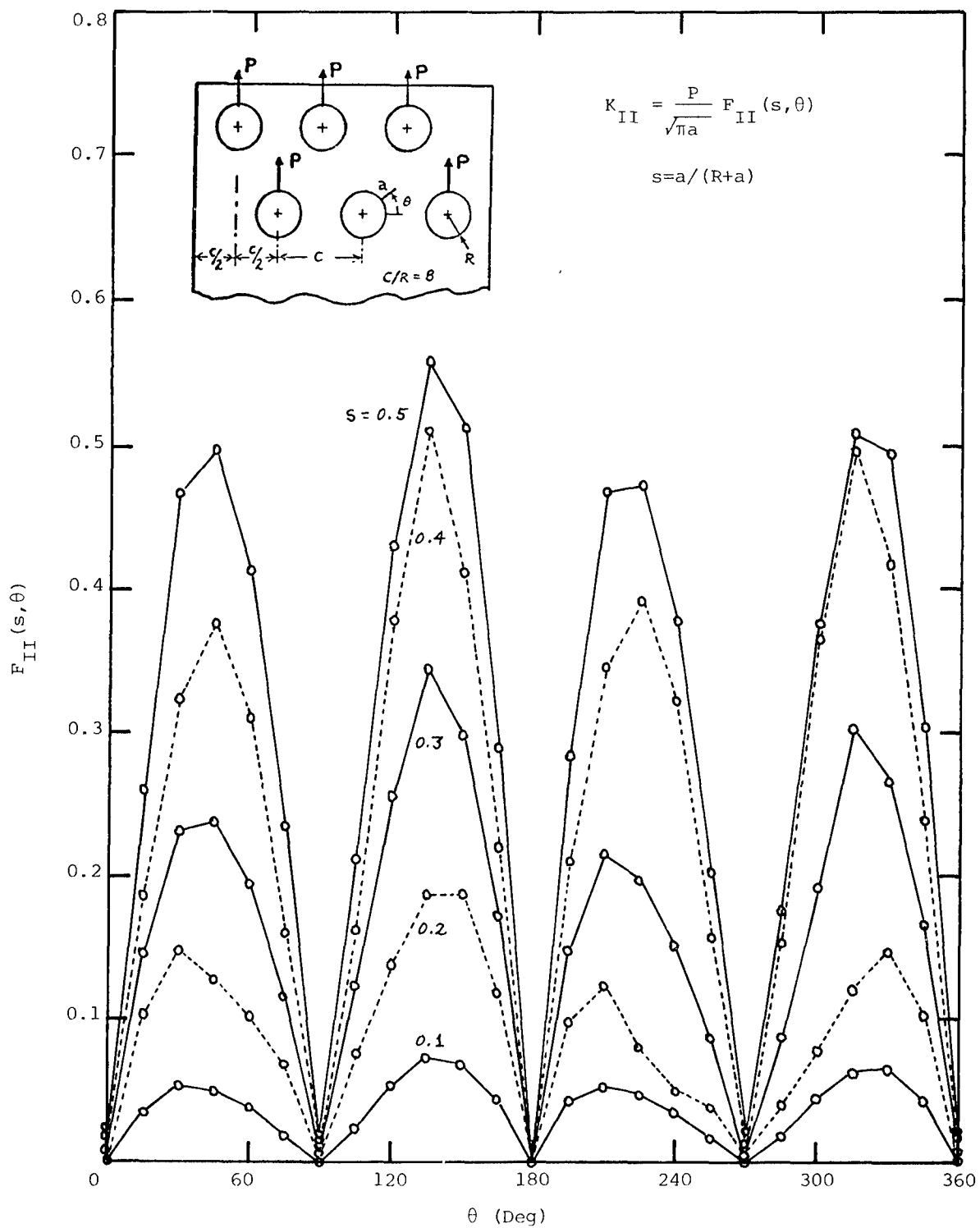


Figure 46. Double Row K_{II} Chart (Lower Center Hole Damaged and Unloaded, $C/D=4$)

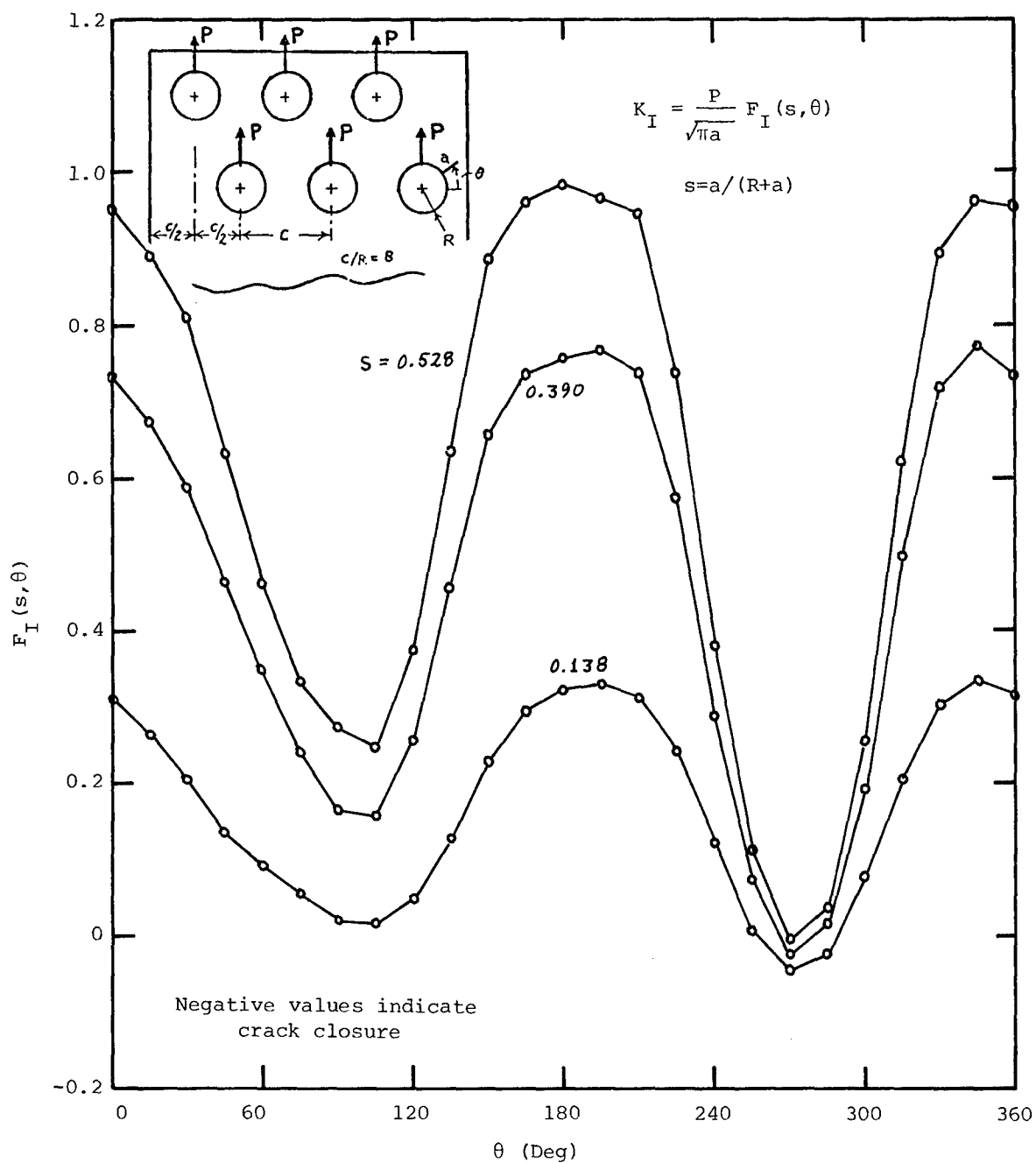


Figure 47. Double Row K_I Chart (Lower Right Hole Damaged, $C/D=4$)

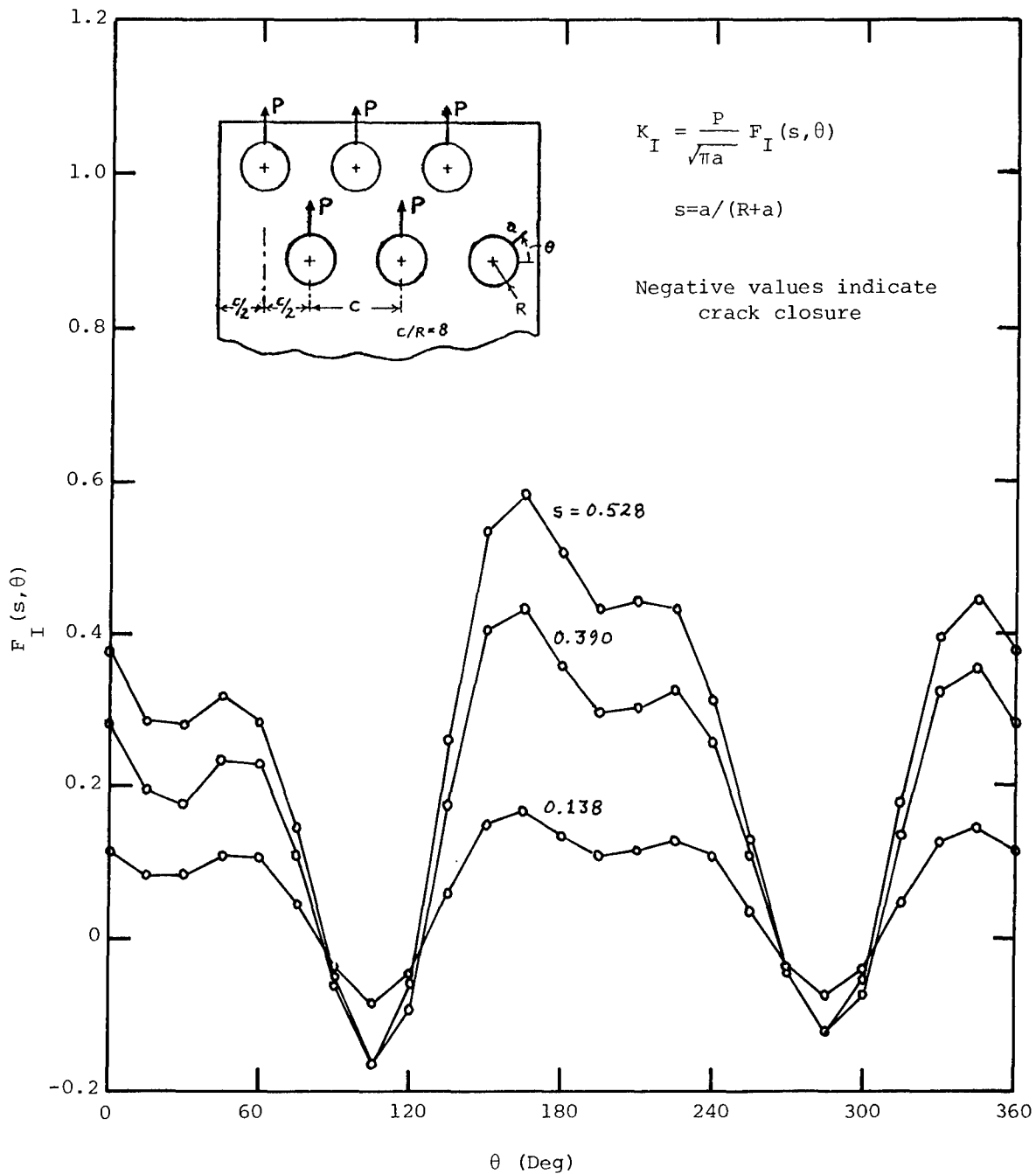


Figure 48. Double Row K_I Chart (Lower Right Hole Damaged and Unloaded, $C/D=4$)

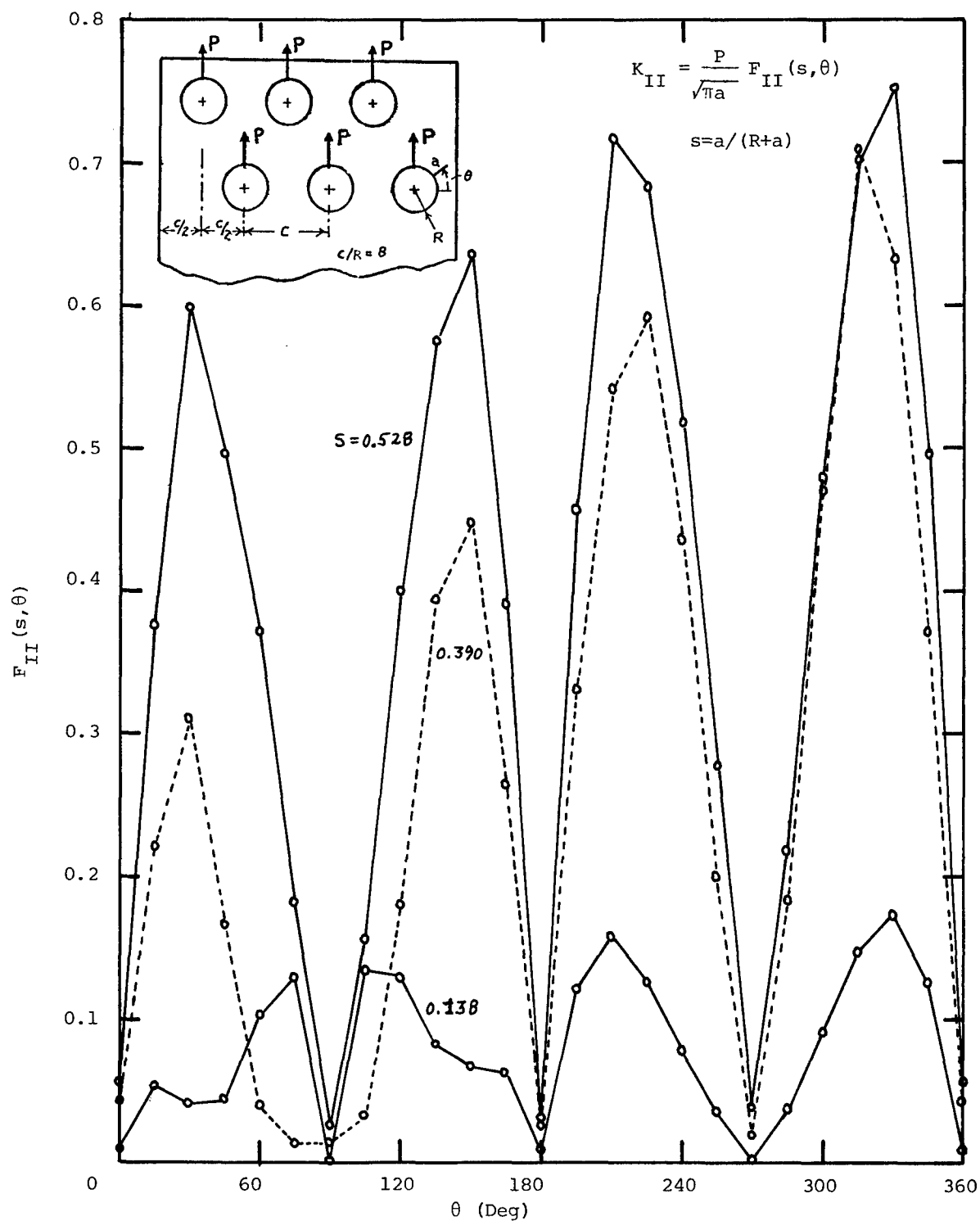


Figure 49. Double Row K_{II} Chart (Lower Right Hole Damaged, $C/D=4$)

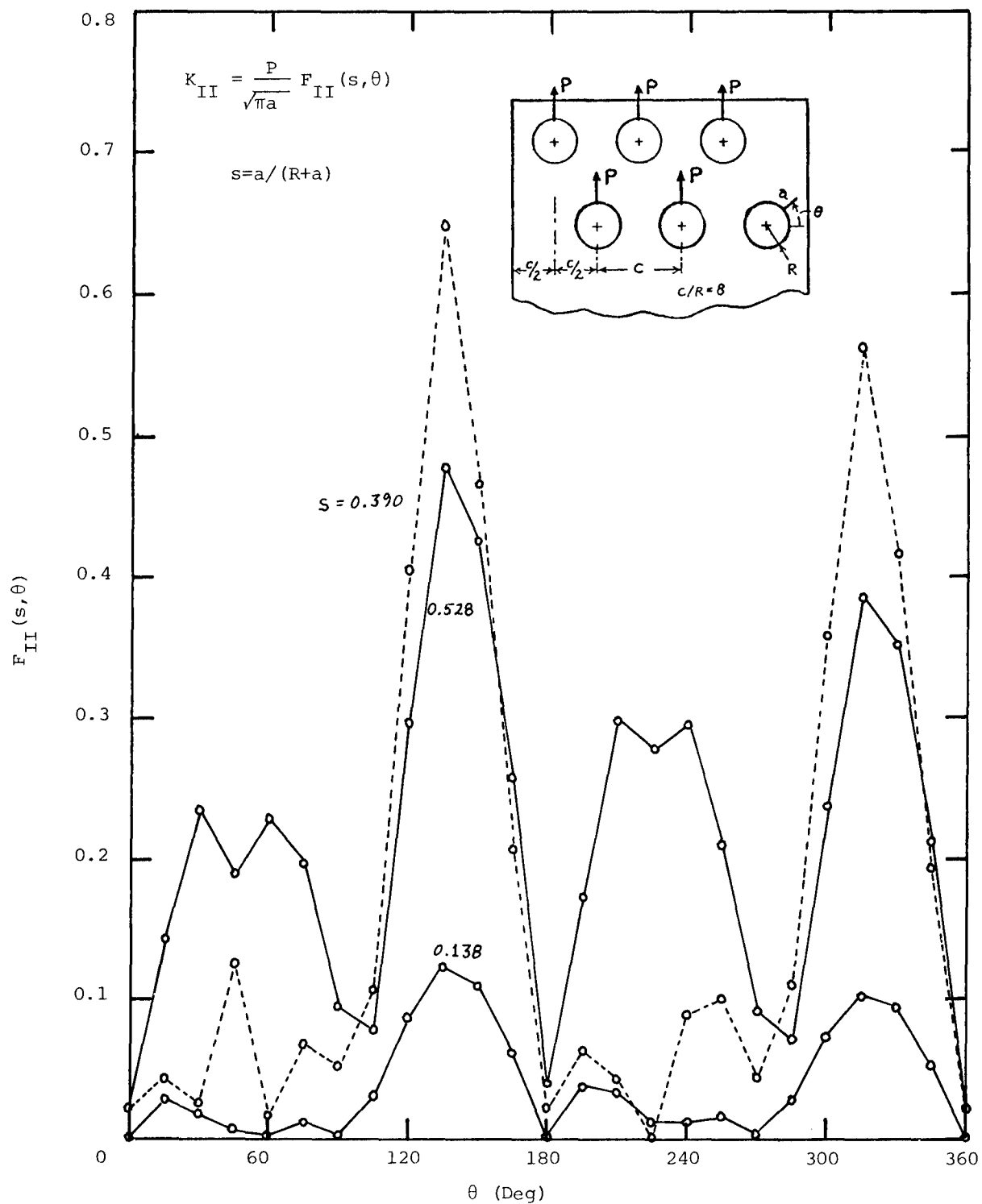


Figure 50. Double Row K_{II} Chart (Lower Right Hole Damaged and Unloaded, $C/D=4$)

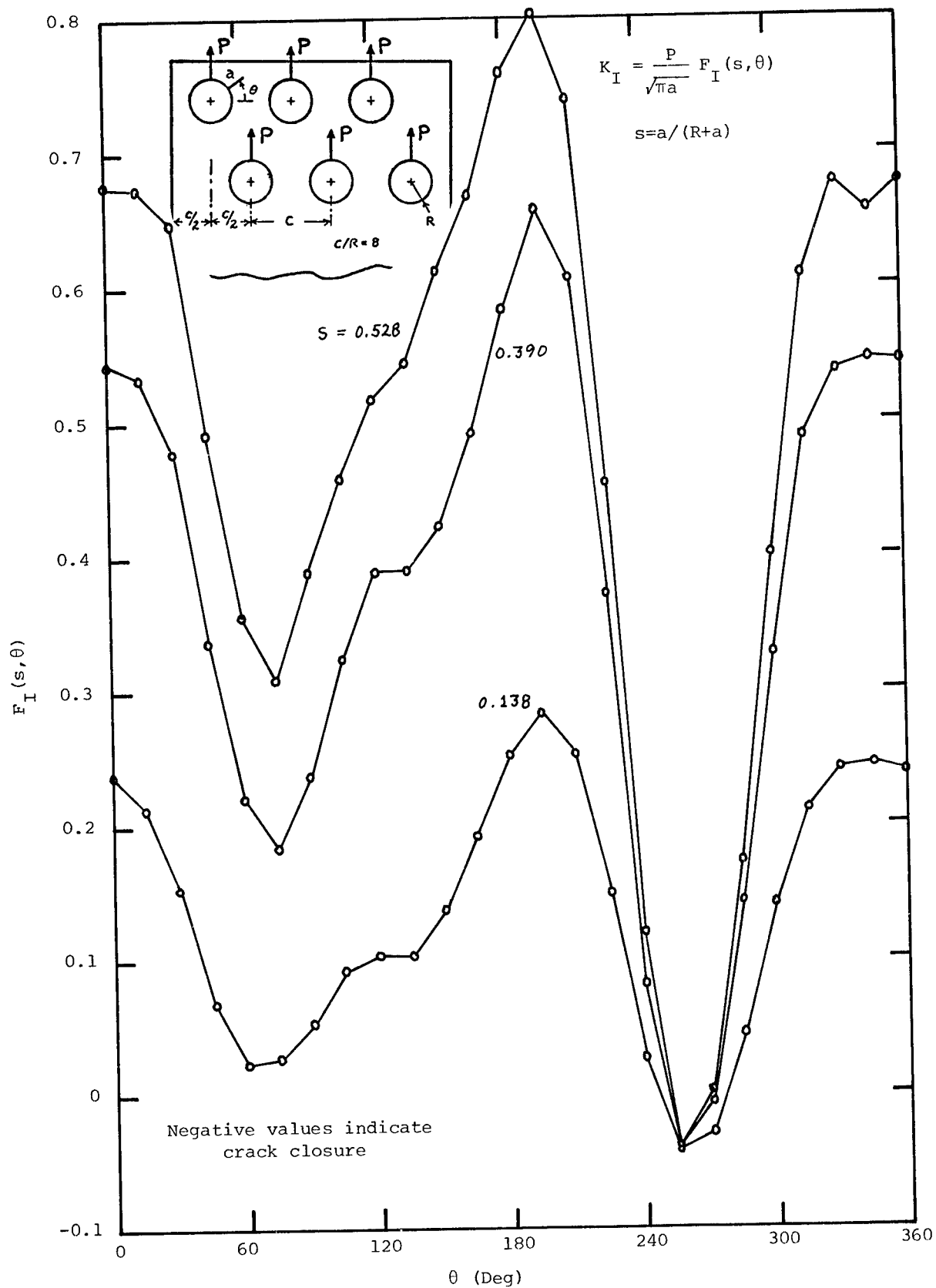


Figure 51. Double Row K_I Chart (Upper Left Hole Damaged, $C/D=4$)

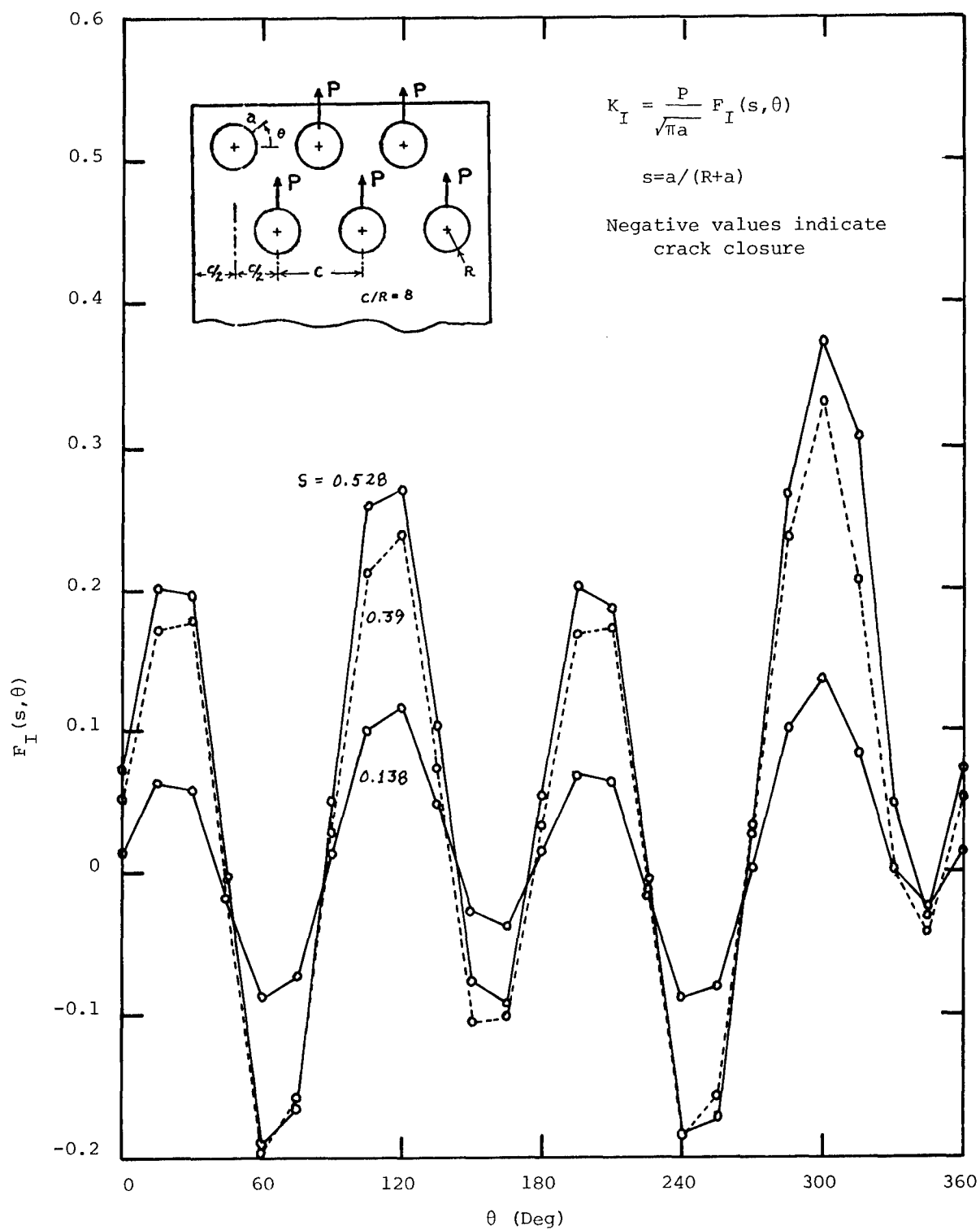


Figure 52. Double Row K_I Chart (Upper Left Hole Damaged and Unloaded, $C/D=4$)

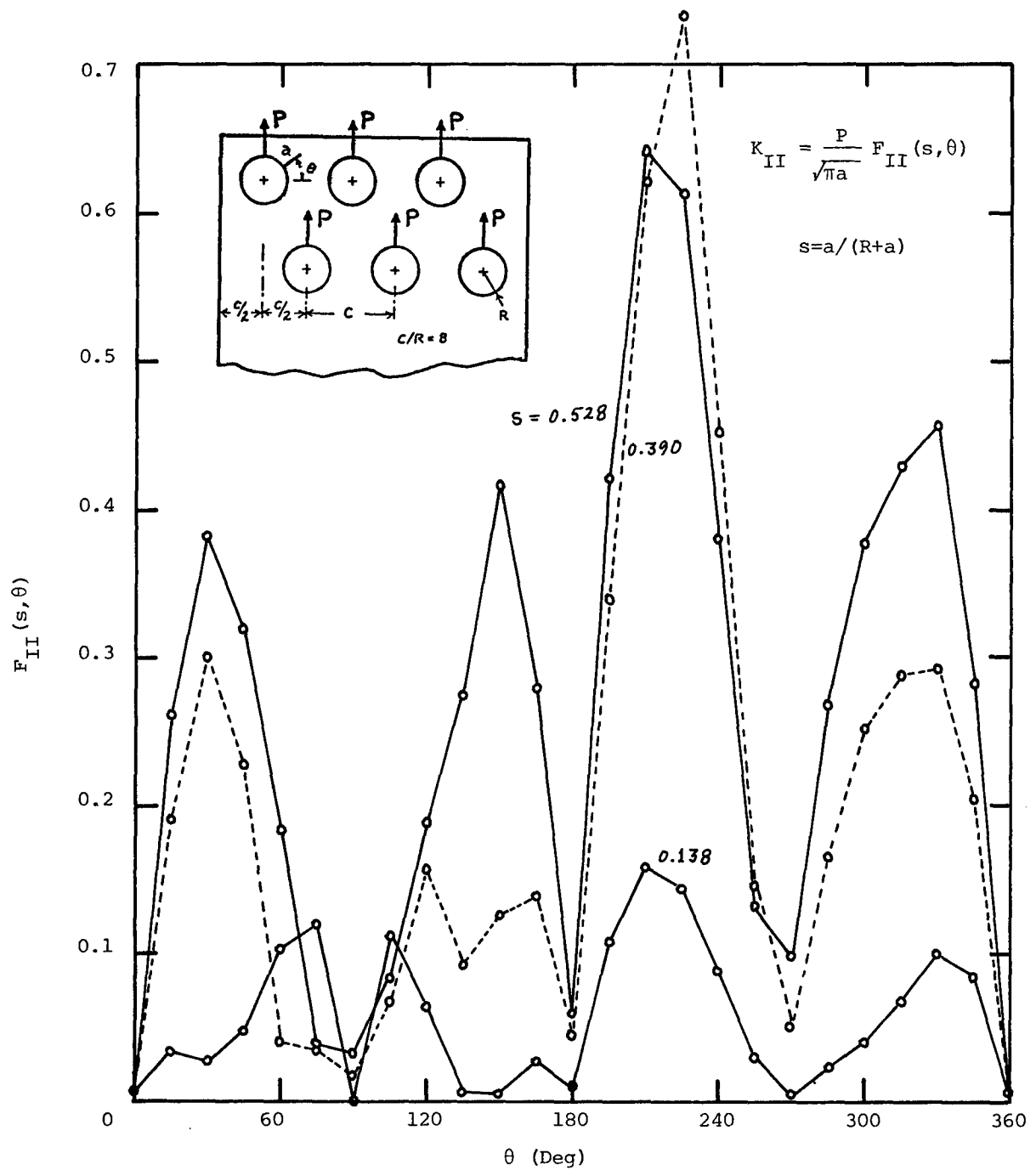


Figure 53. Double Row K_{II} Chart (Upper Left Hole Damaged, $C/D=4$)

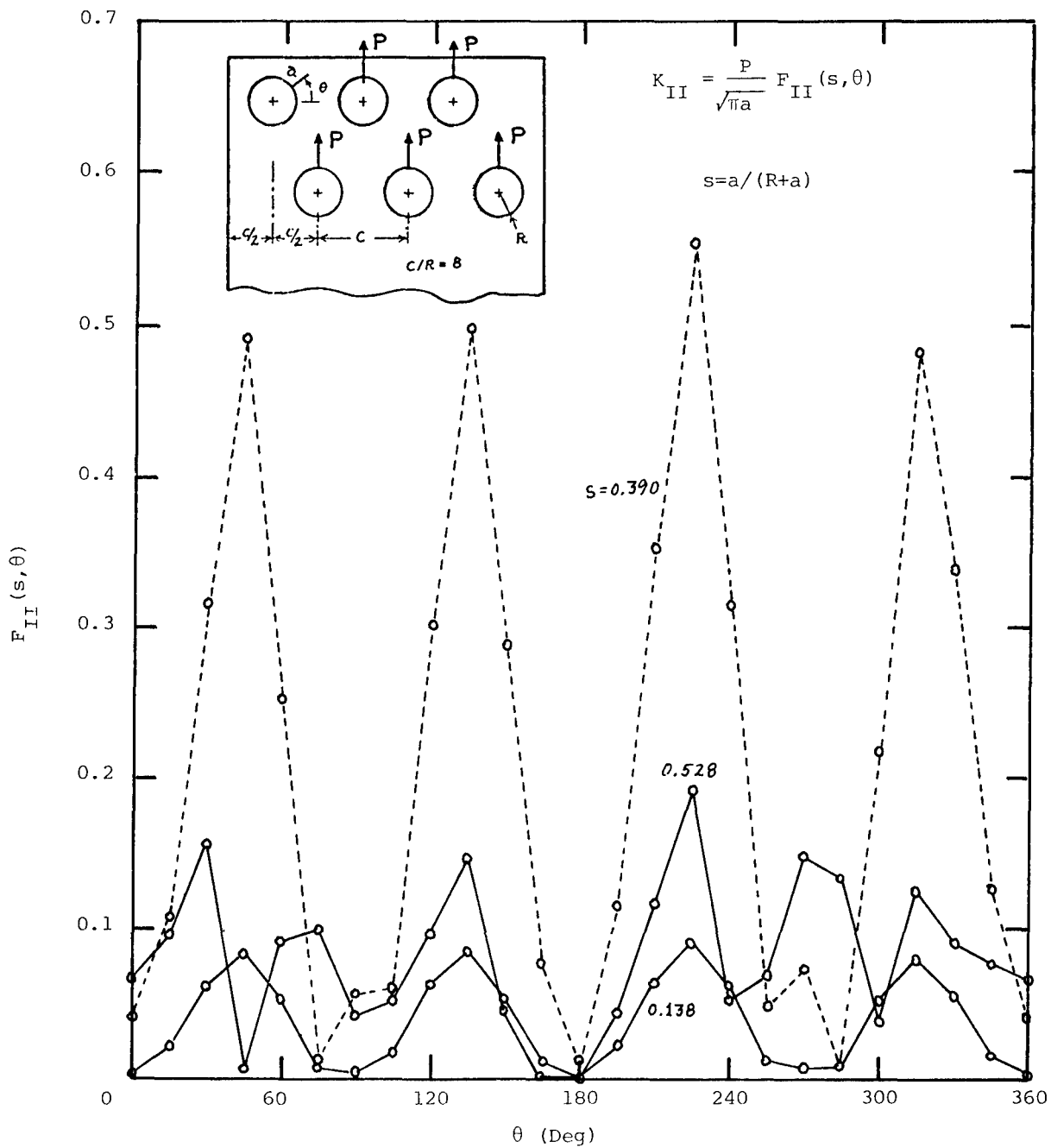


Figure 54. Double Row K_{II} Chart (Upper Left Hole Damaged and Unloaded, $C/D=4$)

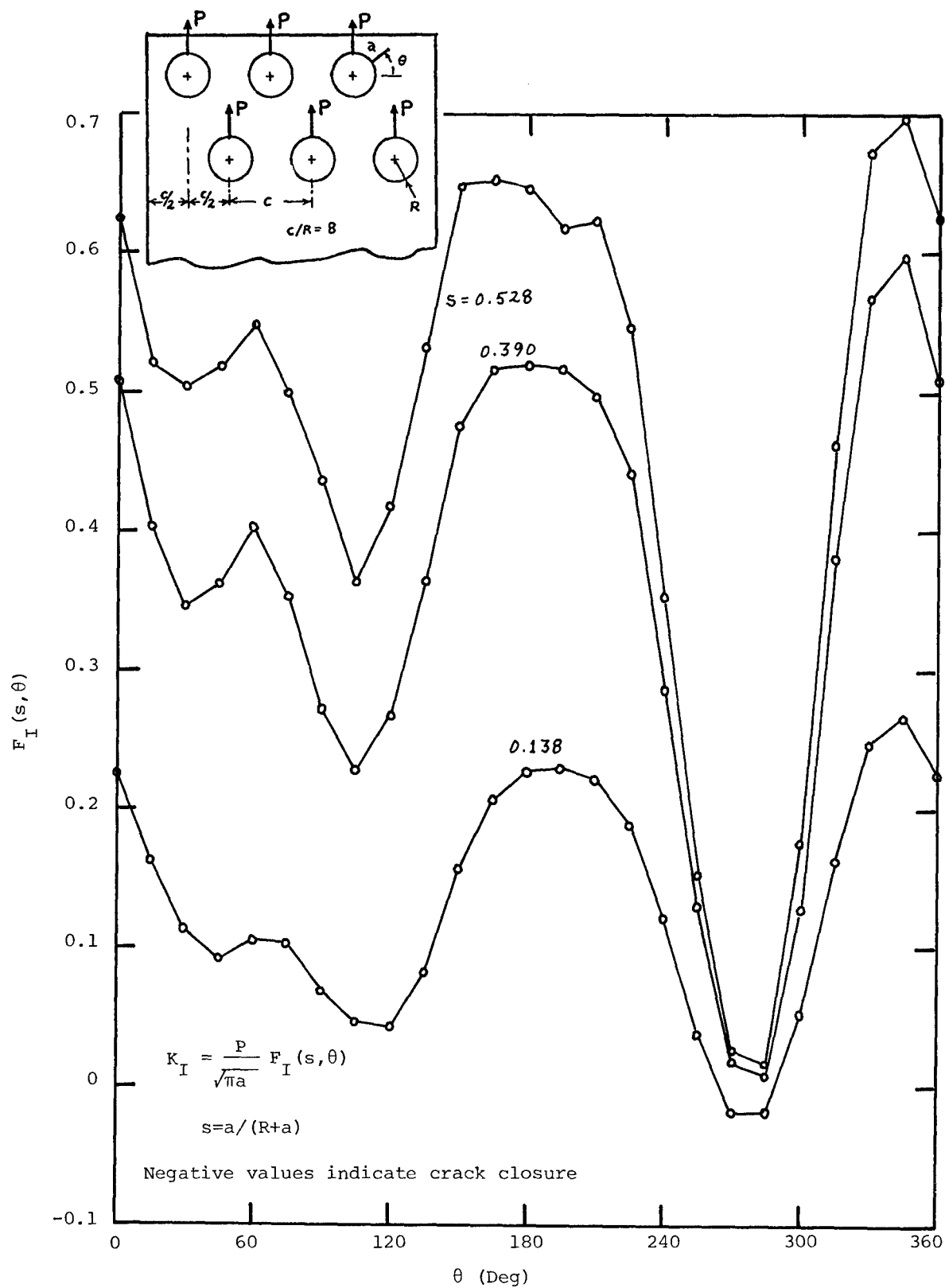


Figure 55. Double Row K_I Chart (Upper Right Hole Damaged, $C/D=4$)

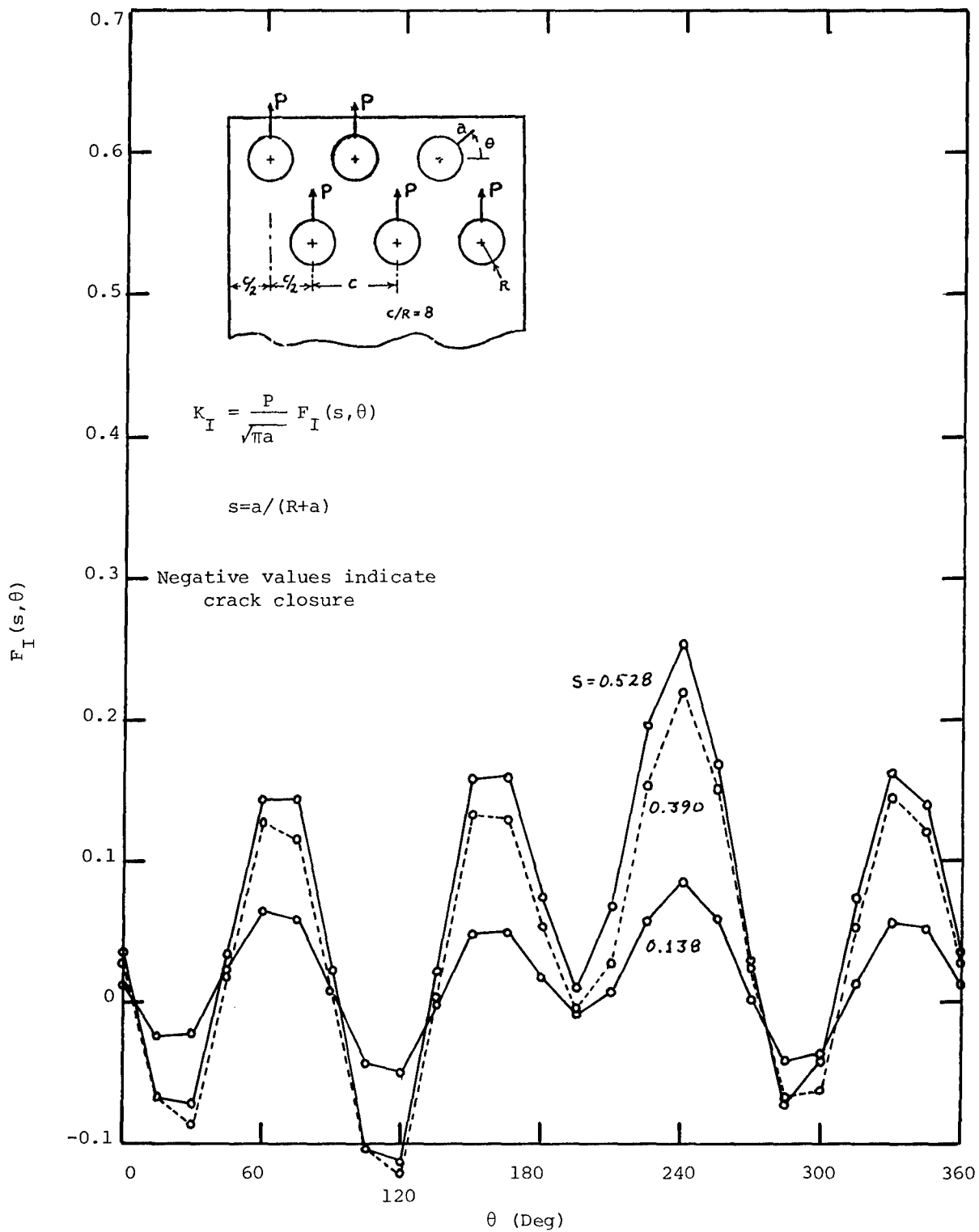


Figure 56. Double Row K_I Chart (Upper Right Hole Damaged and Unloaded, $C/D=4$)

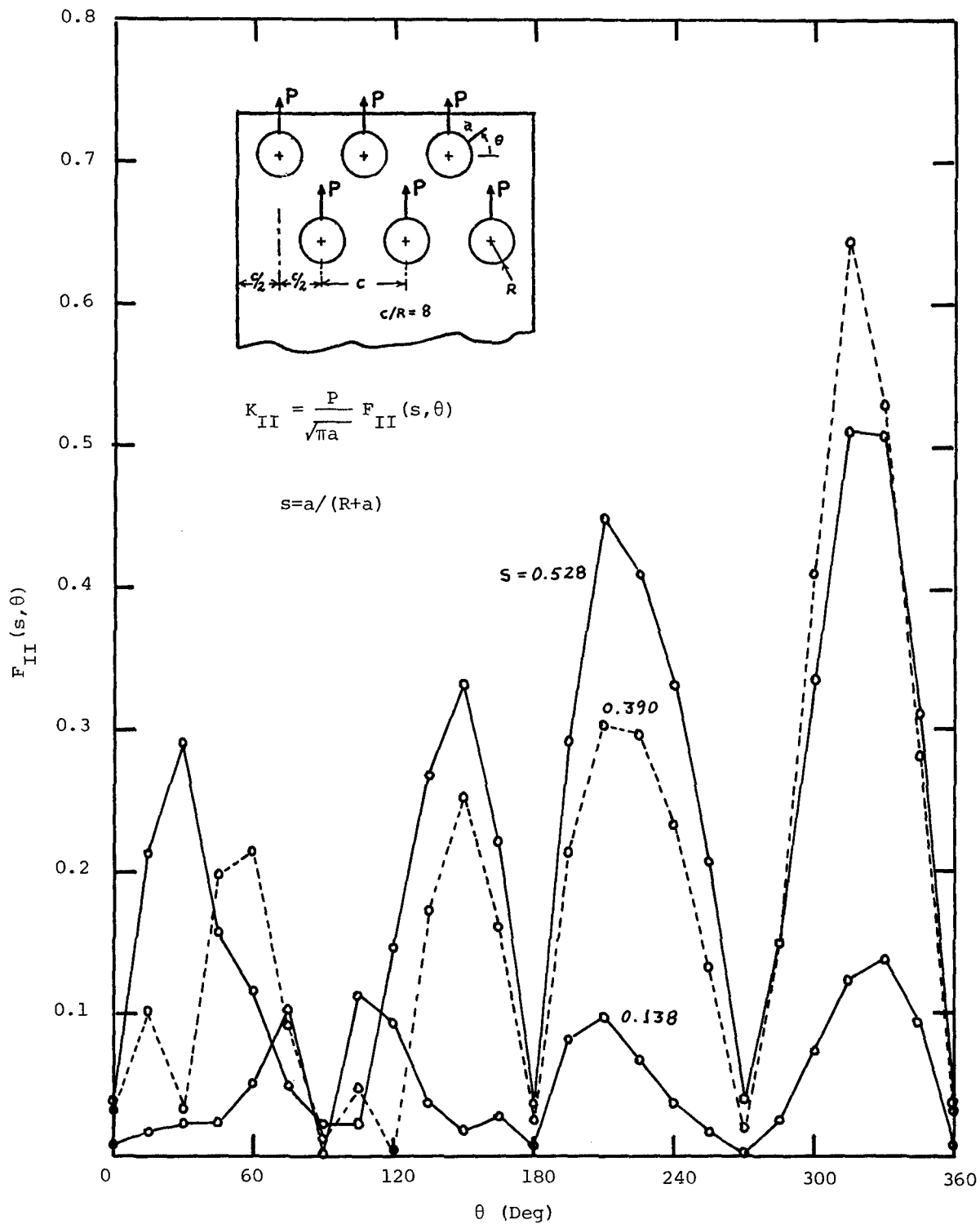


Figure 57. Double Row K_{II} Chart (Upper Right Hole Damaged, $C/D=4$)

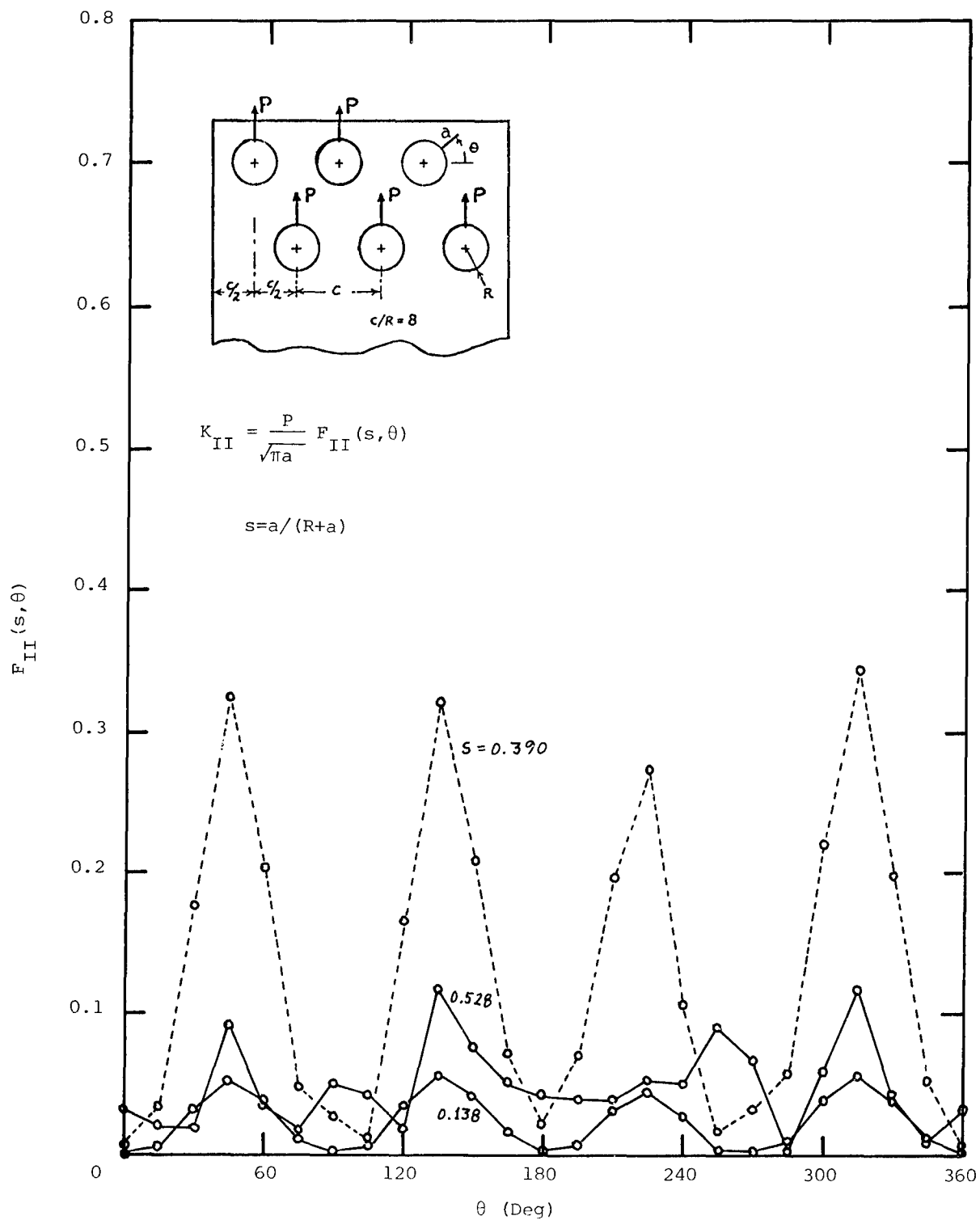


Figure 58. Double Row K_{II} Chart (Upper Right Hole Damaged and Unloaded, $C/D=4$)

TABLE 1
TYPICAL CORE STORAGE AND CPU TIME REQUIREMENTS

Program	Core Storage ⁽¹⁾			(1,2) CPU Time (Min.)
	KBYTES	Decimal Words	Octal Words	
Attachment Lug	250	62,500	172,044	1.1
Rectangular Panel	260 to 300	65,000 to 75,000	176,750 to 222,370	0.8 to 1.0
Single Fastener Row (3)	272	68,000	204,640	0.25 to 1.25
Double Fastener Row (3)	344	86,000	247,760	0.25 to 1.25

- (1) Includes data and object code produced by IBM FORTRAN G-1 and H(0) compilers.
- (2) Times are quoted for one complete set of K_I , K_{II} , solutions, i.e., one set of dimensions and all angular crack positions, on an IBM S-370/168.
- (3) Time and storage quoted for models possessing three fastener holes per row.

TABLE 2
UNIFORM BEARING ($R_2/R_1=1.5$)

$\theta^\circ \backslash a/R_1$.02	.04	.05	.10	.15	.20	.22
0	-.069 0	-.089 0	-.105 0	-.130 0	-.082 0	-.006 .001	.691 .001
11.25	.006 .011	.022 .040	.022 .047	.050 .109	.115 .168	.168 .210	.811 .314
22.5	.145 .028	.228 .028	.255 .031	.377 .099	.473 .184	.495 .277	1.004 .482
33.75	.227 .059	.342 .016	.384 .019	.560 .047	.682 .161	.706 .326	1.046 .626
45	.241 .079	.358 .026	.404 .021	.610 .090	.760 .257	.815 .512	.979 .888
56.25	.244 .072	.372 .018	.428 .042	.683 .231	.884 .461	1.005 .799	.988 1.212
67.5	.256 .049	.411 .058	.487 .095	.834 .320	1.116 .571	1.305 .918	1.129 1.303
78.75	.234 .024	.404 .043	.487 .068	.885 .207	1.226 .357	1.495 .566	1.228 .793
90	.196 .006	.348 .011	.428 .015	.801 .045	1.137 .088	1.424 .136	1.162 .124
101.25	.167 .006	.288 .064	.354 .095	.666 .262	.938 .447	1.163 .679	.921 .793
112.5	.121 .012	.193 .077	.235 .114	.435 .309	.606 .514	.744 .764	.560 .888
123.75	.062 .004	.089 .044	.109 .072	.200 .224	.278 .382	.348 .570	.212 .657
135	.024 .010	.028 .008	.034 .026	.056 .134	.071 .249	.089 .380	-.017 .434
146.25	.001 .006	-.009 .013	-.012 .031	-.036 .128	-.064 .227	-.079 .340	-.156 .387
157.5	-.024 .002	-.064 .022	-.078 .039	-.149 .123	-.212 .202	-.252 .292	-.301 .330
168.75	-.058 0	-.106 .018	-.129 .029	-.236 .080	-.322 .125	-.376 .175	-.404 .198
180	-.066 0	-.121 0	-.148 0	-.268 0	-.360 0	-.420 0	-.440 0

$$K = \frac{P}{\sqrt{\pi a}} F(a/R_1, \theta)$$

Upper values - F_I

Lower values - F_{II}

TABLE 3
UNIFORM BEARING ($R_2/R_1=2$)

$\theta^\circ \backslash a/R_1$.02	.04	.05	.10	.15	.20	.22
0	-.027 0	-.030 0	-.036 0	-.043 0	-.030 0	-.034 0	.300 0
11.25	-.013 .002	-.007 .032	-.009 .037	-.007 .069	.005 .093	-.006 .104	.312 .139
22.5	.021 .004	.047 .038	.051 .044	.073 .095	.086 .142	.063 .179	.341 .250
33.75	.053 .020	.096 .021	.107 .026	.152 .092	.174 .166	.154 .240	.375 .344
45	.073 .035	.125 .007	.141 .016	.216 .104	.264 .206	.270 .320	.422 .441
56.25	.083 .036	.144 .011	.167 .027	.281 .140	.371 .260	.421 .399	.497 .518
67.5	.090 .025	.162 .024	.194 .043	.352 .156	.484 .268	.577 .395	.574 .493
78.75	.095 .011	.176 .020	.215 .034	.402 .104	.558 .168	.677 .238	.609 .299
90	.104 .003	.188 .004	.230 .006	.419 .014	.573 .025	.695 .038	.586 .019
101.25	.105 .004	.177 .034	.216 .050	.386 .130	.523 .205	.627 .288	.501 .297
112.5	.098 .009	.149 .046	.179 .069	.309 .178	.412 .277	.490 .386	.369 .403
123.75	.075 .009	.104 .037	.123 .057	.202 .155	.266 .247	.315 .346	.207 .358
135	.047 .006	.060 .020	.069 .034	.106 .106	.134 .177	.157 .255	.065 .258
146.25	.020 .005	.019 .016	.021 .028	.024 .086	.023 .144	.026 .208	-.048 .212
157.5	-.008 .004	-.022 .015	-.027 .026	-.055 .073	-.079 .119	-.089 .169	-.143 .172
168.75	-.028 .002	-.054 .010	-.064 .017	-.115 .046	-.154 .072	-.171 .100	-.210 .103
180	-.035 0	-.065 0	-.078 0	-.138 0	-.182 0	-.200 0	-.233 0

$$K = \frac{P}{\sqrt{\pi a}} F(a/R_1, \theta)$$

Upper values - F_I
Lower values - F_{II}

TABLE 4
UNIFORM BEARING ($R_2/R_1=2.5$)

$\theta^\circ \backslash a/R_1$.02	.04	.05	.10	.15	.20	.25	.30	.35	.40	.45
0	-.015 0	-.017 0	-.019 0	-.015 0	.001 0	.022 0	.047 0	.075 0	.104 0	.129 0	.182 .001
11.25	-.013 .010	-.009 .038	-.009 .043	.004 .074	.025 .099	.047 .113	.069 .118	.092 .113	.118 .103	.141 .088	.200 .076
22.5	-.004 .002	.012 .032	.002 .034	.048 .069	.077 .108	.101 .138	.119 .158	.133 .167	.150 .169	.171 .166	.244 .175
33.75	.017 .037	.044 .015	.052 .018	.095 .011	.134 .058	.162 .102	.181 .141	.193 .176	.208 .211	.230 .249	.309 .309
45	.044 .076	.080 .063	.091 .065	.147 .021	.199 .038	.240 .090	.270 .142	.293 .198	.316 .266	.343 .347	.415 .465
56.25	.064 .095	.107 .079	.123 .073	.206 .002	.282 .074	.346 .129	.400 .183	.444 .248	.483 .331	.517 .436	.569 .580
67.5	.067 .081	.117 .057	.139 .045	.253 .043	.356 .110	.444 .157	.522 .201	.590 .256	.649 .330	.696 .422	.727 .548
78.75	.059 .042	.115 .022	.143 .011	.281 .049	.397 .088	.496 .111	.585 .132	.665 .159	.739 .196	.797 .244	.817 .310
90	.067 .002	.128 .002	.160 .003	.307 .007	.423 .013	.518 .019	.604 .027	.684 .034	.758 .042	.819 .050	.833 .056
101.25	.085 .022	.143 .001	.174 .016	.316 .088	.428 .136	.520 .169	.599 .200	.668 .235	.728 .278	.773 .329	.772 .390
112.5	.110 .026	.160 .002	.188 .024	.304 .129	.398 .201	.475 .250	.539 .293	.591 .342	.631 .401	.655 .474	.642 .560
123.75	.112 .018	.150 .001	.171 .019	.251 .113	.315 .184	.368 .234	.410 .279	.442 .329	.462 .391	.469 .463	.448 .545
135	.084 .008	.108 .002	.120 .011	.167 .073	.201 .125	.230 .168	.253 .208	.266 .253	.271 .307	.269 .366	.247 .432
146.25	.041 .005	.050 .004	.055 .005	.071 .049	.083 .088	.092 .121	.098 .155	.099 .192	.095 .235	.089 .283	.074 .335
157.5	.005 .008	-.001 .004	-.002 .004	-.014 .041	-.022 .071	-.029 .096	-.035 .121	-.042 .148	-.050 .179	-.054 .212	-.060 .248
168.75	-.015 .007	-.030 .003	-.038 .003	-.071 .027	-.095 .045	-.112 .059	-.127 .072	-.139 .086	-.148 .102	-.152 .119	-.151 .137
180	-.021 0	-.040 0	-.049 0	-.091 0	-.121 0	-.142 0	-.159 0	-.173 0	-.183 0	-.186 0	-.183 0

$$K = \frac{P}{\sqrt{\pi a}} F(a/R_1, \theta)$$

Upper values - F_I
Lower values - F_{II}

TABLE 5
UNIFORM BEARING ($R_2/R_1=3$)

$\theta^\circ \backslash a/R_1$.02	.04	.05	.10	.15	.20	.25	.30	.35	.40	.45
0	-.011 0	-.009 0	-.009 0	.002 0	.020 0	.040 0	.065 0	.084 0	.105 0	.119 0	.154 0
11.25	-.012 .014	-.007 .039	-.006 .043	.010 .069	.031 .090	.051 .101	.069 .103	.086 .095	.103 .082	.118 .065	.163 .051
22.5	-.013 .003	0 .034	.004 .036	.029 .067	.055 .100	.073 .125	.084 .138	.092 .141	.104 .135	.120 .125	.184 .124
33.75	-.004 .030	.016 .010	.021 .012	.053 .013	.082 .054	.102 .091	.112 .121	.118 .146	.127 .168	.146 .190	.222 .227
45	.015 .067	.040 .056	.048 .058	.089 .022	.127 .027	.157 .071	.177 .113	.191 .156	.207 .207	.230 .264	.299 .343
56.25	.034 .084	.066 .073	.077 .069	.139 .010	.197 .048	.246 .092	.284 .135	.316 .186	.344 .251	.372 .328	.421 .428
67.5	.042 .070	.080 .054	.097 .045	.185 .024	.265 .077	.333 .113	.392 .149	.441 .192	.485 .249	.519 .317	.544 .404
78.75	.043 .036	.088 .021	.110 .013	.220 .035	.312 .066	.388 .085	.455 .103	.516 .124	.568 .153	.607 .187	.618 .233
90	.055 .002	.105 .002	.131 .003	.250 .006	.342 .010	.416 .014	.481 .019	.541 .024	.594 .028	.635 .034	.640 .036
101.25	.070 .018	.117 0	.143 .013	.258 .071	.348 .109	.420 .134	.481 .158	.533 .183	.576 .213	.606 .249	.600 .288
112.5	.091 .021	.132 .001	.155 .019	.250 .104	.325 .162	.387 .200	.438 .233	.478 .269	.507 .313	.524 .363	.507 .421
123.75	.095 .014	.127 0	.144 .016	.211 .092	.264 .149	.307 .189	.342 .225	.367 .263	.381 .309	.386 .361	.365 .417
135	.074 .004	.095 .001	.106 .010	.146 .062	.177 .103	.201 .137	.221 .169	.232 .205	.236 .245	.234 .290	.214 .335
146.25	.039 .001	.047 .002	.053 .006	.069 .041	.082 .071	.091 .097	.098 .124	.100 .153	.098 .187	.094 .223	.080 .258
157.5	.008 .003	.005 .003	.005 .004	-.001 .032	-.004 .055	-.006 .075	-.009 .095	-.012 .116	-.016 .140	-.018 .164	-.024 .188
168.75	-.010 .004	-.021 .002	-.026 .002	-.049 .021	-.064 .034	-.075 .045	-.084 .056	-.090 .067	-.096 .079	-.096 .091	-.095 .103
180	-.015 0	-.029 0	-.036 0	-.066 0	-.086 0	-.100 0	-.111 0	-.119 0	-.124 0	-.123 0	-.120 0

$$K = \frac{P}{\sqrt{\pi a}} F(a/R_1, \theta)$$

Upper values - F_I

Lower values - F_{II}

TABLE 6
COSINE BEARING ($R_2/R_1=1.5$)

$\theta^\circ \backslash a/R_1$.02	.04	.05	.10	.15	.20	.22
0	.037 0	.092 0	.116 0	.268 0	.458 0	.639 0	1.038 0
11.25	.079 .004	.150 .008	.180 .001	.347 .022	.528 .058	.677 .137	1.062 .139
22.5	.156 .011	.255 .003	.293 .011	.479 .051	.639 .094	.731 .184	1.079 .148
33.75	.199 .026	.309 .014	.349 .027	.534 .053	.675 .066	.736 .095	1.038 .005
45	.197 .040	.303 .018	.341 .023	.519 .003	.654 .038	.714 .102	.946 .265
56.25	.172 .042	.273 .004	.312 .004	.500 .080	.651 .178	.742 .333	.888 .545
67.5	.137 .030	.236 .013	.279 .029	.497 .133	.692 .264	.846 .466	.905 .686
78.75	.101 .021	.200 .007	.249 .020	.505 .101	.754 .207	.981 .365	.971 .518
90	.131 .008	.243 .008	.301 .008	.588 .006	.863 .001	1.115 .001	1.046 .025
101.25	.214 .012	.346 .057	.416 .082	.722 .199	.986 .317	1.179 .472	1.062 .539
112.5	.234 .017	.353 .082	.416 .120	.683 .299	.884 .470	1.005 .670	.880 .751
123.75	.182 .025	.258 .074	.299 .106	.470 .254	.597 .390	.669 .546	.557 .598
135	.116 .016	.157 .038	.179 .057	.271 .146	.337 .235	.373 .336	.279 .361
146.25	.062 .009	.080 .020	.090 .031	.129 .090	.154 .151	.168 .223	.093 .239
157.5	.015 .005	.012 .015	.012 .024	.008 .069	.003 .116	.004 .170	-.051 .183
168.75	-.019 .001	-.038 .009	-.046 .015	-.082 .042	-.108 .069	-.115 .099	-.154 .108
180	-.031 0	-.055 0	-.066 0	-.114 0	-.147 0	-.157 0	-.190 0

$$K = \frac{P}{\sqrt{\pi a}} \quad F(a/R_1, \theta)$$

Upper values - F_I

Lower values - F_{II}

TABLE 7
COSINE BEARING ($R_2/R_1=2$)

$\theta^\circ \backslash a/R_1$.02	.04	.05	.10	.15	.20	.22
0	.022 0	.055 0	.068 0	.143 0	.219 0	.263 0	.521 0
11.25	.030 .002	.067 .014	.081 .011	.156 .003	.226 .008	.263 .033	.516 .019
22.5	.048 0	.093 .017	.108 .010	.181 .002	.238 .010	.256 .038	.496 .005
33.75	.061 .009	.111 .009	.125 .004	.194 .005	.238 .009	.241 .004	.460 .060
45	.061 .020	.110 .001	.124 .001	.190 .021	.234 .050	.237 .082	.427 .156
56.25	.049 .025	.096 .005	.111 .001	.187 .042	.244 .093	.270 .157	.421 .238
67.5	.037 .019	.083 .003	.101 .005	.196 .052	.281 .108	.343 .180	.450 .256
78.75	.034 .017	.085 .007	.109 .002	.234 .035	.348 .082	.441 .138	.491 .195
90	.070 .008	.132 .008	.163 .008	.310 .004	.435 .006	.536 .015	.529 .033
101.25	.116 .010	.186 .034	.222 .047	.376 .102	.498 .146	.586 .195	.536 .200
112.5	.130 .008	.194 .041	.227 .062	.372 .156	.480 .235	.548 .318	.475 .335
123.75	.118 .015	.165 .040	.190 .059	.298 .143	.379 .216	.430 .294	.349 .305
135	.089 .014	.119 .024	.135 .037	.206 .091	.258 .142	.290 .199	.210 .200
146.25	.054 .011	.070 .014	.079 .021	.117 .055	.145 .090	.165 .131	.090 .129
157.5	.020 .007	.023 .009	.026 .014	.037 .038	.046 .064	.058 .093	-.008 .092
168.75	-.005 .002	-.012 .004	-.014 .008	-.024 .022	-.028 .037	-.019 .053	-.076 .053
180	-.013 0	-.025 0	-.029 0	-.046 0	-.055 0	-.047 0	-.100 0

$$K = \frac{P}{\sqrt{\pi a}} F(a/R_1, \theta)$$

Upper values - F_I

Lower values - F_{II}

TABLE 8
COSINE BEARING ($R_2/R_1=2.5$)

$\theta^\circ \backslash a/R_1$.02	.04	.05	.10	.15	.20	.25	.30	.35	.40	.45
0	.015 0	.039 0	.049 0	.116 0	.177 0	.234 0	.290 0	.344 0	.397 0	.438 0	.484 .001
11.25	.019 .020	.046 .034	.058 .032	.125 .027	.188 .028	.243 .027	.294 .020	.343 .003	.390 .022	.428 .054	.478 .090
22.5	.028 .022	.060 .040	.072 .034	.140 .019	.201 .018	.251 .020	.292 .015	.327 .002	.362 .030	.394 .070	.457 .112
33.75	.034 0	.069 .013	.080 .005	.141 .013	.195 .011	.237 .002	.269 .003	.294 .001	.319 .008	.349 .023	.425 .034
45	.032 .033	.066 .028	.075 .034	.128 .035	.178 .023	.218 .008	.249 .007	.273 .023	.298 .044	.330 .069	.415 .110
56.25	.021 .059	.051 .058	.061 .059	.118 .040	.175 .018	.224 .001	.264 .021	.298 .053	.334 .100	.374 .160	.454 .246
67.5	.010 .058	.038 .060	.050 .059	.120 .033	.192 .012	.257 .005	.316 .030	.370 .070	.424 .128	.476 .203	.543 .301
78.75	.004 .049	.035 .053	.051 .051	.145 .030	.236 .011	.318 .008	.394 .034	.465 .070	.532 .118	.590 .174	.632 .242
90	.043 .009	.087 .011	.111 .012	.226 .010	.323 .003	.405 .007	.482 .018	.553 .028	.621 .038	.676 .044	.700 .050
101.25	.102 .004	.160 .018	.190 .032	.319 .090	.418 .119	.498 .130	.566 .137	.627 .149	.680 .167	.721 .196	.726 .233
112.5	.138 .021	.198 .007	.229 .030	.357 .130	.455 .192	.532 .228	.595 .255	.643 .286	.676 .326	.692 .375	.672 .436
123.75	.152 .007	.206 .016	.232 .037	.333 .130	.409 .192	.470 .230	.517 .261	.551 .296	.568 .339	.569 .391	.539 .450
135	.128 .009	.167 .019	.186 .033	.255 .090	.306 .129	.348 .158	.380 .187	.400 .218	.407 .255	.403 .297	.374 .340
146.25	.079 .013	.101 .014	.112 .021	.153 .048	.185 .070	.211 .091	.231 .115	.244 .141	.247 .170	.243 .200	.223 .228
157.5	.032 .006	.040 .004	.044 .009	.062 .025	.077 .040	.091 .056	.103 .074	.111 .093	.114 .112	.116 .132	.110 .149
168.75	.002 0	0 .001	0 .001	-.001 .012	.002 .021	.006 .031	.012 .041	.017 .050	.022 .060	.030 .069	.032 .076
180	-.007 0	-.012 0	-.014 0	-.022 0	-.025 0	-.024 0	-.020 0	-.016 0	-.010 0	-.001 0	.005 0

$$K = \frac{P}{\sqrt{\pi a}} F(a/R_1, \theta)$$

Upper values - F_I

Lower values - F_{II}

TABLE 9
COSINE BEARING ($R_2/R_1=3$)

$\theta^\circ \backslash a/R_1$.02	.04	.05	.10	.15	.20	.25	.30	.35	.40	.45
0	.014 0	.036 0	.048 0	.107 0	.161 0	.209 0	.253 0	.295 0	.333 0	.358 0	.387 0
11.25	.015 .021	.039 .035	.050 .033	.109 .030	.163 .031	.209 .030	.250 .023	.285 .007	.319 .015	.344 .043	.379 .071
22.5	.015 .023	.042 .041	.052 .036	.109 .025	.160 .025	.199 .027	.230 .021	.254 .005	.279 .022	.302 .057	.355 .090
33.75	.013 .003	.040 .016	.049 .009	.096 .006	.139 .004	.171 .003	.193 .007	.209 .003	.226 .008	.249 .024	.321 .035
45	.007 .028	.032 .023	.038 .029	.078 .032	.116 .023	.146 .013	.166 .002	.181 .010	.197 .025	.224 .040	.305 .068
56.25	-.001 .052	.021 .053	.027 .056	.070 .045	.114 .032	.150 .020	.178 .004	.201 .022	.227 .058	.259 .104	.335 .164
67.5	-.005 .052	.016 .057	.024 .058	.078 .044	.135 .032	.184 .022	.229 .002	.268 .031	.309 .078	.348 .136	.406 .208
78.75	-.005 .046	.019 .052	.031 .052	.107 .040	.181 .027	.246 .012	.306 .011	.359 .043	.410 .082	.449 .128	.479 .181
90	.035 .009	.071 .011	.090 .012	.184 .010	.262 .004	.328 .006	.387 .017	.442 .028	.490 .038	.528 .044	.539 .051
101.25	.087 .001	.136 .017	.161 .030	.267 .078	.345 .100	.407 .107	.459 .111	.504 .116	.542 .127	.568 .144	.565 .165
112.5	.114 .017	.164 .006	.189 .025	.295 .108	.373 .159	.435 .187	.483 .208	.519 .230	.542 .258	.550 .293	.527 .331
123.75	.127 .005	.171 .013	.192 .031	.276 .108	.338 .158	.387 .189	.425 .214	.451 .240	.462 .272	.460 .309	.431 .348
135	.108 .009	.141 .016	.157 .028	.216 .074	.258 .106	.293 .130	.319 .152	.335 .177	.340 .205	.335 .235	.308 .265
146.25	.069 .013	.088 .012	.098 .018	.135 .040	.163 .056	.186 .072	.204 .090	.214 .111	.216 .133	.214 .156	.194 .175
157.5	.030 .007	.038 .004	.042 .008	.060 .019	.075 .029	.089 .041	.101 .056	.109 .070	.113 .085	.115 .100	.108 .110
168.75	.004 .001	.004 .001	.005 .001	.008 .008	.014 .014	.021 .022	.028 .030	.035 .038	.041 .045	.048 .051	.049 .055
180	-.004 0	-.007 0	-.008 0	-.010 0	-.008 0	-.004 0	.001 0	.008 0	.015 0	.024 0	.028 0

$$K = \frac{P}{\sqrt{\pi a}} F(a/R_1, \theta)$$

Upper values - F_I
Lower values - F_{II}

TABLE 10
RANGE OF PARAMETER STUDY FOR
FASTENER ROW PROGRAMS

Fastener hole diameter = 0.625 inch
Fastener hole radius, R = 0.3125 inch

Crack Size, a (in.)	$s=a/(R+a)$	a/R
0.005	0.0158	0.016
0.03	0.0875	0.096
0.05	0.138	0.16
0.10	0.242	0.32
0.20	0.390	0.64
0.30	0.490	0.96
0.35	0.528	1.12

TABLE 11
SINGLE FASTENER ROW (CENTER HOLE
DAMAGED, C/D=4)

a/R	.016	.096	.16	.32	.64	.96	1.12
θ°	.0158	.0875	.138	.242	.390	.490	.528
90	-.019 0	.020 0	.054 0	.149 0	.223 0	.304 0	.331 0
75	-.041 .098	.020 .089	.058 .116	.161 .014	.234 .042	.307 .056	.321 .072
60	-.073 .184	.023 .050	.058 .085	.183 .056	.276 .032	.358 .152	.373 .201
45	-.080 .226	.042 .029	.081 .021	.215 .008	.341 .089	.438 .255	.473 .295
30	-.060 .187	.082 .052	.141 .007	.286 .130	.434 .207	.549 .325	.595 .364
15	-.022 .085	.119 .015	.194 .025	.344 .112	.490 .142	.590 .189	.631 .220
0	.028 .007	.149 .006	.228 .010	.367 .012	.521 .038	.611 .048	.656 .054
-15	.088 .013	.168 .042	.242 .090	.367 .151	.546 .254	.625 .298	.657 .330
-30	.129 .084	.170 .056	.227 .116	.326 .201	.523 .406	.600 .448	.649 .481
-45	.122 .157	.135 .050	.172 .090	.238 .126	.403 .429	.462 .415	.506 .430
-60	.076 .168	.069 .030	.089 .048	.119 .043	.211 .278	.257 .272	.278 .287
-75	.027 .104	.012 .008	.018 .016	.026 .021	.086 .108	.113 .125	.121 .134
-90	.007 0	-.009 0	-.009 0	-.012 0	.041 0	.060 0	.070 0

$$K = \frac{P}{\sqrt{\pi a}} F(s, \theta)$$

Upper values - F_I
Lower values - F_{II}

TABLE 12
SINGLE FASTENER ROW (CENTER HOLE
DAMAGED, C/D VARIED)

$\frac{a}{R}$ θ°	C/D = 3.2			C/D = 3.6			C/D = 4.8		
	.16	.64	1.12	.16	.64	1.12	.16	.64	1.12
s	.138	.390	.528	.138	.390	.528	.138	.390	.528
90	.053 0	.230 0	.349 0	.054 0	.226 0	.338 0	.055 0	.222 0	.320 0
75	.061 .119	.256 .023	.372 .111	.059 .117	.242 .035	.340 .088	.056 .114	.222 .052	.294 .053
60	.074 .093	.322 .009	.460 .250	.065 .092	.292 .016	.405 .220	.050 .081	.252 .054	.334 .174
45	.111 .034	.429 .154	.601 .360	.093 .026	.377 .116	.525 .324	.064 .014	.296 .051	.407 .252
30	.177 .021	.535 .255	.739 .424	.156 .013	.475 .228	.654 .392	.120 .002	.377 .178	.512 .320
15	.227 .035	.585 .169	.772 .262	.208 .029	.529 .154	.690 .238	.174 .018	.434 .123	.546 .190
0	.259 .010	.614 .038	.804 .044	.242 .010	.560 .038	.718 .050	.210 .010	.465 .039	.572 .059
-15	.276 .100	.650 .278	.825 .366	.256 .094	.590 .264	.726 .346	.221 .084	.484 .239	.565 .309
-30	.267 .129	.648 .457	.828 .546	.244 .122	.575 .427	.721 .508	.204 .108	.452 .377	.547 .438
-45	.208 .101	.504 .503	.642 .503	.187 .095	.445 .458	.564 .460	.150 .083	.342 .388	.425 .386
-60	.110 .056	.266 .330	.346 .339	.098 .052	.234 .301	.309 .309	.076 .044	.176 .247	.231 .250
-75	.025 .020	.109 .130	.153 .164	.021 .018	.096 .118	.136 .147	.014 .015	.070 .094	.098 .114
-90	-.007 0	.055 0	.083 0	-.008 0	.046 0	.076 0	-.008 0	.034 0	.059 0

$$K = \frac{P}{\sqrt{\pi a}} F(s, \theta)$$

Upper values - F_I

Lower values - F_{II}

TABLE 13
SINGLE FASTENER ROW (CENTER HOLE
DAMAGED AND UNLOADED, C/D=4)

a/R	.16	.64	1.12
θ°	.138	.390	.528
90	- .012 0	-.048 0	- .093 0
75	- .014 .005	-.059 .011	- .100 .029
60	- .013 .012	-.064 .056	- .099 .068
45	0 .018	-.016 .102	- .027 .102
30	.017 .016	.043 .088	.061 .094
15	.022 .010	.065 .037	.094 .055
0	.026 .001	.058 .013	.092 .033
-15	.022 .004	.063 .003	.093 0
-30	.030 .005	.090 .003	.138 .002
-45	.034 .005	.104 .025	.151 .042
-60	.024 .005	.077 .047	.113 .057
-75	.008 .003	.038 .026	.056 .034
-90	.001 0	.002 0	.037 0

$$K = \frac{P}{\sqrt{\pi a}} F(s, \theta)$$

Upper values - F_I
Lower values - F_{II}

TABLE 14

SINGLE FASTENER ROW (LEFT HOLE
DAMAGED, C/D=4)

a/R \ θ°	.016	.096	.16	.32	.64	.96	1.12
s	.0158	.0875	.138	.242	.390	.490	.528
0	.029 .007	.152 .007	.232 .013	.374 .024	.532 .067	.626 .094	.672 .108
15	-.014 .085	.137 .014	.217 .026	.378 .113	.538 .129	.648 .159	.690 .178
30	-.047 .185	.108 .046	.174 .016	.337 .155	.508 .230	.633 .321	.685 .351
45	-.068 .220	.063 .017	.108 .034	.255 .046	.406 .160	.516 .286	.561 .315
60	-.068 .178	.030 .060	.069 .096	.199 .030	.303 .033	.404 .191	.429 .232
75	-.040 .096	.019 .093	.056 .122	.154 .004	.236 .001	.324 .103	.350 .120
90	-.020 0	.016 0	.049 .003	.143 .012	.222 .030	.317 .044	.353 .049
105	-.041 .099	.017 .086	.052 .122	.156 .027	.239 .080	.322 .013	.342 .024
120	-.078 .188	.012 .039	.044 .077	.168 .084	.269 .104	.354 .115	.366 .170
135	-.091 .229	.017 .044	.050 .009	.175 .039	.290 .012	.382 .235	.412 .286
150	-.072 .188	.052 .061	.104 .001	.234 .105	.368 .193	.480 .360	.524 .416
165	-.029 .086	.101 .015	.172 .027	.312 .116	.451 .170	.555 .252	.601 .298

$$K = \frac{P}{\sqrt{\pi a}} F(s, \theta)$$

Upper values - F_I

Lower values - F_{II}

TABLE 14
(Concluded)

$\theta^\circ \backslash \begin{matrix} a/R \\ s \end{matrix}$.016	.096	.16	.32	.64	.96	1.12
	.0158	.0875	.138	.242	.390	.490	.528
180	.029 .007	.153 .006	.234 .007	.375 .001	.535 .011	.634 .009	.685 .009
195	.095 .009	.189 .046	.268 .095	.404 .163	.597 .268	.685 .304	.725 .336
210	.137 .077	.190 .069	.252 .133	.361 .247	.568 .480	.639 .503	.685 .534
225	.126 .152	.141 .068	.179 .111	.242 .183	.402 .541	.446 .490	.485 .500
240	.074 .163	.062 .042	.079 .064	.098 .079	.170 .348	.201 .324	.215 .336
255	.025 .100	.001 .013	.002 .025	-.001 .039	.040 .144	.054 .162	.056 .173
270	.006 0	-.018 0	-.023 .002	-.036 .007	.002 .014	.011 .018	.015 .019
285	.023 .101	.003 .008	.004 .018	.004 .020	.052 .099	.070 .121	.075 .133
300	.068 .163	.055 .025	.069 .047	.094 .034	.174 .254	.210 .277	.224 .300
315	.110 .155	.113 .042	.144 .085	.199 .100	.349 .393	.402 .423	.439 .448
330	.116 .085	.146 .051	.199 .113	.286 .185	.470 .405	.541 .477	.590 .520
345	.081 .015	.155 .042	.226 .092	.345 .155	.516 .277	.595 .342	.628 .351

$$K = \frac{P}{\sqrt{\pi a}} F(s, \theta)$$

Upper values - F_I
Lower values - F_{II}

TABLE 15
DOUBLE FASTENER ROW (CENTER HOLE
IN UPPER ROW DAMAGED, C/D=4)

$\frac{a}{R}$.016	.096	.16	.32	.64	.96	1.12
θ°	.0158	.0875	.138	.242	.390	.490	.528
0	.029 .011	.155 .006	.237 .007	.382 .003	.543 .014	.632 .009	.675 .010
15	-.051 .110	.119 .013	.195 .028	.354 .125	.490 .158	.589 .218	.626 .251
30	-.103 .259	.081 .053	.141 .006	.302 .140	.432 .186	.554 .311	.602 .349
45	-.122 .338	.045 .033	.085 .015	.241 .017	.362 .034	.479 .208	.522 .242
60	-.102 .303	.028 .046	.067 .077	.216 .048	.315 .085	.427 .097	.456 .136
75	-.055 .176	.027 .086	.069 .109	.194 .012	.275 .073	.380 .018	.410 .025
90	-.025 0	.030 0	.070 .001	.188 .004	.271 .009	.386 .013	.429 .015
105	-.050 .175	.038 .085	.082 .109	.213 .012	.301 .065	.409 .038	.439 .050
120	-.095 .303	.044 .041	.086 .072	.242 .064	.351 .102	.466 .098	.495 .144
135	-.116 .340	.057 .040	.100 .007	.261 .007	.387 .012	.505 .189	.550 .229
150	-.100 .260	.086 .059	.147 .001	.309 .125	.437 .151	.561 .292	.611 .333
165	-.050 .110	.120 .015	.196 .026	.355 .118	.487 .138	.588 .197	.625 .229

$$K = \frac{P}{\sqrt{\pi a}} F(s, \theta)$$

Upper values - F_I

Lower values - F_{II}

TABLE 15
(Concluded)

$\theta^\circ \backslash \frac{a}{R}$.016	.096	.16	.32	.64	.96	1.12
	.0158	.0875	.138	.242	.390	.490	.528
180	.029 .011	.155 .006	.237 .009	.382 .004	.542 .029	.632 .032	.674 .034
195	.119 .036	.180 .043	.259 .092	.385 .148	.586 .255	.666 .284	.700 .311
210	.118 .153	.185 .060	.247 .124	.343 .203	.573 .430	.652 .462	.708 .492
225	.170 .270	.146 .059	.187 .102	.245 .128	.449 .498	.514 .465	.565 .480
240	.108 .286	.071 .038	.091 .061	.111 .045	.229 .346	.279 .330	.304 .351
255	.040 .180	.005 .012	.009 .023	.004 .023	.079 .146	.099 .164	.104 .180
270	.014 0	-.015 0	-.016 .001	-.032 .004	.032 .009	.044 .014	.052 .017
285	.044 .181	.016 .011	.023 .023	.024 .022	.104 .155	.128 .185	.135 .207
300	.114 .288	.086 .034	.110 .056	.139 .029	.267 .330	.320 .333	.348 .360
315	.176 .270	.159 .051	.202 .095	.266 .104	.476 .452	.575 .446	.598 .467
330	.181 .153	.190 .055	.254 .118	.351 .188	.578 .393	.660 .443	.718 .476
345	.120 .036	.181 .042	.260 .090	.387 .141	.585 .235	.665 .264	.700 .289

$$K = \frac{P}{\sqrt{\pi a}} F(s, \theta)$$

Upper values - F_I
Lower values - F_{II}

TABLE 16

DOUBLE FASTENER ROW (CENTER HOLE
IN LOWER ROW DAMAGED, C/D=4)

a/R \ θ°	.016	.096	.16	.32	.64	.96	1.12
s	.0158	.0875	.138	.242	.390	.490	.528
0	.046 .009	.243 .007	.374 .012	.604 .019	.872 .062	1.036 .082	1.119 .093
15	-.011 .123	.219 .006	.342 .076	.586 .198	.841 .265	1.018 .355	1.092 .410
30	-.044 .261	.187 .024	.284 .080	.514 .258	.763 .437	.954 .646	1.040 .722
45	-.066 .317	.128 0	.192 .088	.390 .120	.589 .377	.744 .616	.811 .682
60	-.071 .275	.061 .076	.105 .137	.263 .036	.373 .214	.494 .464	.519 .545
75	-.049 .162	.009 .101	.039 .145	.146 .054	.208 .087	.294 .238	.306 .277
90	-.033 0	-.016 0	.003 .001	.085 .005	.138 .011	.220 .016	.243 .019
105	-.057 .160	-.004 .102	.022 .145	.123 .054	.176 .079	.259 .215	.270 .247
120	-.083 .270	.043 .081	.083 .144	.232 .056	.331 .241	.450 .466	.474 .589
135	-.076 .307	.115 .010	.175 .098	.371 .150	.563 .438	.720 .645	.784 .706
150	-.049 .250	.182 .017	.278 .087	.510 .275	.763 .484	.956 .675	1.042 .749
165	-.013 .117	.220 .009	.342 .080	.588 .206	.849 .291	1.030 .385	1.107 .442

$$K = \frac{P}{\sqrt{\pi a}} F(s, \theta)$$

Upper values - F_I
Lower values - F_{II}

TABLE 16
(Concluded)

a/R	.016	.096	.16	.32	.64	.96	1.12
θ°	.0158	.0875	.138	.242	.390	.490	.528
180	.046 .010	.245 .007	.376 .010	.609 .011	.881 .041	1.051 .052	1.136 .059
195	.130 .013	.266 .065	.386 .143	.596 .237	.897 .403	1.047 .493	1.116 .553
210	.192 .111	.267 .086	.360 .189	.524 .316	.845 .663	.988 .779	1.073 .847
225	.181 .217	.210 .080	.269 .155	.376 .210	.632 .731	.736 .762	.807 .801
240	.109 .232	.100 .053	.126 .095	.170 .100	.297 .517	.368 .548	.397 .584
255	.035 .141	0 .019	-.001 .042	-.003 .065	.067 .225	.103 .272	.112 .297
270	.005 0	-.040 0	-.054 .001	-.080 .005	-.024 .012	-.003 .020	.006 .023
285	.032 .138	-.011 .019	-.015 .041	-.024 .062	.040 .207	.072 .242	.081 .260
300	.104 .225	.081 .056	.103 .099	.136 .114	.252 .518	.316 .529	.340 .562
315	.175 .209	.192 .086	.246 .160	.343 .231	.585 .762	.680 .770	.746 .804
330	.188 .103	.256 .092	.346 .193	.503 .329	.816 .695	.948 .797	1.027 .863
345	.129 .007	.262 .067	.381 .145	.585 .246	.883 .426	1.025 .519	1.091 .582

$$K = \frac{P}{\sqrt{\pi a}} F(s, \theta)$$

Upper values - F_I
Lower values - F_{II}

TABLE 17

DOUBLE FASTENER ROW (CENTER HOLE)
IN LOWER ROW DAMAGED AND UNLOADED, C/D=4)

a/R	.016	.096	.16	.32	.64	.96	1.12
θ°	.0158	.0875	.138	.242	.390	.490	.528
0	.024 .006	.134 0	.209 .001	.348 0	.527 .019	.654 .021	.721 .023
15	-.009 .060	.140 .030	.209 .072	.354 .125	.517 .179	.649 .250	.708 .290
30	-.015 .142	.149 .037	.203 .098	.339 .181	.486 .309	.619 .453	.687 .512
45	-.017 .200	.127 .036	.162 .086	.274 .157	.379 .365	.481 .485	.534 .529
60	-.023 .208	.063 .030	.078 .063	.146 .127	.175 .300	.245 .401	.266 .446
75	-.024 .144	-.005 .014	-.010 .034	.014 .091	.005 .153	.041 .227	.045 .256
90	-.023 0	-.040 0	-.056 .001	-.057 .004	-.082 .012	-.061 .018	-.059 .021
105	-.027 .150	-.026 .018	-.037 .037	-.026 .100	-.049 .157	-.019 .206	-.016 .225
120	-.026 .224	.039 .045	.045 .080	.095 .179	.108 .374	.176 .422	.195 .452
135	-.014 .221	.115 .060	.147 .110	.253 .239	.358 .508	.460 .551	.512 .579
150	-.008 .164	.155 .053	.210 .114	.353 .234	.519 .401	.655 .501	.723 .549
165	-.003 .076	.150 .034	.221 .078	.372 .145	.553 .214	.691 .280	.754 .318

$$K = \frac{P}{\sqrt{\pi a}} F(s, \theta)$$

Upper values - F_I
Lower values - F_{II}

TABLE 17
(Concluded)

a/R	.016	.096	.16	.32	.64	.96	1.12
θ°	.0158	.0875	.138	.242	.390	.490	.528
180	.026 .006	.136 0	.212 0	.351 .006	.539 .004	.672 0	.742 0
195	.083 .008	.138 .030	.207 .074	.326 .113	.531 .202	.653 .272	.712 .317
210	.131 .078	.146 .037	.200 .097	.291 .140	.511 .333	.624 .453	.691 .512
225	.130 .156	.125 .034	.160 .082	.223 .079	.407 .384	.486 .462	.529 .503
240	.085 .174	.064 .028	.079 .058	.106 .045	.206 .316	.257 .368	.279 .406
255	.031 .110	-.002 .012	-.005 .030	-.012 .043	.039 .155	.064 .197	.071 .219
270	.004 0	-.034 0	-.047 .001	-.074 .005	-.040 .012	-.028 .020	-.023 .024
285	.017 .113	-.021 .015	-.029 .032	-.046 .046	-.009 .151	.011 .171	.017 .184
300	.064 .187	.037 .040	.046 .070	.059 .082	.135 .365	.182 .369	.201 .393
315	.113 .181	.108 .053	.140 .100	.197 .137	.361 .495	.434 .501	.481 .526
330	.123 .104	.145 .051	.198 .110	.293 .174	.508 .411	.614 .484	.674 .530
345	.082 .024	.143 .034	.212 .078	.335 .124	.538 .234	.655 .294	.711 .336

$$K = \frac{P}{\sqrt{\pi a}} F(s, \theta)$$

Upper values - F_I
Lower values - F_{II}

REFERENCES

1. Military Specification, "Airplane Damage Tolerance Requirements", MIL-A-83444 (USAF), June 1974.
2. Bowie, O.L., Freese, C.E. and Neal, D.M., "Solution of Plane Problems of Elasticity Utilizing Partitioning Concepts", ASME Paper No. 73-APM-C, 1973.
3. Tada, H., Paris, P.C. and Irwin, G.R., The Stress Analysis of Cracks Handbook, DEL Research Corporation, Hellertown, Pennsylvania, 1973.
4. Pian, T.H.H., "Crack Elements", Proc. World Congress on Finite Element Methods in Structural Mechanics (J. Robinson, ed.), Bournemouth, Dorset, England, 12-17 October 1975, pp. F1-F39.
5. Pian, T.H.H., "Derivation of Element Stiffness Matrices by Assumed Stress Distributions", AIAA J, Vol. 2, July 1964, pp. 1333-1336.
6. Tong, P., Pian, T.H.H. and Lasry, S.J., "A Hybrid Element Approach to Crack Problems in Plane Elasticity", Int J Num Meth Eng, Vol. 7, 1973, pp. 297-308.
7. Orringer, O. and French, S.E., "FEABL (Finite Element Analysis Basic Library) User's Guide", Aeroelastic and Structures Research Laboratory, MIT, ASRL TR 162-3, AFOSR-TR-72-2228, August 1972. (Currently undergoing revision.)
8. Orringer, O., "Fracture Mechanics Analysis of an Attachment Lug", Aeroelastic and Structures Research Laboratory, MIT, ASRL TR 177-1, AFFDL-TR-75-51, January 1976.
9. Stalk, G. and Orringer, O., "Fracture Mechanics Analysis of Centered and Offset Fastener Holes in Stiffened and Unstiffened Panels under Uniform Tension", Aeroelastic and Structures Research Laboratory, MIT, ASRL TR 177-2, AFFDL-TR-75-70, April 1976.
10. Orringer, O. and Stalk, G., "Fracture Mechanics Analysis of Single and Double Rows of Fastener Holes Loaded in Bearing", Aeroelastic and Structures Research Laboratory, MIT, ASRL TR 177-3, AFFDL-TR-75-71, April 1976.

11. Lin, K.Y., "The Stress Intensity of a Crack at an Interface Between Two Materials", Aeroelastic and Structures Research Laboratory, MIT, ASRL TR 162-5, AFOSR-TR-73-1917, June 1973.
12. Orringer, O., Lin, K.Y., Stalk G., Tong, P. and Mar, J.W., "Application of the Assumed-Stress Hybrid Method to Finite Element Analysis in Fracture Mechanics", presented at Session 31, ASCE National & Structural Engineering Convention, New Orleans, La., 16 April 1975.
13. Lin, K.Y., Tong, P. and Orringer, O., "Effect of Shape and Size on Hybrid Crack-Containing Finite Elements", Computational Fracture Mechanics (E.F. Rybicki and S.E. Benzley, ed.), Proc. ASME Second National Congress on Pressure Vessels and Piping, San Francisco, Cal., 23-27 June 1975, pp. 1-20.
14. Lin, K.Y. and Mar, J.W., "Finite Element Analysis of Stress Intensity Factors for Cracks at a Bi-Material Interface", to appear in Int J Fract Mech, February 1976.
15. Desai, C.S. and Abel, J.F., Introduction to the Finite Element Method, Van Nostrand Reinhold Company, 1970.
16. Isida, M., "On the Determination of Stress Intensity Factors for Some Common Structural Problems", J Eng Fract Mech, Vol. 2, 1970 pp. 61-79.
17. Pustejovsky, M.A., "Fatigue Crack Propagation in Titanium Under General In-Plane Loading", PhD Thesis, Department of Aeronautics and Astronautics, MIT, February 1976.